PROUDMAN OCEANOGRAPHIC LABORATORY

REPORT NO. 1

A feasibility study for the development of a joint surge and wave model

J. Wolf, K.P. Hubbert and R.A. Flather

1988

DOCUMENT DATA SHEET

AUTHOR J. WOLF, K.P. HUBBERT AND R.A. FLATHER

PUBLICATION DATE 1988

TITLE A feasibility study for the development of a joint surge and wave model

REFERENCE
Proudman Oceanographic Laboratory, Report No. 1, 109 pp.

ABSTRACT

This report is a preliminary investigation of the interactions between surface waves and the longer period motions due to tides and surges. The aim is to study the feasibility of developing a combined model of tides, surges and waves with particular application to flood prediction. The theoretical background of the interactions between tide and surge motion and the surface waves is summarised. The modified equations for the conservation of momentum for tide and surge motion and conservation of wave spectral energy density are derived. Some calculations of the magnitude of the interaction terms have been made, using results of existing surge/tide and wave models.

ISSUING ORGANISATION
Proudman Oceanographic Laboratory
Bidston Observatory
Birkenhead, Merseyside L43 7RA
UK

Director: Dr B S McCartney

TELEPHONE 051 653 8633

TELEX 628591 OCEAN BG

TELEFAX 051 653 6269

KEYWORDS
WAVES
TIDES
SURGES
MODELLING

CONTRACT

PROJECT PK36

PRICE £26.00

CONTENTS PAGE NO.

1.	Introduction	7
2.	Surge models	8
3.	Wave models	9
4.	Interactions between surge and wave models	12
	4.1 Effects of waves on surges	12
	4.2 Effects of surges and tides on waves	16
5.	Order of magnitude of interaction processes	22
	5.1 Effects of waves on surges	23
	5.2 Effects of surges and tides on waves	31
6.	Discussion	35
7.	Conclusions and recommendations	37
	Appendix	39
	References	50
	List of Symbols	56
	List of Tables	59
	Tables	60
	List of Figures	68
	Figures	70

1. INTRODUCTION

Wind wave and surge/tide models have been developed independently over many years (e.g. GOLDING, 1983; the SWAMP GROUP, 1985; FLATHER, 1984; PROCTOR & FLATHER, 1983). A good understanding of the capabilities and limitations of each type of model has evolved, to the point where there is now some confidence in the results produced and these results are of practical value for routine prediction of waves and water levels. Although they are at present treated separately, a wind event that causes wind waves would also generate a storm surge and vice versa, so clearly their generation is closely related and there are several known mechanisms by means of which the waves and the mean flow or water level associated with tide and surge can interact, each component of the total motion affecting the others. In very shallow water, where accurate prediction of waves, surges and tides is essential for coastal protection (MAFF, 1985), the influence of these interactions may be substantial.

At earlier stages in the development of wind wave and surge models, efforts were concentrated first on the basic requirements, for example, the provision of accurate surface wind fields fundamental to the success of both types of model. Subsequently, attention turned to improving the representation of important physical processes and including some processes initially neglected. For example, surge/tide interaction was shown to be important in shallow water regions (BANKS, 1974) and its inclusion, by developing non-linear models in which tide and surge were treated together, led to improved water level estimates. Now it appears that interactions between wind waves and the surge/tide motion may also be significant and should no longer be ignored. With this in view, the present study aims to examine the relevant interaction mechanisms, estimate their magnitude and hence their probable significance, and to consider the feasibility of developing a combined wave/surge/tide model taking account of the important interactive processes. Likely problem areas are identified.

The structure of the report is as follows. The present status of surge and wave models is first reviewed; surge models being described in Section 2 and wave models in Section 3. In Section 4, the interactive mechanisms linking waves and surge/tide motion are set out, considering first the effect of waves on surges and then the effect of surge and tide on waves, with relevant references to the literature. Estimates of the probable order of magnitude of each mechanism are then attempted, making use of directional wave energy spectra

and tide/surge currents and elevations for representative locations and selected storm events derived from wave and surge/tide model simulations. These are presented in Section 5. The practical implementation of interaction effects in a combined wave/surge/tide prediction system is discussed in Section 6, and conclusions and recommendations are summarised in Section 7.

2. SURGE MODELS

We consider the surge model developed at the Institute of Oceanographic Sciences (now Proudman Oceanographic Laboratory), though similar models have been developed and are in regular use in other countries. These models are reviewed in HEAPS (1983) and MURTY (1984). The model considered here is used for operational storm surge prediction at the U.K. Meteorological Office (henceforth referred to as M.O.) and is described in detail in PROCTOR & FLATHER (1983). It is based on the mass-conservation and momentum equations in depth-averaged form, solving these equations by finite difference methods on a regular grid (Fig. 2.1) covering the NW European shelf seas to produce time series of elevation and current associated with tides and surges. A slightly extended version of the operational model, shown in Fig. 2.2, has been used in some of the computations described later.

The equations in vector notation are:

$$\frac{\partial \underset{\sim}{u}}{\partial t} + \underset{\sim}{u}.\underset{\sim}{\nabla u} + 2\,\underset{\sim}{\Omega} \times \underset{\sim}{u} + g\underset{\sim}{\nabla}\left\{\zeta + \frac{p_a}{\rho g}\right\} + \frac{\underset{\sim}{\tau}_s - \underset{\sim}{\tau}_B}{\rho D} + A_H \nabla^2 \underset{\sim}{u} = 0 \quad , \tag{2.1}$$

$$\frac{\partial \zeta}{\partial t} + \underset{\sim}{\nabla}.(D\underset{\sim}{u}) = 0 \quad , \tag{2.2}$$

where $\underset{\sim}{u}$ is the depth averaged current velocity vector,

ζ is the elevation of the sea surface above its undisturbed level,

$\underset{\sim}{\Omega}$ is the planetary angular velocity,

D is the total water depth (= $h+\zeta$ where h is the undisturbed water depth),

g is the gravitational acceleration,

$\underset{\sim}{\tau}_S, \underset{\sim}{\tau}_B$ are the surface wind stress and bottom stress respectively,

p_a is the atmospheric pressure,

ρ is the density of sea water, assumed constant,

and A_H is a horizontal eddy viscosity coefficient.

At present, the surface stress, $\underset{\sim}{\tau}_s$, is assumed to be related to the surface wind velocity at 10m, $\underset{\sim}{U}_{10}$, by a quadratic law:

$$\underset{\sim}{\tau}_s = C_S \rho_a \underset{\sim}{U}_{10} |\underset{\sim}{U}_{10}| , \tag{2.3}$$

where ρ_a is the density of air and C_s is a surface drag coefficient. This drag coefficient itself varies with wind-speed:

$$C_s = (0.63 + 0.066 |\underset{\sim}{U}_{10}|).^{-3} , \tag{2.4}$$

for $\underset{\sim}{U}_{10}$ in ms^{-1} (SMITH & BANKE, 1975). Equation (2.4) is an empirical result, reflecting the increasing roughness of the sea surface with increasing wind speed.

The bottom stress, $\underset{\sim}{\tau}_B$, is (similarly) related to the depth-mean current by a quadratic friction law:

$$\underset{\sim}{\tau}_B = C_B \rho \underset{\sim}{u} |\underset{\sim}{u}| , \tag{2.5}$$

where C_B takes a constant value of 0.0025.

These equations are solved by time-stepping on a regular grid of 1/3° latitude by 1/2° longitude, using tide and surge input at the open boundaries, just beyond the continental shelf edge (Fig. 2.1) and atmospheric pressure and surface winds derived from the M.O. 15-level atmospheric model (GADD, 1985) to drive the motion.

A boundary condition requiring zero normal flow at land boundaries is imposed, and along open boundaries, a gravity wave radiation condition is employed which also permits the introduction of externally generated tides and surges. Details are given in PROCTOR & FLATHER (1983).

3. WAVE MODELS

Most operational wave models solve the energy balance equation for the two-dimensional wave energy density spectrum $E(f,\theta,\underset{\sim}{x},t)$ (the SWAMP GROUP, 1985), where f and θ are the wave frequency and direction at location $\underset{\sim}{x}$ and time t ($f = \omega/2\pi$, where ω is the wave angular frequency). This equation is generally

written

$$\frac{\partial E}{\partial t} + \underset{\sim}{\nabla}.(\underset{\sim g}{c} E) = S \ , \qquad (3.1)$$

where E is the wave energy density spectrum (divided by $\frac{1}{2}\rho g$)

$\underset{\sim g}{c}$ is the group velocity of a particular spectral component,

and S is a source function, representing sources and sinks of wave energy.

Equation (3.1) may be integrated numerically by time-stepping on a finite difference spatial grid. The two models considered here are the M.O. wave model (GOLDING, 1983) and the WAM group model (KOMEN, 1986) running at the European Centre for Medium Range Weather Forecasting (ECMWF). Both these models are undergoing development, so only general comments about their features will be made.

The main differences between most wave models lie in the specification of the source term S. This may be expanded as

$$S = S_{in} + S_{nl} + S_{ds} \ , \qquad (3.2)$$

where S_{in} represents the energy input from the wind,

S_{nl} is the redistribution of energy within the spectrum by non-linear interactions,

and S_{ds} is the dissipation of energy by wave breaking and bottom friction.

The main wind input source function, S_{in}, represents an exponential rate of wave growth, and is given by SNYDER ET AL (1981) as

$$S_{in} = \frac{\beta\rho_a}{\rho} f\, E(F,\theta)\left(\frac{U\cos(\theta-\Psi)}{c} - 1\right) \quad \text{if } \frac{U\cos(\theta-\Psi)}{c} > 1 \ , \qquad (3.3)$$

$$= 0 \text{ otherwise} \ ,$$

where β is a constant,

U is the wind speed at some height (replaced by u_*, the friction velocity, in the WAM model),

Ψ is the wind direction,

c is the phase speed.

The phase speed is given by

$$c = \frac{\omega_o}{k} = \sqrt{\frac{g}{k} \tanh kh} \quad , \tag{3.4}$$

where k is the wavenumber of waves of frequency f($k = 2\pi/\lambda$, with λ = wavelength), and ω_o is the wave angular frequency as seen by an observer moving with the current, the 'intrinsic' frequency.

In the M.O. model, this source term has an additional linear growth rate component allowing for the initial growth of waves from flat calm. The WAM model requires an initial wave field to be specified or else no growth occurs.

The dissipation term, S_{ds}, consists of two parts, the first being a representation of wave-breaking or whitecapping, given by HASSELMANN (1974). The second component of dissipation is bottom friction. A quadratic bottom friction term is used, relating the stress to the wave particle velocity at the sea-bed. For the M.O. model this term is

$$S_{ds} = \frac{\phi_1 \, c_g}{2\pi g k} |\langle \underset{\sim}{u} \rangle| \, E(f,\theta) \left(\frac{gk}{2\pi f \cosh kh} \right)^2 \quad , \tag{3.5}$$

where

$$\langle \underset{\sim}{u} \rangle = \left\{ \iint \left(\frac{gk}{2\pi f \cosh kh} \right)^2 \quad E(f,\theta) \, df \, d\theta \right\}^{\frac{1}{2}} \tag{3.6}$$

$\langle \underset{\sim}{u} \rangle$ represents a mean sea-bed wave velocity and ϕ_1 is taken to be 0.005.

The main difference between the M.O. model and the WAM model is in the non-linear wave-wave interaction term, S_{nl}, which causes energy to be redistributed within the spectrum. The term is a rather complicated multiple integral over wavenumber space (see HASSELMANN & HASSELMANN, 1985, for its definition). The M.O. model is a 'hybrid' model which does not include this term explicitly, but represents its effect by forcing the wind-sea energy (associated with waves which are being generated by the local wind) to fit a prescribed spectral shape at all times. The JONSWAP spectrum (HASSELMANN ET AL, 1973) is used. The WAM model, however, does include the S_{nl} term explicitly, being a so-called 'third-generation' model, and consequently there are no imposed restrictions on the shape of the spectrum. Effectively, then, the M.O. model distinguishes between wind-sea and 'swell' (that part of the motion not being actively generated by the local wind) in its treatment of these processes, whereas the WAM model does not.

The M.O. model does, however, include depth-refraction, i.e. changes in the

group velocity of the waves due to variations in mean water depth, whereas the WAM model, in its present version, does not.

4. INTERACTIONS BETWEEN SURGE AND WAVE MODELS

The interactions between surges, tides and waves may be divided into two groups: (i) the effects of waves on surges; and (ii) the effect of tide plus surge elevations and currents on waves. It will be assumed that the scales of motion are sufficiently disparate that the longer period motions (tides and surges) appear as a change in mean elevation and current to the waves, while some statistics of the wave field may be used to parameterize the effect of waves on the surge. The various effects are listed and an attempt is made to quantify them in the following sections. Linear wave theory is used (KINSMAN, 1965). Note that there are interactions between tides and surges and waves which may be already partially included empirically in the surge model, for example in the empirical expression of SMITH & BANKE (1975) for the surface drag coefficient (equation 2.4). Much of the energy input from the wind enters the wave field first, and is then transmitted rapidly to the mean flow by dissipative processes acting on the waves.

4.1 Effects of waves on surges

Referring to equations (2.1) and (2.2), the possible effects of waves on the surge prediction are listed below.

4.1.1 Non-linear interactions

There will be an additive effect of wave-induced mean flow and change in water depth (wave set-up or set-down). These are second-order effects of the waves. For example, the waves generate a mean momentum density produced by a mean flow in the surface layer (above the trough level of the waves). This may be equated to a depth-averaged mean velocity, u_M, in the wave direction, of

$$u_M = \frac{ga^2}{2cD} , \qquad (4.1.1)$$

where a is the wave amplitude for a train of monochromatic waves (LeBLOND & MYSAK, 1978). Wave breaking also contributes to the mean flow.

Wave set-up (or set-down) is described by the theory developed by Longuet-Higgins and Stewart and summarised in LONGUET-HIGGINS & STEWART (1964). See also JAMES (1983). It arises from a 'radiation stress', which is defined as the excess momentum flux due to the waves. For waves travelling in the positive x direction we have

$$R_{xx} = \tfrac{1}{2}\rho g a^2 \left(\frac{2kD}{\sinh 2kD} + \frac{1}{2}\right), \quad R_{xy} = R_{yx} = 0, \quad R_{yy} = \tfrac{1}{2}\rho g a^2 \frac{kD}{\sinh 2kD}, \qquad (4.1.2)$$

where R_{xx} is the flux of x-momentum in the x-direction, etc.
Horizontal gradients in the radiation stress must be balanced by other terms in the momentum equation. If the waves are entering shallow water without breaking, the radiation stress is increasing; this is balanced by a set-down in mean water level, $\bar{\zeta}$, such that,

$$\frac{d\bar{\zeta}}{dx} = -\frac{1}{\rho g D}\frac{dR_{xx}}{dx} . \qquad (4.1.3)$$

Inside the breaker zone, the wave energy decreases towards the shore and so does the radiation stress, leading to an increase in mean water level ('set-up'). Values for this near-shore set-up are more empirical, dependent on the wave-breaking process, but generally related to the bottom slope (BATTJES, 1974)

$$\frac{d\zeta}{dx} = -A_S \frac{dh}{dx} , \qquad (4.1.4)$$

where A_S is an empirical constant.

All the extra terms in the equation of motion for the mean flow, due to waves, are summarised for example in LeBLOND & MYSAK (1978). If $\underset{\sim}{\Gamma}/\rho D$ represents the extra terms due to the action of waves in the momentum equations for the mean flow (2.1), then

$$\frac{\underset{\sim}{\Gamma}}{\rho D} = \frac{1}{2\rho D}\underset{\sim}{\nabla}\{(\underset{\sim}{c} - 2\underset{\sim}{c}_g).\langle \underset{\sim}{M}\rangle\} - \frac{\underset{\sim}{u}}{\rho D}(\underset{\sim}{\nabla}.\langle \underset{\sim}{M}\rangle) + \frac{\langle \underset{\sim}{M}\rangle}{\rho D} \times (\underset{\sim}{\nabla} \times \underset{\sim}{u}) , \qquad (4.1.5)$$

where $\langle \underset{\sim}{M}\rangle$ is the mean momentum of the waves,

$$\langle \underset{\sim}{M}\rangle = \frac{\langle Q\rangle \underset{\sim}{k}}{\omega_o} , \quad \langle \underset{\sim}{M}\rangle . \underset{\sim}{c} = \langle Q\rangle , \qquad (4.1.6)$$

where $\langle Q\rangle$ is the wave energy density ($= \frac{1}{2}\rho g a^2$ for monochromatic waves).

In equation (4.1.5), it is assumed that the mean flow velocity $\underset{\sim}{u}$ is

independent of depth. The first term on the right-hand side includes the contribution of radiation stress, being purely an effect of the waves. The last two terms come from the non-linear interactions of waves and current.

For wave spectra the momentum will be given by

$$\langle \underset{\sim}{M} \rangle = \tfrac{1}{2}\rho g \int_0^\infty \int_0^{2\pi} \frac{\underset{\sim}{k}}{2\pi f} E(f,\theta) d\theta \, df \, . \qquad (4.1.7)$$

So, for example in Cartesian coordinates

$$\langle \underset{\sim}{M} \rangle_x = \rho g \int_0^\infty \int_0^{2\pi} \frac{k\cos\theta}{f} E(f,\theta) d\theta \, df, \quad \langle \underset{\sim}{M} \rangle_y = \frac{\rho g}{4\pi} \int_0^\infty \int_0^{2\pi} \frac{k\sin\theta}{f} E(f,\theta) d\theta \, df \quad , \qquad (4.1.8)$$

$$c_g = \frac{\partial \omega}{\partial k} = \frac{c}{2} \left(1 + \frac{2kD}{\sinh 2kD}\right), \text{ using (3.4)}, \qquad (4.1.9)$$

so that

$$(\underset{\sim}{c} - 2\underset{\sim}{c}_g) . \langle \underset{\sim}{M} \rangle = -\rho g D \int_0^\infty \int_0^{2\pi} \frac{k}{\sinh 2kD} E(f,\theta) d\theta \, dF \, . \qquad (4.1.10)$$

4.1.2 Surface stress

The sea surface roughness is substantially determined by the wave field and so the surface drag coefficient (and hence the wind stress driving the surge motion) is a function of the wave field. In fact, the surface stress at the air-sea interface should be identical in the three models concerned: the atmospheric model, the surge model and the wave model. This may be difficult to achieve when the mechanisms of wave growth and turbulence are not fully understood, but some consistency is desirable. The momentum transferred from the wind to the sea must subsequently be divided between the surge and the waves (DONELAN, 1979). Most of the momentum transferred from the wind to the waves is passed on to the mean flow by dissipation, but part is retained by the waves during the development of a wind-sea.

A quadratic law is used to relate the surface stress to the wind speed at 10m in the present surge model (equation 2.3). The drag coefficient is only empirically related to the surface wind speed at 10m (equation 2.4) and not directly to the wave field.

Some other models used for the calculation of the drag coefficient are discussed in the Appendix. A similar analysis has been made by GEERNAERT ET AL

(1986). In a neutral atmospheric boundary layer, the velocity profile for the surface wind may be taken to be logarithmic. The drag coefficient, C_s, may then be obtained from a roughness length representing the sea surface, z_o (in metres),

$$C_S = \left[\frac{K}{\ln(z/z_o)}\right]^2 \quad , \tag{4.1.11}$$

where z = 10m, and K is von Karman's constant ($\simeq$0.4).

The roughness length, z_o, should be related to some length scale representative of the surface waves, and will presumably therefore be related to wind fetch and duration as well as the magnitude of the wind velocity. The surface roughness is also moving at the phase speed of the waves and this should be taken into account. Details of the calculation of the drag coefficient from the wave field are given in sub-section 5.1.2. One of the outstanding problems in formulating a model for the surface drag coefficient is in understanding how important is the long wave and swell contribution to the surface roughness. It seems that the most important contribution is from the high frequency waves and these adjust quickly to the local wind hence the success of simple wind-speed dependent drag coefficients such as (2.4), but the long waves may have a significant effect and these are dependent on non-local winds and wave-age.

4.1.3 Bottom stress

The bottom stress acting on the surge will be affected by the turbulence introduced at the sea-bed in the wave boundary layer. This has been studied, for example, by GRANT & MADSEN (1979) and CHRISTOFFERSEN & JONSSON (1985), henceforth termed CJ. The water must be sufficiently shallow for the orbital velocities of the waves to be non-zero at the sea-bed. This implies $h<\lambda/2$. The same argument as for the surface stress suggests that the bottom stress in both the wave and surge models should not be independent. CJ show how the total instantaneous bed stress, $\underset{\sim}{\tau}_B$, can be split up into a mean flow component, $\underset{\sim}{\tau}_{BC}$, and a wave component, $\underset{\sim}{\tau}_{BW}$, i.e.

$$\underset{\sim}{\tau}_B = \underset{\sim}{\tau}_{BC} + \underset{\sim}{\tau}_{BW} \tag{4.1.12}$$

where $$|\underset{\sim}{\tau}_{BC}| = \tfrac{1}{2}C_{BC}\rho|\underset{\sim}{u}|^2 , \qquad (4.1.13)$$

$$|\underset{\sim}{\tau}_{BW}| = \tfrac{1}{2}C_{BW}\rho\,|\underset{\approx}{u}_{WBM}|^2 ,$$

$\underset{\sim}{u}$ is the depth-mean current,

$\underset{\sim}{u}_{WBM}$ is the wave-particle current just outside the wave boundary layer,

and C_{BC}, C_{BW} are friction coefficients.

The friction coefficients are interdependent and are obtained in CJ by iteration. The details of their determination are given in sub-section 5.1.3. The limitations of the method of CJ are that the current is assumed steady, with no Coriolis effect, the waves are monochromatic and the eddy viscosity is assumed time-invariant. Recent work by YOO & O'CONNOR (1987) suggests a similar method avoiding iteration.

Two models of the eddy viscosity profile are used by CJ, both employing a parabolic viscosity in the upper, current, boundary layer. The first model, for 'large' bed roughness (low wave-current regimes), assumes a constant viscosity in the wave boundary layer (WBL), while the second, for 'small' bed roughness, has a viscosity in the WBL which increases with height above the bed. Much more sophisticated turbulence models could be envisaged and this is an area in which there will doubtless be fundamental developments, (e.g. KING, DAVIES & SOULSBY, 1985).

4.2 Effects of surges and tides on waves

The surge and tide will affect the wave field, due to:

(a) changes in water depth; and

(b) the presence of a mean current.

These will result in differences in the generation, propagation and dissipation of the waves depending on the surge/tide motion, plus some energy transfers between the waves and the mean flow field. A comprehensive review of the wave-current interactions is given by PEREGRINE & JONSSON (1983). LeBLOND & MYSAK (1978) and PHILLIPS (1977) cover the theoretical derivations of the formulae stated below.

4.2.1 Wave generation

As mentioned in sub-section 4.1.2, the surface stress applied to both the surge and wave models should ideally be consistent. DONELAN (1979) discusses the proportions in which the momentum transferred from the wind is distributed between the mean flow and waves. The presence of a mean current will change the effective fetch of the wind and the relative velocity which should be used in calculating the surface stress (effective wind). In practice, the way in which energy is input to the wave model is designed to achieve the correct rate of wave growth in an empirical way. More sophisticated formulations in this area may therefore be difficult to implement (see Section 6), but further work in the fields of wave growth and atmospheric boundary layer research must be monitored.

4.2.2 Wave propagation

Present operational wave models may calculate refraction due to changes in the undisturbed water depth. However, they do not generally account for changes in the water depth or the current due to surges and tides which will also result in changes in various wave parameters. The main effects of these are the Doppler shift of wave frequency and further refraction, causing changes in wavelength, period and wave direction due to changes in wave phase and group velocity. The derivation of the refraction equations is first outlined.

The fundamental equation is

$$\frac{\partial \underset{\sim}{k}}{\partial t} + \underset{\sim}{\nabla}\omega = 0 \ , \qquad (4.2.1)$$

sometimes referred to as the 'conservation of crests',

where $$\omega = \omega_o + \underset{\sim}{k}.\underset{\sim}{u} \ . \qquad (4.2.2)$$

$\underset{\sim}{k}$ is the wavenumber vector and $\underset{\sim}{\omega}_o$ is the wave angular frequency as seen by an observer moving with the current $\underset{\sim}{u}$ and satisfies the dispersion relationship

$$\omega_o = \underset{\sim}{k}.\underset{\sim}{c} = \sqrt{gk \tanh kD} \ , \qquad (4.2.3)$$

for linear wave theory, where $k = |\underset{\sim}{k}|$. ω may be called the 'apparent' or observed frequency (as seen by a stationary observer). ω_o may be called the

'intrinsic', relative or Doppler-shifted frequency.

Equation (4.2.2) describes the Doppler shift of frequency of waves travelling on a current. Equations (4.2.1) to (4.2.3) lead to the refraction equations in their most general form:

$$\frac{\partial \omega}{\partial t} + (\underset{\sim}{u} + \underset{\sim}{c}_g).\underset{\sim}{\nabla}\omega = \underset{\sim}{k}.\frac{\partial \underset{\sim}{u}}{\partial t} + \frac{\partial \omega_o}{\partial D}\frac{\partial D}{\partial t} , \tag{4.2.4}$$

$$\frac{\partial \omega_o}{\partial t} + (\underset{\sim}{u} + \underset{\sim}{c}_g).\underset{\sim}{\nabla}\omega_o = -D\underset{\sim}{\nabla}.\underset{\sim}{u}\frac{\partial \omega_o}{\partial D} - \underset{\sim}{c}_g.(\underset{\sim}{k}.\underset{\sim}{\nabla})\underset{\sim}{u} , \tag{4.2.5}$$

and

$$\frac{\partial \underset{\sim}{k}}{\partial t} + (\underset{\sim}{u} + \underset{\sim}{c}_g).\underset{\sim\sim}{\nabla k} = -\frac{\partial \omega_o}{D}\underset{\sim}{\nabla} D - \underset{\sim}{k}.\underset{\sim\sim}{\nabla u} - \underset{\sim}{k} \times (\underset{\sim}{\nabla} \times \underset{\sim}{u}) , \tag{4.2.6}$$

(using the continuity equation $\frac{\partial D}{\partial t} + \underset{\sim}{\nabla}.(D\underset{\sim}{u}) = 0$) .

$\underset{\sim}{c}_g$ is given by

$$\underset{\sim}{c}_g = \frac{\underset{\sim}{k}}{k}\frac{\partial \omega_o}{\partial k} = c_g\frac{\underset{\sim}{k}}{k} . \tag{4.2.7}$$

In a time-invariant flow, equation (4.2.4) may be rewritten

$$\frac{d\omega}{dt} = 0 , \tag{4.2.8}$$

where

$$\frac{d}{dt} = \frac{\partial}{\partial t} + (\underset{\sim}{u} + \underset{\sim}{c}_g).\underset{\sim}{\nabla} ,$$

i.e. the frequency is constant along the characteristics or 'rays', describing the direction of wave energy propagation, which are given by

$$\frac{d\underset{\sim}{x}}{dt} = \underset{\sim}{u} + \underset{\sim}{c}_g . \tag{4.2.9}$$

This leads to Snell's Law, commonly used for the refraction of waves in shoaling water, using $\omega = \underset{\sim}{k}.\underset{\sim}{c}$ = constant along a wave ray, assuming $\underset{\sim}{u} = o$. The wave speed given by equation (3.4) is reduced as the water depth decreases, leading to a reduction in the wavelength of the waves and a change in direction of propagation.

Now the full form of the spectral energy balance equation is derived. The

fundamental conserved quantity, as obtained by BRETHERTON & GARRETT (1969), is 'wave-action density', defined as energy divided by intrinsic frequency, $\langle Q\rangle/\omega_o$, which obeys

$$\frac{\partial}{\partial t}\frac{\langle Q\rangle}{\omega_o} + \underset{\sim}{\nabla}.\{(\underset{\sim}{u} + \underset{\sim}{c}_g)\frac{\langle Q\rangle}{\omega_o}\} = 0 \ , \qquad (4.2.10)$$

(neglecting energy input and dissipation, temporarily). We actually require the equation in terms of a spectral energy budget however. The wave-action contained in an element δA of the wavenumber plane is $N(\underset{\sim}{k})\delta A$ where $N(\underset{\sim}{k})$ is the wave-action density wave-number spectrum, so (using $N \equiv N(\underset{\sim}{k})$)

$$\frac{\partial}{\partial t}(N\delta A) + \underset{\sim}{\nabla}.\{(\underset{\sim}{u} + \underset{\sim}{c}_g)N\delta A\} = \frac{S'(\underset{\sim}{k})\delta A}{\omega_o} \ , \qquad (4.2.11)$$

where the RHS is the re-introduced source term.
It may be shown (e.g. PHILLIPS, 1977) that

$$\frac{\partial}{\partial t}\delta A + \underset{\sim}{\nabla}.\{(\underset{\sim}{u} + \underset{\sim}{c}_g)\delta A\} = 0 \ , \qquad (4.2.12)$$

thus

$$\frac{d}{dt}N(\underset{\sim}{k}) = \frac{\partial}{\partial t}N(\underset{\sim}{k}) + (\underset{\sim}{u} + \underset{\sim}{c}_g).\nabla N(\underset{\sim}{k}) = \frac{S'(\underset{\sim}{k})}{\omega_o} \qquad (4.2.13)$$

is now the basic conservation equation, i.e. $N(\underset{\sim}{k})$ is conserved along a ray (in the absence of wave generation or dissipation). We now convert this to an equation in terms of the energy density spectrum in frequency and direction space, $E(\omega_o,\theta)$.

$$N(\underset{\sim}{k}) = \frac{E'(k)}{\omega_o} = \frac{c_g}{\omega_o k}E(\omega_o,\theta) \ , \qquad (4.2.14)$$

so that (using $E \equiv E(\omega_o,\theta)$, $S \equiv S(\omega_o,\theta)$), (4.2.13) becomes

$$\frac{dE}{dt} + \frac{E}{c_g}\frac{dc_g}{dt} - \frac{E}{k}\frac{dk}{dt} - \frac{E}{\omega_o}\frac{d\omega_o}{dt} = S \ , \qquad (4.2.15)$$

or, including explicitly the differentiation with respect to the dependent variables, ω_o and θ,

$$\frac{dE}{dt} + \frac{\partial E}{\partial \omega_o}\frac{d\omega_o}{dt} + \frac{\partial E}{d\theta}\frac{d\theta}{dt} + \frac{E}{c_g}\frac{dc}{dt}_g - \frac{E}{k}\frac{dk}{dt} - \frac{E}{\omega_o}\frac{d\omega}{dt}_o = S, \qquad (4.2.16)$$

$\frac{d\omega_o}{dt}$ is given by equation (4.2.5). $\frac{dk}{dt}$ and $\frac{d\theta}{dt}$ are obtained from (4.2.6):-

$$\frac{dk}{dt} = \frac{k}{k} \cdot \frac{dk}{dt} = \frac{-k.\nabla D}{k}\frac{\partial \omega_o}{\partial D} - \frac{k.(k.\nabla)u}{k}, \qquad (4.2.17)$$

$$\frac{d\theta}{dt} = \frac{1}{k^2}\left|k \times \frac{dk}{dt}\right| = \frac{-1}{k^2}\frac{\partial \omega_o}{\partial D}\left|k \times \nabla\right| D - \frac{k.}{k^2}\left|k \times \nabla\right| u . \qquad (4.2.18)$$

$$\frac{dc}{dt}_g = \frac{dc}{\partial t}_g\frac{dD}{dt} + \frac{\partial c}{\partial k}_g\frac{dk}{dt}$$

$$= \frac{\partial c_g}{\partial D}(-D\nabla.u + c_g.\nabla D) + \frac{\partial c_g}{\partial k}\left\{\frac{-k.\nabla D}{k}\frac{\partial \omega_o}{\partial D}\frac{-k.(k.\nabla)u}{k}\right\}, \qquad (4.2.19)$$

so the wave energy equation becomes, after some manipulation,

$$\frac{dE}{dt} + E\nabla.u + \frac{\partial}{\partial \sigma}\left(E\frac{d\sigma}{dt}\right) + \frac{\partial}{\partial \omega_o}\left(E\frac{d\omega_o}{dt}\right) - \frac{E}{\omega_o}\frac{d\omega_o}{dt} + E\left(\frac{\partial c_g}{\partial D} - \frac{1}{c_g}\frac{\partial c_g}{\partial K}\frac{\partial \omega_o}{\partial D}\right)k.\nabla D = S . \qquad (4.2.20)$$

We have used the relations

$$\frac{\partial}{\partial \theta}\left(\frac{k.\left|k \times \nabla\right| u}{k^2}\right) = \nabla.u - \frac{2k.(k.\nabla)u}{k^2}, \quad \frac{\partial}{\partial \theta}\left(\left|k \times \nabla\right| D\right) = -k.\nabla D ,$$

and $$\frac{\partial}{\partial \omega_o}\left(\frac{d\omega_o}{dt}\right) = \frac{1}{c_g}\frac{\partial}{\partial k}\left(\frac{d\omega_o}{dt}\right) = \frac{-k.(k.\nabla)u}{k^2} - \frac{k}{c_g}\frac{\partial c_g}{\partial k}\frac{k.(k.\nabla)u}{k^2} - \frac{D}{c_g}\frac{\partial c_g}{\partial D}\nabla.u .$$

Equation (4.2.20) thus allows for the effects of current and depth refraction and the transfer of energy to or from the mean flow by means of the radiation stress working on the current shear.

4.2.3 Wave dissipation

The two mechanisms for wave energy dissipation are wave breaking and bottom friction. In the WAM model, dissipation is based on the white-capping formulation of HASSELMANN (1974) i.e.

$$S_{ds} = -3.33.10^{-5}\bar{\omega}\left(\frac{\omega}{\bar{\omega}}\right)^{2}\left(\frac{\alpha}{\alpha_{PM}}\right)^{2}E \ , \qquad (4.2.21)$$

where the coefficients have been determined empirically (KOMEN, 1986). $\bar{\omega}$ is the mean frequency, defined as

$$\bar{\omega} = \frac{\iint E\omega \ d\theta \ dF}{\iint E \ d\theta \ dF} \ .$$

α is an integral wave steepness parameter

$$\alpha = \frac{\iint E \ d\theta \ df}{\bar{\omega}^4 \ g^2}$$

and $\alpha_{PM} = 4.57.10^{-3}$ is the theoretical value of α for a Pierson-Moskowitz spectrum. The dissipation is thus related to the wave energy. However from the point of view of wave-current interactions, it is thought that surface current shear may enhance wave breaking (PEREGRINE & JONSSON, 1983). It would be possible to extend the depth-averaged surge and tide model from 2D into 3D in order to include these effects. A technique allowing vertical profiles of current to be extracted from the depth-averaged values might be used e.g. DAVIES (1988). An eddy viscosity profile must be chosen, relating it to the known physical parameters of wind-speed, current, depth and stratification if possible. This has not been fully determined. The method would give an estimate of the surface current shear and also the near-bed profile of current and the bottom stress allowing the bottom friction to be more accurately predicted. Further interactions between waves and vertical current shear have been reviewed in SROKOSZ (1985).

Bottom friction only affects the waves when they are in sufficiently shallow water for the wave particle velocity to be non-zero at the sea-bed. The M.O. wave model uses a quadratic friction law relating the energy dissipation to the near-bed wave particle velocity, assuming a constant friction coefficient (equation (3.5)). However, the wave and current friction coefficients should be related as discussed in sub-section 4.1.3. The effective eddy viscosity, μ, is related to the turbulence produced in both the wave and current boundary layers.

The method of CJ (shown in sub-section 5.1.3) can be used to provide both current and wave friction factors. It could perhaps be extended to use the vertical current profile extracted as discussed above.

5. ORDER OF MAGNITUDE OF INTERACTION PROCESSES

Some concurrent wave and surge model data was available for a period in January-February 1983, which was quite stormy, and this was used to calculate the magnitude of the various terms already outlined. Tide and surge elevations and currents were available from an extended shelf model (Fig. 2.2) for the period 1 January - 10 February 1983. Directional wave spectra at 6-hourly intervals for the same period were obtained from the M.O. wave model. Some further 3-hourly wave spectra for 11 selected locations and 6 selected storms (corresponding to 'WHIST' - the Wave HIndcast STudy) produced by the WAM model, were obtained from ECMWF. The periods are given in Table 5.1 and locations in Table 5.2 and shown in Figure 5.1. A subset of these locations and periods were used for the calculations described here. In particular, the severe storm on 1 February 1983 was examined. The station locations are such that water depths, generally, increase northwards, from point 1 in the southern North Sea to point 11 off the Norwegian coast. However, station 6 is in relatively deep water in the Norwegian Trench.

The magnitude of the various interaction terms in the equations was calculated to provide an indication of their relative importance. A full assessment of the interaction effects would require the wave and surge models to be run again, including the interaction terms. This has not yet been done, but is planned at a subsequent stage.

Shown in Figs. 5.2(a), (b) and (c) are the total surface elevations and the east- and north-directed current velocity components (u, v respectively) calculated by the tide and surge model for the first 40 days of 1983, encompassing 5 of the WHIST storms. The semidiurnal tidal signal is clearly distinguishable at most locations. The tidal elevations have an amplitude of about 1m. During storm events the surge elevations perturb the tidal signal by a significant amount at the shallower locations but are small in depths over 100m. For point number 1, an elevation range of 4 metres is indicated, which is very significant compared with the undisturbed water depth of 20m at that point. The tidal current velocities are clearly much greater in shallow water regions than in deep water regions. The perturbations of the current velocity by the

surge are less noticeable at shallower locations than in deeper water. The maximum current speed of about 60 cm/s at Station 1 is not much enhanced by the surge. The effects of the surge are more marked at the deeper locations where a background tidal signal of amplitude about 10 cm/s may be doubled in the presence of the surge and there are strong oscillations of diurnal period at Stations 7 to 11 probably triggered by the storm events. The large magnitudes of the effects of meteorological forcing upon the tidal model are illustrated in these figures.

Shown in Fig. 5.2(d) are surface wind vectors for the eleven locations during the WHIST storms, provided by the M.O. North is towards the top of the page. The wind fields from this model are used as input to the tide/surge and wave models described earlier. For the first three WHIST storms, the predominant wind direction is towards ENE. For the fourth storm, the winds are predominantly towards the SE. During the final storm, there is a sharp change in the wind direction in the early part of the storm.

It is interesting to observe the effect of this sudden change in the wind direction upon the wave spectrum. Shown in Fig. 5.2(e) are consecutive spectra from the WAM model for point number 5 at the start of the fifth WHIST storm. The sudden change in direction and freshening of the wind has led to an energetic swell pattern and a small wind-sea at 12z on 1 February, 1983. A comparison of spectra for the two models is given in Fig. 5.2(f). There are quite large differences in the swell predictions, with far more swell predicted by the WAM model on this particular occasion. The differences between the two models may be attributed to their differing treatments of the swell part of the spectrum and wave growth.

Profiles of significant wave height at the eleven locations are presented in Fig. 5.2(g). At the start of a storm, there is a sharp rise in the value of this parameter although the background level is quite high (M.O. model). Differences between the two sets of predictions can again be attributed to the differing model formulations. Maximum values of significant wave height of about 5m are predicted for the shallower stations during storms 4 and 5, while the maximum is about 12m at the deeper stations attained during storms 2 and 3.

5.1 Effects of waves on surges

The most important effects will be discussed in turn.

5.1.1 Non-linear interactions.

From equation (4.1.5) it may be seen that these effects depend upon the existence of horizontal gradients of wave energy and momentum and current velocity. These terms are likely to be small in general but may be large locally and therefore tend to depend on model resolution (as for the non-linear advective terms in the surge model).

The first part of equation (4.1.5) is the radiation stress contribution. In deep water, $c = 2c_g$ and this becomes zero. In very shallow water ($h<\lambda/20$), $c = c_g$ and this term may be important. One of the most important effects which has been observed is wave 'set-up' (LONGUET-HIGGINS & STEWART, 1964) or, more correctly, outside the breaker-zone, wave 'set-down'. Here, the momentum balance is between a mean sea-level gradient (in the direction of the wave propagation) and the radiation stress gradient, leading to

$$\bar{\zeta} = \frac{-\langle Q \rangle}{\rho g^{o}} \frac{k}{\sinh 2kD} = -\int_{o}^{\infty}\int_{o}^{2\pi} \frac{E(f,\theta)k}{2\sinh 2kD} \, d\theta \, df \, , \qquad (5.1.1)$$

for the increase in sea-level due to the presence of the waves. This will be most important right at the coast in very shallow water. Inside the breaker zone, the set-down becomes a set-up, i.e. increase in water level. This region is not resolved by the present wave and surge models, having grid sizes of a few tens of kilometres. The maximum set-down is 1.2cm achieved at station 4 during storm 5, using the WAM wave predictions which give slightly larger values than the M.O. waves. The set-down increases rapidly as the water depth reduces, as shown (for monochromatic waves) in Table 5.3. Only the longer waves are in "shallow" water for depths of 20m, i.e. wave periods of greater than 5 seconds. Shorter waves generate no set-down. The mean wave period (zero-up-crossing period) for station 1 is about 5 seconds rising to 6 or 7 seconds at the height of the storm and the set-down is very small. Table 5.3 shows how the set-down associated with a 'typical' swell period of 10 seconds and a 'typical' wind-sea period of 5 seconds (taken from M.O. wave model prediction for station 1) increases with increasing wave height and decreasing water depth. At station 1 the wind-sea significant wave height reaches a maximum of 4.5m during the time period 1 January - 9 February 1983; the swell significant wave height reaches 1.9m (swell will be strongly dissipated in this shallow water). The set-down might exceed 10cm in less than 5m of water but will only be 1-2cm in 10m of

water and so should be negligible except very near shore. (This estimate does not include the effects of wave breaking which occurs in the surf zone within a few hundred meters of the shoreline, where set-down becomes set-up).

The other terms in the radiation stress energy transfer are $(\underset{\sim}{u}\underset{\sim}{\nabla}.\langle\underset{\sim}{M}\rangle)/\rho D$ and $(\langle\underset{\sim}{M}\rangle \times \underset{\sim}{\nabla} \times \underset{\sim}{u})/\rho D$. The contribution of these terms does not disappear in deep water but will be reduced because of the inverse relationship with water depth. An order of magnitude analysis of the equation of motion is given below. The mean flow momentum equation, equation (2.1), with the extra terms due to waves, equation (4.1.5), becomes

$$\frac{\partial \underset{\sim}{u}}{\partial t} + \underset{\sim}{u}.\underset{\sim}{\nabla}\underset{\sim}{u} + 2\underset{\sim}{\Omega}\times\underset{\sim}{u} + g\underset{\sim}{\nabla}\zeta + \frac{1}{\rho}\underset{\sim}{\nabla}p_a + \frac{\underset{\sim}{\tau}_s}{\rho D} - \frac{\underset{\sim}{\tau}_B}{\rho D} + A_H\nabla^2\underset{\sim}{u}$$
$$= \frac{1}{2\rho D}\underset{\sim}{\nabla}\{(\underset{\sim}{c} - 2\underset{\sim}{c}_g).\langle\underset{\sim}{M}\rangle\} - \frac{\underset{\sim}{u}.\langle\underset{\sim}{M}\rangle}{\rho D} + \frac{\langle\underset{\sim}{M}\rangle \times \underset{\sim}{\nabla}\times\underset{\sim}{u}}{\rho D}. \qquad (5.1.2)$$

The order of magnitude of the amplitude of each of these terms under three different scenarios is set out in Table 5.4. Some fundamental assumptions have been made:

(i) The mean current and elevation have an M_2 tidal period of 12.4 hours, the current amplitude is 1m s^{-1} and the elevation amplitude is 1m. This is representative of a large part of the area of the North Sea within a factor of 2 (FLATHER, 1987). The surge will have a similar periodicity to the tide;

(ii) the wind speed is 20m/s representing a strong wind event with an associated atmospheric pressure gradient of 3.10^{-3} N m^{-3}(Pa m^{-1}),

(iii) the horizontal eddy viscosity is related to the cross-sectional area of the model grid-box. It is chosen as 5D m^2s^{-1} for a grid of 1/3° latitude by ½° longitude. The grid size of the model is assumed to be 30km by 30km everywhere;

(iv) spatial gradients are determined by the wave-length of the tidal wave for the long period motion but by the grid size of the model for sub-grid scale motion i.e. surface waves, and for the advective term which will be determined by the resolution of the bottom topography; and

(v) the wave momentum per unit surface area $\langle\underset{\sim}{M}\rangle$ is 1000kg $m^{-1}s^{-1}$. This represents a reasonable range of wave conditions from a 7m significant wave height in 50m of water with period 10 seconds and phase speed 15ms^{-1} to a 5m significant wave height in 10m of water with period 5 seconds and phase speed 7ms^{-1}. For comparison, the maximum value of

momentum calculated from the wave model spectra was 2.6 10^3 kg $m^{-1}s^{-1}$ for the WAM model at station 4 during the 4th WHIST storm.

The Coriolis parameter ($f_c = 2\Omega\sin\phi$, here ϕ = latitude) was chosen to be the value at 55°N i.e. $f_c = 1.2.10^{-4}$ rads.s^{-1}. The densities of water and air were taken to be, respectively, ρ = 1025 kg m^{-3} and ρ_a = 1.25 kg m^{-3}.

The three scenarios were:

(a) depth = 50m, grid size = 30km, A_H = 250 m^2 s^{-1};

(b) depth = 10m, grid size = 30km, A_H = 50 m^2 s^{-1}; and

(c) depth = 10m, grid size = 5km, A_H = 8 m^2 s^{-1}.

For case (a) the three radiation stress terms are three orders of magnitude smaller than the dominant terms in the equation of motion, such as the elevation gradient. For case (b) in shallower water, the difference is two orders of magnitude. Reducing the grid size in case (c) brings these terms within one order of magnitude of the dominant terms. Thus the radiation stress terms are likely to be important only in depths less than 10m, but the grid resolution could have a marked effect on the magnitude of these terms (as well as on the advective term) whereas the long-wave terms will not be substantially affected.

5.1.2 Surface stress

Time series of surface drag coefficient at the selected locations were computed by a method taking account of surface waves. For comparison, the original formula of Smith and Banke (equation 2.4) was used.

The method was derived from KITAIGORODSKII (1973). A roughness length related to the root mean square wave height is determined, and corrected for the motion of the roughness elements relative to the wind. The wind profile is assumed to take the classic logarithmic form in a frame of reference moving with the waves:

$$U(z) - c = \frac{u_*}{K} \ln\left(\frac{z}{z_o}\right) ,$$

which leads to

$$U(z) = \frac{u_*}{K} \ln\left(\frac{z}{z'_o}\right) = U_z , \qquad (5.1.3)$$

where

$$z'_o = z_o \exp\left(\frac{-Kc}{u_*}\right), \qquad (5.1.4)$$

or, substituting for u_* from equation (5.1.2),

$$z'_o = z_o \left(\frac{z}{z_o}\right)^{-c/(U_z - c)} . \qquad (5.1.5)$$

If z_o is related to the frequency spectrum of wave energy, $E(\omega)$ by

$$z_o = A_K \left[2\int_o^\infty E(\omega)d\omega\right]^{\frac{1}{2}} , \qquad (5.1.6)$$

then a first approximation to z'_o can be taken as

$$z'_o = A_K \left[2\int_o^\infty E(\omega)\left(\frac{z}{z_o}\right)^{-2c/(U_z-c)}d\omega\right]^{\frac{1}{2}} , \qquad (5.1.7)$$

using z_o from equation (5.1.6). The factor A_K was taken from KITAIGORODSKII (1973) to be $0.12\sqrt{2\pi}$. The drag coefficient, C_s, is then given by

$$C_s = \left[\frac{K}{\ln(z/z'_o)}\right]^2 . \qquad (5.1.8)$$

This gave too high a value for the drag coefficient throughout. The drag coefficient was therefore normalised by a factor 0.383, empirically derived to give the same mean stress in the central North Sea as the Smith and Banke formula (FLATHER & WOLF, 1986; Appendix).

A comparison of the drag coefficient calculated from equations (5.1.7) and (5.1.8) with that calculated from equation (2.4) for the M.O. wave spectra and the WAM spectra is shown in Fig. 5.3. The wave-modified coefficient follows the same basic trend as the Smith and Banke (SB) calculation, the wave height and hence z_o and C_s increasing with wind-speed. There are some systematic differences however. At the shallower locations (lower significant wave heights) the drag coefficient is slightly lower than the SB value, but at the deeper locations it is somewhat larger. There is a tendency for maximum enhancement of the drag coefficient to be obtained at the peaks in the time series, particularly early in the storm events. The WAM wave data give rather higher values of the drag coefficient than the M.O. data, mainly due to larger significant wave heights. The increase in C_s can be up to 50% over the SB values. This implies substantial increases in surface stress at the peak of the storm event.

The present formula (5.1.7) does not allow for any effect of the relative direction of wind and waves. Recent work by DONELAN (personal communication) suggests that a method for including the full directional information in calculations of the surface drag coefficient is feasible. Eventually it would be hoped to include the same input source function as used in the wave model to calculate the surface stress directly.

5.1.3 Bottom stress

Time series of the bottom drag coefficient are computed similarly, using different models for the bottom stress (all assuming a quadratic friction law). The original formula is (equation (2.5))

$$\underset{\sim}{\tau}_B = C_B \rho \underset{\sim}{u} |\underset{\sim}{u}| \ , \tag{5.1.9}$$

where C_B is assumed to take the constant value of 0.0025.
This has been used extensively for surge and tidal modelling.

The alternative bottom drag formulation is taken from CJ, with some modifications to allow the use of wave spectra, employing the following algorithm to calculate the coefficients C_{BC} and C_{BW} (equation (4.1.9)).

(1) Obtain the current friction factor for the case where there are no waves. We choose $C_{BC} = 0.005$ and derive an appropriate Nikuradse length scale, l_N, from the formula

$$l_N = 11h \exp(-K\sqrt{2/C_{BC}}). \tag{5.1.10}$$

(2) Compute parameter J from the model I formula (large roughness, low wave-current) in CJ:

$$J = \left\{ \frac{b\, u_{WBM}^2}{l_N^2\, \omega_a^2} \right\}^{1/3} , \tag{5.1.11}$$

where $b = 0.0747$, $\omega_a = \omega_p + \underset{\sim}{k}_p . \underset{\sim}{u}$, ω_p is the peak frequency of the bottom wave-current spectra,

and $$u_{WBM} = \left[\int_0^\infty \frac{\omega}{\sinh kh} \int_0^{2\pi} E(\omega,\theta)\, d\theta\, d\omega \right]^{\frac{1}{2}} . \tag{5.1.12}$$

(3) If $J \leq 3.47$, continue using model I, if not use model II. Calculate first approximation to C_{BW} (assuming no current).

Model I : $C_{BW} = \frac{2b}{J}$

Model II : $C_{BW} = \left[\frac{2K^2}{\ln(30KJ\exp(-2\xi))}\right]^2$, $(\xi = 0.5013)$ (5.1.13)

(4) Keeping C_{BC} constant, iterate the following calculations of σ,m,J and C_{BW}

until sufficient accuracy is obtained for C_{BW}:

$$\sigma = \frac{C_{BC}}{C_{BW}} \left(\frac{u_c}{u_{WBM}} \right)^2 , \tag{5.1.14}$$

$$m = \sqrt{1 + \sigma^2 + 2\sigma \left| \cos (\delta - \theta_p) \right|} , \tag{5.1.15}$$

where δ is the direction of the mean current velocity,
and θ_p is the direction of the waves (i.e. direction of the peak of the spectrum of wave-generated bottom currents),

$$J = \frac{u_{WBM}}{l_N \omega_a} \sqrt{m C_{BW}/2} , \tag{5.1.16}$$

$$\left.\begin{aligned} &\text{Model I} \quad : \quad C_{BW} = \frac{2bm}{J} \\ &\text{Model II} \quad : \quad C_{BW} = \frac{2K^2}{m[\ln(30Ke^{-2\xi}J)]^2} \end{aligned}\right\} \tag{5.1.17}$$

(5) The thickness of the wave boundary layer, Δ_w, the apparent roughness, l_A, and the current friction factor, C_{BC}, are then computed:

$$\left.\begin{aligned} &\text{Model I} \quad : \quad \Delta_w = r l_N \frac{\pi}{\sqrt{2}} \sqrt{bJ} \qquad (r = 0.450) \\ &\text{Model II} \quad : \quad \Delta_w = nKJl_N \qquad (n = 0.367) \end{aligned}\right\} \tag{5.1.18}$$

$$\left.\begin{aligned} &\text{Model I} \quad : \quad l_A = 30\Delta_w \exp\left[\frac{-K\Delta_w}{bl_N}\right]^{\sqrt{\sigma/m}} \\ &\text{Model II} \quad : \quad l_A = l_N \left[\frac{30\Delta w}{l_N}\right]^{1-\sqrt{\sigma/m}} \end{aligned}\right\} \tag{5.1.19}$$

$$C_{BC} = \frac{2K^2}{[\ln (11h/l_A]^2} \quad . \tag{5.1.20}$$

Steps (4) and (5) are repeated until sufficient accuracy is obtained for C_{BC}.

Some comparisons of the current friction factor for both wave models with the original value (C_B = 0.0025 = $C_{BC}/2$) are shown in Fig. 5.4. The two wave models give very similar results. In general, the current friction factor during the storms is about 50% higher than if there were no waves present. For the selected grid points, all in more than 20m of water, CJ model I seemed to be preferred (by their criterion), i.e. large bed roughness and low wave-current velocity. This might change somewhat if the Nikuradse length scale, l_N, were chosen independently rather than from equation (5.1.10) which makes it proportional to the depth in order to give a uniform quadratic friction coefficient. $l_N (=30z_o$, where z_o is a roughness length representative of the sea-bed) should depend upon the characteristics of the sea-bed.

Both the surface and bottom drag coefficients seem to be increased by the presence of waves, according to the models used. The important effect in the surge model will be the difference between the surface and bottom stresses, the net amount of driving force applied to the water, $\underset{\sim}{\tau}_S - \underset{\sim}{\tau}_B$. This is more difficult to determine without actually running the model since τ_B depends upon the current in a non-linear way. From the above calculations, the surface drag seems to be increased most in deep water while the bottom drag is increased most in shallow water, so the wave effects will not cancel out directly. Also, the surface drag is affected most by the short waves in an undeveloped sea, while the bottom drag is affected most by long waves and swell, so there will be some time lag between the two effects. Shown in Fig. 5.5 are (a) the surface stress, (b) the bottom stress and (c) the difference (surface-bottom stress) for the 5 points using the WAM model wave data only. The bottom stress is the total stress including tidal currents which may be seen to dominate in shallower locations, points 1 and 2. As already discussed, the waves increase surface and bottom drag, which is reflected in the stresses. The bottom stress is more important in the shallow areas where the bottom velocities are larger and the waves smaller. The surface stress dominates in the deeper water where bottom stress is much reduced. It must be remembered, however, that the stresses are more effective in shallow water since they are divided by depth in the momentum equation (2.1). The largest increases in surface stress are seen when there is a rapid change in wind direction, e.g. storm 5 at point 5, as the depression

passes over.

5.2 Effect of surges and tides on waves

5.2.1 Wave generation

The calculation of the surface stress requires the relative velocity between the wind and the current. The highest wind speeds encountered in a North Sea storm (e.g. WHIST storm, 1-2 February 1983) are of the order of $30ms^{-1}$ with associated depth-mean currents of the order of $1ms^{-1}$ in the shallower regions of the southern North Sea. Here, the water is well mixed vertically and the surface current will not differ very substantially from the depth-mean current. More generally, DAVIES & FLATHER (1987) give a surface current to wind speed ratio of the order of 2-3% in shallow water and 4-5% in deep water (the larger values are associated with larger shear in the near-surface current profile). These velocity values would give a change in the effective wind speed of up to 5% if the current and wind directions coincide. However the effect of vertical current shear has not been considered here and the average velocity over the depth of wave influence is probably more appropriate, say 3% of wind speed.

5.2.2 Wave propagation

The effects of surges and tides on wave propagation are expected to be most significant in shallow water where the current velocities and elevations are highest. The changes in the total water depth as a result of surge and tide are also more significant here. The Doppler shift of frequency, given by equation (4.2.2), as a result of waves travelling on a current, varies from as much as 10% of the apparent angular frequency of the waves to a stationary observer in the shallow water regions of the southern North Sea to less than 1% in deep water.

Part of the refraction problem has been dealt with in the M.O. model by GOLDING (1983) and GAO (1986) has put forward a scheme for inclusion in the WAM model. These include depth refraction by bottom topography only but the method should be the same for the full refraction by depth and currents.

An application of equations (4.2.4), (4.2.5) and (4.2.6) was made by BARBER (1949) to calculate the variation in period of waves arriving in SW England after crossing the Celtic Sea tidal stream. This work suggested that changes in

depth vary throughout the region of interest. Their highest values, of the order of 10^{-1} to 10^{-2}, are to be found on the edge of the continental shelf, whilst in the southern North Sea, off the English coast, the highest values, for the present model grid, are of the order of 10^{-4}. Investigation of the depth gradients with a more refined model grid (namely four times greater in each direction), revealed these gradients to be a factor of 10 or more greater in some areas of the southern North Sea. Clearly, the magnitude of the depth gradient terms is dependent upon the accuracy with which the model grid can resolve the bathymetry. Taking the example of a 5-second period wave of amplitude 1m the wave energy density is about 5000 J m^{-2}. For a depth gradient of 10m in 30km, i.e. 3.10^{-4}, in 20m of water depth the last term on the LHS of equation (4.2.20) has a magnitude of 0.03 Jm^{-2} s^{-1}, i.e. 5% of the estimated input source term. For longer waves the input source term is reduced and the depth refraction enhanced, e.g. for a 10-second wave with the other parameters fixed S_{in} = 0.20 Jm^{-2} s^{-1} while the depth refraction term becomes 0.07, i.e. 30% of S_{in}.

In addition to being affected by changes in bathymetry, waves are also refracted as a result of changes in tidal/surge elevation. Shown in Tables 5.5, 5.6 and 5.7 are the variations in wavenumber, wave group velocity and the maximum change in direction of the refracted waves, respectively, as a result of a change in water depth for a range of frequencies. The point chosen is point number 1 in the southern North Sea, with an undisturbed water depth of 20m. The depth range covers $\pm$2m tidal/surge elevation. This range was observed in the WHIST storm of 1-2 February 1983 and these elevation values lie well within extreme estimates (FLATHER, 1987). The frequency range covers the significant part of the spectrum (determined by observation of spectra predicted by the WAM and MO wave models) and the individual values correspond to the discrete values of the WAM model.

The lower frequency components of the spectrum are most affected by the change in water depth. For the wave parameters tabulated, there is a change of $\pm$5% about the undisturbed value for the elevation range $\pm$2m. The higher frequency components of the spectrum are progressively less affected by the tidal/surge elevations, as high frequency waves (shorter wavelengths) are effectively always in deep water. The influence of wave refraction as a result of tidal/surge elevation becomes progressively less significant as the undisturbed water depth increases and is negligible in the deepest parts of the North Sea.

The maximum change in direction of the waves as a result of refraction is

the apparent period of swell at about 18s period of up to ± 1 second could be produced due to crossing the tidal stream.

Ray tracking models (CAVALERI & RIZZOLI, 1981) are commonly used to predict the wave climate at a coastal location. Such models usually cover a small area of the coastal sea and can be used to predict the coastal conditions deriving input from a lower resolution operational wave model. These ray models need to account for refraction by the currents and localised effects such as diffraction and shoaling (TOWNEND & SOWELL, 1985). CHAO (1987) has used a ray model to predict the wave field in the Columbia River entrance on the west coast of the United States. His model incorporated current refraction as the interactions of waves and currents in this region have been found to be very important. VINCENT (1979) examined the interaction between waves and tidal currents in the southern North Sea. A tidal modulation in wave height of amplitude 25cm was observed, of which half could be explained by a simple model of tidal currents. The rest might be due to depth refraction which was not considered. ARANUVACHAPUN (1977) constructed refraction diagrams for the southern North Sea which show the marked effects of the sandbanks off Norfolk on ray paths.

It is possible to estimate the magnitude of the refraction terms in the wave energy equation (4.2.20) without solving it fully as part of surge and wave model calculations. For comparison the input source term S_{in} may be estimated, e.g. using the M.O. model form

$$S_{in} = \frac{1}{2}\rho g\,(X + YE(f,\theta)) \quad J\ m^{-2}\ s^{-2} \qquad (5.2.1)$$

from GOLDING (1983), where

$$X = \frac{6.10^{-8}}{2\pi f_{max}}\, U^2_{19.5} \cos^2(\theta - \Psi) \qquad \text{For } f = f_{max},\ |\theta - \Psi| < 90°$$

$$= 0 \qquad \text{otherwise ,}$$

and $$Y = 6.10^{-2}\, \frac{\rho a}{\rho}\, 2\pi f \left\{ \frac{U}{c} \cos(\theta - \Psi) - 1 \right\} \quad \text{if } \frac{U}{c}\cos(\theta - \Psi) > 1$$

$$= 0 \qquad \text{otherwise .}$$

Here f_{max} = 0.324 Hz, $U_{19.5}$ = wind-speed at 19.5m above sea surface, Ψ = wind direction. Using $U_{19.5} = 20 ms^{-1}$ and taking a wave amplitude of 1m and period 5 seconds in 20m of water depth would give $S_{in} = 0.76\ J\ m^{-2}\ s^{-1}$ (with no waves the energy input would be $0.06\ J\ m^{-2}\ s^{-1}$).

The term $\partial\omega_o/\partial D = \omega_o k/\sinh 2kD$ is of the order of $10^{-2} - 10^{-3}$ rads $m^{-1}\ s^{-1}$ in shallow water but tends to zero in deep water. The spatial gradients of

greatest for the swell components of the spectrum, with typical values of 2-2.5°. Such values are well below the present directional resolutions of both the wave models considered here (22.5° for the M.O. model and 30° for the WAM model).

Referring once again to the refraction equations (equations (4.2.4) - (4.2.6)), the temporal current velocity and surface elevation gradients are likely to be of the order of 10^{-5} (ms^{-2} and ms^{-1} respectively). The magnitudes of the remaining spatial gradients are dependent upon the resolution of the model grid, as before. For the present model grid, the highest velocity gradients in the southern North Sea are of the order of $10^{-5}s^{-1}$. Inserting these values in equation (4.2.20) leads to a change in over 1 hour of up to 2°. Taking a typical wave group velocity of $10ms^{-1}$ would mean the waves travel about 30km in 1 hour, i.e. about 1 grid box of the present surge model, and the surge and tidal currents obtained from that model could cause a change in wave direction of as much as 2° over that distance. Locally, the gradients of current will increase with the spatial resolution of the model until a resolution of the order of the tidal excursion is achieved (KOMEN & RIEPMA, 1981) so the effects may increase with increased model resolution.

The energy balance equation (4.2.20) may be integrated over all frequencies and directions, and using the dispersion relation (4.2.3), to give

$$\frac{d\langle Q\rangle}{dt} + \frac{1}{2}\rho g \underset{\sim}{\nabla}.\underset{\sim}{u} \int_0^\infty \left(1+\frac{kd}{\sinh 2kD}\right) \int_0^{2\pi} E \, d\theta \, df + \frac{1}{4}\rho g \int_0^\infty \left(1+\frac{2kD}{\sinh 2kD}\right) \int_0^{2\pi} \frac{\underset{\sim}{Ek}.(\underset{\sim}{k}.\underset{\sim}{\nabla})\underset{\sim}{u}}{k^2} \, d\theta \, df$$

$$+ \pi\rho g \int_0^\infty \left(\frac{\cosh kD - kD \sin kD}{kD \cosh kD + \sinh kD \cosh^2 kD}\right) \int_0^{2\pi} \underset{\sim}{Ek}.\underset{\sim}{\nabla}H \, d\theta \, df$$

$$= \frac{1}{2}\rho g \int_0^\infty \int_0^{2\pi} S \, d\theta \, df \quad , \qquad (5.2.2)$$

where $\langle Q\rangle = \frac{1}{2}\rho g \int_0^\infty \int_0^{2\pi} E \, d\theta \, df$ is the total energy density (Jm^{-2}). This equation was applied to the 6-hourly wave spectral data available from the M.O. model, together with the total water levels and currents from the surge and tide model, for the 40 day period at 4 stations (1, 3, 5 and 9), to produce time series of each of the terms. The nonlinear transfer terms and some of the refraction terms which move energy from one frequency band to another or change its

direction do not appear. Effects on individual spectral components can therefore be larger or smaller than the effect on the total energy. The source terms were calculated as in GOLDING (1983), i.e. including wind input, dissipation and bottom friction. The depth gradients at the selected stations were taken from the surge model. The results are shown in Fig. 5.6(a) and (b). Fig. 5.6(a) is a time series plot of the terms included in a wave model without interaction with tides and surges. The propagation term is

$$\frac{\partial \langle Q \rangle}{\partial t} + \frac{1}{2}\rho g \int_0^{\infty}\int_0^{2\pi} \underset{\sim}{c}_g . \nabla \underset{\sim}{E} \, d\theta \, df$$

and is mainly balanced by the source terms on the RHS of (5.2.2). The depth refraction term (with no tide and surge elevation) is not negligible however, except at point no. 3 where the depth gradient is zero. It is interesting to see that this term reaches its largest values at the deepest station. Point no. 9 is on the edge of the Norwegian trench in 175m of water and the depth gradients are of order 10^{-3}. During the storm events, long period waves of large amplitude are being refracted by the bottom topography at this station. Fig. 5.6(b) contains the interaction terms compared for reference with the depth refraction term and plotted on a larger scale. The current refraction plus radiation stress terms are of similar magnitude to the depth refraction at the shallower stations. Inclusion of the tide and surge elevation does not modify the depth refraction term significantly at the above stations. In less than 10m of water this may become important. The advection of the waves by tidal and surge currents is of about the same magnitude as the current refraction. Table 5.8 shows the mean absolute values of various terms over the whole period normalised with respect to the dissipation source term at the 4 stations. It would suggest that the modification of the waves by tide and surge currents could have a significant effect over the whole of the North Sea.

6. DISCUSSION

An important part of the interaction between waves and surges is in the surface stress. The atmospheric model, surge model and wave model all presently use empirical parameterizations of the momentum transfer between air and sea and ultimately these ought to be interlinked in a more sophisticated boundary layer model. However this is seen as a long term problem, and in the short term some improvement in the empirical formulae, making them more consistent with one

another, could be hoped for. The momentum transferred from the air to the long period motion in the sea is mostly through the intermediate stage of surface waves so the generation and dissipation of the waves is fundamental to the driving of the surge motion, and some preliminary calculations have shown that the stage of development of the waves can significantly modify the effective drag coefficient for the surge. There seems a great deal of scope for further investigation in this area, following up work being carried out in measurements of air-sea momentum transfer.

The bottom boundary layer is also treated empirically in the surge and wave models and there is much room for improvement. Again, preliminary calculations show that the drag coefficients can be substantially modified by interaction between surge and tide and waves. Unlike the surface stress which can be important in deep water, for waves at least, this will be most effective in shallow water.

The refraction of waves by tide and surge currents as well as water depth changes can be significant throughout the North Sea and its cumulative effect may result in modified wave predictions in the southern North Sea. Long period waves are particularly affected and calculations suggest that the large amplitude of long period wave energy generated in storm events in the North Atlantic may result in significant refraction at the continental shelf edge. Surge and tidal currents are much larger in shallow water but wave energy tends to be much less which counteracts this.

Parallel models of surge and tide and waves could be set up, incorporating the interaction terms, to examine the integrated effect of the terms whose magnitude has been discussed. The models would need to exchange data, say once per hour (simulation time). The wave model requires spatial gradients of current $\underset{\sim}{\nabla}.\underset{\sim}{u}$ and $\underset{\sim}{\nabla} \times \underset{\sim}{u}$ and total water level D at each grid-point. The surge model requires the total wave momentum $\langle \underset{\sim}{M} \rangle$ and momentum gradients $\underset{\sim}{\nabla}.\langle \underset{\sim}{M} \rangle$ plus the divergence of the integral $F = \int_0^\infty \int_0^{2\pi} E\ (1 - 2c_g/c)$ i.e. $\underset{\sim}{\nabla}F$, and a surface drag coefficient obtained from some integral of the wave spectrum. Also once per hour the surge/tide and wave bottom velocities would be used to obtain values of the bottom drag coefficient for each model. A hindcast period needs to be chosen with sufficient observed sea level, current and wave data to test the modified models, e.g. a WHIST storm.

An examination of wave data available, preferably with simultaneous current measurements is needed. It should be possible to see tidal modulation of wave height and relate this to the modification of wave propagation by tide and

surge. Detecting changes in generation and dissipation of waves may be more difficult and for this a good data set with detailed current and wave data at several locations over several storms would be required.

7. CONCLUSIONS AND RECOMMENDATIONS

(i) The various interactions between surface waves and long period motion, i.e. surge and tide, have been reviewed. There is sufficient theoretical work in existence to suggest that various interaction mechanisms could be usefully included in existing wave and surge models.

(ii) The most important effects of the waves on the surge and tide are in modifying the surface and bottom stresses. Transfer of momentum by radiation stresses is negligible except very near shore.

(iii) Advection and refraction of the wave field by surge and tidal currents may be important throughout the North Sea. The effects of surge and tide elevations on the waves will probably be small except in shallow water. The tide and surge currents will also introduce turbulence at the sea-bed, modifying the bottom friction felt by the waves. This type of wave dissipation is important in shallow water.

(iv) Surge and wave models incorporating the interaction effects should be run in parallel in hindcast mode for a small number of storm events, exchanging data at intervals of 1 hour, for example. Events must be selected with sufficient observational data for comparison; a WHIST storm might be suitable.

(v) The wave model should incorporate all the refraction terms and it is expected that improved directional resolution will be required, e.g. 10° initially. Development of a suitable numerical scheme is important.

(vi) The available observed wave and current data must be examined for interaction effects. Detection of the finer details may require a specifically designed observational exercise.

(vii) Near the coast, i.e. from about 10km offshore, a good prediction of sea level will probably require a more detailed local wave model, e.g. a ray-tracking model or a high spatial resolution spectral model, incorporating the coastal morphology. This would allow for the effects of shallow water wave breaking and set-up while the tide and surge conditions would effectively remain constant. The surge and tide levels could also be corrected for the coastal depth profile, possibly allowing for inundation of drying areas.

(viii) Some tuning of the combined wave and surge models may be required,

particularly with respect to the sea-bed roughness parameter which is common to both models.

(ix) Some experiments with a three-dimensional tide/surge model would be desirable to assess the influence of vertical current shear on the waves and provide better estimates of surface and bottom stress.

ACKNOWLEDGEMENTS

We wish to acknowledge helpful discussions with M. Donelan, G. Komen, P. Janssen J. Ewing and H. Tolman. Thanks are due to Mrs J. Campbell for preparing the diagrams and Mrs L. Parry and Mrs J. Huxley for typing the manuscript. The work was funded by the Ministry of Agriculture, Fisheries and Food.

APPENDIX - Influence of surface waves

For completeness, we reproduce and summarise here sections of two reports (FLATHER & WOLF, 1986 and WOLF & FLATHER, 1986) describing some earlier work examining the possible influence of surface waves on the sea surface drag coefficient and hence on storm surges. This work was funded by ESSO Exploration and Production U.K. Ltd. under contract EP007R.

A1 Introduction

The aim of the work was to investigate the possibility of using information on surface waves from a wave model to improve the estimation of wind-stress. The first part contains a review of methods which have been suggested in the literature. The next sections concern the application of a chosen method to the wave spectra to obtain wind-stress fields and then the use of these in the surge model. The results were compared with the results obtained by conventional methods for a 10-day period at the end of the first WHIST period i.e. 0z 31 January - 0z 10 February 1983.

A2 Literature review

The starting point of most work is the assumption that the velocity profile in a neutral atmospheric boundary layer obeys a logarithmic law (e.g. KITAIGORODSKII, 1973, p.11) so that

$$U(z) = \frac{u_*}{K} \ln\left(\frac{z}{z_o}\right) , \qquad (A1.1)$$

where $U(z)$ is the mean wind-speed at a height z above a stationary surface, u_* is the 'friction velocity', K is von Karman's constant and z_o is the roughness length. By definition the stress at the surface is

$$\tau = -\overline{\rho u'\omega'} = \rho u_*^2 = \rho C_S U^2(z) ,$$

where C_S is a drag coefficient relating the wind-stress and the wind speed at height z.

Hence $$C_S = \frac{u_*^2}{U^2(z)} = \left[\frac{K}{\ln(z/z_o)}\right]^2 \quad . \qquad (A2.2)$$

The problem of determining the drag coefficient becomes that of obtaining the roughness length z_o. The stress can be divided into 'skin friction' and 'form drag'. When the flow is fully turbulent (which is almost always the case over the sea) the form drag dominates and z_o is related to the size of the surface irregularities. Much experimental work has been done on measuring the wind-stress and mean velocity profile over the sea, and so determining the drag coefficient and roughness length directly e.g. see the review by GARRATT (1977). Form drag over land seems proportional to $U^2(z)$ but over water to $U^3(z)$ (MUNK, 1955). One wishes to relate C_S and z_o to known quantities such as the height of surface irregularities and the mean wind-speed. However there has been a large amount of scatter in the observed values of C_S. Three types of model seem to have emerged.

(i) The drag coefficient has been observed to increase approximately linearly with wind-speed, at least for intermediate wind-speeds, such that

$$C_S = 10^{-3}.(A + BU_{10}), \qquad (A2.3)$$

where U_{10} is the wind speed at 10m above the surface in ms^{-1}. Various values attributed to A and B by different workers are given in Table A1. However this empirical relationship does not allow for the stage of wave development and gives little information on the drag mechanism.

(ii) The roughness length has been related to the friction velocity squared

$$z_o = \frac{a_c U_*^2}{g}, \qquad (A2.4)$$

where g is the gravitational acceleration and a_c is a constant. This has been termed 'Charnock's relation' and was derived on dimensional grounds (CHARNOCK, 1955). However quite a large amount of variation in the 'constant' a_c has been determined, and again it does not allow explicitly for the surface waves. This formulation has been found to give similar agreement with experimental results to the linear drag law (WU, 1982). Some modifications to this method have been suggested e.g. including wave slope (HSU, 1974) or a dimensionless wave height allowing for wind drift and swell (MELVILLE, 1977).

(iii) The roughness length should be related to some length scale representative of the surface waves, in particular the significant wave height,

H. However the values of z_o which have been observed are much smaller than would be obtained from a stationary solid surface with the same shape (KITAIGORODSKII & VOLKOV, 1965). Two suggested reasons are either that the roughness length is more dependent on wave slope than on wave height e.g. MUNK (1955) or that some allowance must be made for the relative motion of the waves and the wind (KITAIGORODSKII & VOLKOV, 1965). The former gives a bias towards the high frequency waves which are shorter and hence steeper for the same amplitude than the low frequency waves, but which contribute less to the significant wave height. Assuming the equilibrium range form of the wave frequency spectrum $E(\omega)\alpha\omega^{-5}$ this method reduces to Charnock's relation (BYRNE, 1983) but if the waves are not in equilibrium with the wind a different result may be obtained. The simplest correction for wave mobility is to assume that the wind profile is the same in a frame of reference moving with the wave phase speed c as it would be over an equivalent stationary surface, i.e.

$$U(z) - c = \frac{u_*}{K} \ln \left(\frac{z}{z_o}\right), \qquad \text{(A2.5)}$$

(KITAIGORODSKII, 1973) so that

$$U(z) = \frac{u_*}{K} \ln \left(\frac{z}{z'_o}\right), \qquad \text{(A2.6)}$$

where

$$z'_o = z_o \exp(-Kc/u_*). \qquad \text{(A2.7)}$$

This implies that the faster the waves travel the more the effective roughness z'_o is reduced relative to that which would apply for a stationary surface, z_o. By the deep water dispersion relation

$$c = g/\omega \qquad \text{(A2.8)}$$

where is the wave frequency, so that the low frequency longer wavelength waves travel faster and contribute less to the roughness.

DONELAN (1982) has used these ideas to calculate a drag coefficient composed of two parts. The wave energy frequency spectrum is divided into a long wave part with frequencies up to twice the spectral peak frequency, ω_p, and a short wave part containing all the higher frequency energy. The longer waves are allowed to travel in an off-wind direction which has been observed to occur when the gradient of fetch with direction is large (DONELAN, 1980). Each part produces a drag coefficient which is corrected for an appropriate relative speed of wind and waves and then combined to give a single value of C_S.

There is some doubt as to what happens if the waves are travelling faster than

the wind or in opposition to it. TAYLOR & GENT (1978) use a numerical model of wind-stress which suggests that for waves travelling against the wind the drag is much larger than for waves travelling with the wind. However the DONELAN (1982) model breaks down when the waves are travelling at 90° to the wind direction. There is little observational evidence of this situation and it is unclear what effect swell might have on the roughness length.

A3 Wave spectral data

Wave data, for use in the investigation, were provided by the Meteorological Office from their wave models. The data were of two types (i) the full directional spectra, only available every 6 hours, and (ii) some integrated spectral parameters such as significant wave height, supplied every hour.

The integrated wave parameters are the total significant wave height and zero up-crossing period, the wind sea wave height and period and the swell height and principal period and direction. Also supplied are the wind speed and direction. By definition in the model the wind sea peak frequency may be determined from the wind sea wave height H_W and wind-speed U_{10}, i.e.

$$\omega_P = \left(\frac{10^{-4} + 7.10^{-4}.(\gamma - 1)E}{\bar{E}_W}\right)^{\frac{1}{4}}, \qquad \text{(A3.1)}$$

where $\bar{E}_W$ is the total energy of the wind-sea part of the spectrum. By definition of significant wave height (e.g. CARTER, 1982),

$$\bar{E}_W = \left(\frac{H_W}{4}\right)^2 .$$

Here, $$\gamma = 1.0 + 2.3\left\{1-\left(\frac{\bar{E}_W}{\bar{E}P_M}\right)^2\right\},$$

where the total energy of the Pierson-Moskowitz spectrum, E_{PM}, is given by

$$\bar{E}_{PM} = \left(\frac{U_{10}}{1.4g}\right)^4 .$$

ϵ is the peak width (= 0.08).

This frequency does not always coincide with the actual spectral peak in the full directional spectrum since the swell may contribute a large amount of energy at lower frequencies.

The directional spectra were supplied for 14 discrete frequency bands and 16 directions and stored on tape in a compact form. For each data time there was one record containing all the spectral data (224 numbers per grid-point) for each whole row of the model grid. These had to be decoded sequentially before performing any integration. The peak frequency ω_p of the spectrum was determined using wind-sea wave height selected from the integrated data in equation (A3.1).

A4 Comparison of different stress formulations

Various possible formulations for the drag coefficient were selected based on the literature survey.

(i) SMITH & BANKE (1975). The standard formulation of drag coefficient currently used in the shelf model was used as a basis for comparison

$$C_S = 10^{-3}.(0.63 + 0.066U_{10}) \quad . \tag{A4.1}$$

This will be termed method SB.

(ii) KITAIGORODSKII (1973). This relates the roughness length to the wave height modified by a factor dependent on the difference between the wind speed and wave phase speed, c (=g/ω),

$$z'_o = A_K\left[\, 2\int_o^\infty E(\omega)\exp\left(\frac{-2Kc}{u_*}\right)d\omega\right]^{\frac{1}{2}} \quad , \tag{A4.2}$$

where $E(\omega)$ is the wave energy frequency spectrum. The logarithmic wind profile is used to substitute for u_* giving

$$z'_o = A_K\left[2\int_o^\infty E(\omega)\left(\frac{z}{z_o}\right)^{-2c/(U_z-c)}d\omega\right]^{\frac{1}{2}} \quad ,$$

with U_z now the wind speed at height z where z_o is the immobile roughness length

$$z_o = A_K\left[2\int_o^\infty E(\omega)d\omega\right]^{\frac{1}{2}} = \frac{A_K H}{2\sqrt{2}} \quad , \tag{A4.3}$$

where H is the significant wave height (CARTER, 1982).

Then $C_S=[K/\ln(z/z_o)]^2$. A simplified formulation is

$$z'_o = z_o \left(\frac{z}{z_o}\right)^{-C_p/(U_z - C_p)} , \qquad (A4.4)$$

which only requires knowledge of the significant wave height and spectral peak frequency ω_p. This method will be called K1 and the full integration of the frequency spectrum weighted by a function of the local phase speed will be called K2. The parameter A is given by KITAIGORODSKII (1973) to be $0.12\sqrt{2\pi}$ for the K1 method. The same value is used in K2.

(iii) BYRNE (1983). This relates the roughness length to the wave slope so that

$$z_o = \frac{f_w}{2\pi g} \int_{\omega_1}^{\infty} E(\omega)\omega^2 \, d\omega \quad . \qquad (A4.5)$$

where $\omega_1=g/U_{10}$ i.e. limiting integration to the part of the spectrum with waves travelling slower than the wind-speed. Byrne states that f_w should lie between 0.1 and 1 but no value was recommended so f_w was arbitrarily chosen to be 1. This method is labelled B1. A modification of this method whereby the integral was weighted by the same factor as in K2 was also used,

i.e.

$$z'_o = \frac{f_w}{2\pi g} \int_{\omega_1}^{\infty} E(\omega)\omega^2 \left(\frac{z}{z_o}\right)^{-c/(U_z - c)} d\omega \quad . \qquad (A4.6)$$

which is called B2.

(iv) DONELAN (1982). Two roughness lengths are calculated;

$$\left.\begin{aligned} Z_{LW} &= A_o \left[\int_o^{2\omega p} E(\omega)\,d\omega\right]^{\frac{1}{2}} \\ Z_{SW} &= A_o \left[\int_{2\omega p}^{\infty} E(\omega)\,d\omega\right]^{\frac{1}{2}} \end{aligned}\right\} \qquad (A4.7)$$

A_o is determined empirically to be 1/80.

Two drag coefficients are then obtained

$$C_{LW} = \left[\frac{K}{\ln(z/z_{LW})}\right]^2 \frac{|\cos\theta|}{U^2_{10}} \left|U_{10} - \frac{0.83C_p}{\cos\theta}\right| \left\{ U_{10} - \frac{0.83C_p}{\cos\theta} \right\}$$

$$\} \qquad \text{(A4.8)}$$

$$C_{SW} = \left[\frac{K}{\ln(z/z_{SW})}\right]^2 \left\{\frac{U_{10} - 1.66C_p}{U_{10}}\right\}^2$$

where θ is the angle between the direction of the waves at the peak of the spectrum and the wind. The factor 0.83 is included since it is assumed that when $U_{10}/c_p = 0.83$ the spectrum is fully developed and the long waves contribute nothing to the total drag (DONELAN, 1982). Then

$$C_S = (C_{LW} + C_{SW})\ (0.07 + 0.2\ln Re_s)\ ,$$

where Re_s is a sea-state Reynolds' number allowing the drag coefficient to vary with the degree of whitecap coverage, $Re_s = U_{10}s/\nu$, with s the rms deviation of the sea surface and ν the kinematic viscosity of air. This will be called method D.

In all the above models it was assumed that the drag becomes zero whew the wave phase speed exceeds the wind speed (or $U_{10}/0.83$ for method D). Only the wind-sea part of the spectrum was included, defining the swell as all frequencies less than 0.8 of the wind-sea peak frequency and all directions further than 90° away from the wind direction.

A comparison of methods SB, K1, K2, B1, B2 and D was made at six locations marked on Fig. A1. Their positions are given in Table A2. They were selected to give a variety of wave climates for comparison. The last 10 days of the first data period were chosen i.e. 0z 31 Jan. - 0z 10 Feb. 1983. The wind stress magnitude at each position was calculated every 6 hours by the six methods. Method SB was taken to be the standard for comparison as it is well tested in surge models so that it presumably produces the right order of magnitude of stress. The initial comparisons are shown in Figures A2 to A4.

Figure A2 shows the two Kitaigorodskii methods K1 and K2 with SB. Method K1 gives about the same magnitude of stress as SB but K2 is generally much larger. This is due to the uncertainty in applying the same value of constant A in both K1 and K2. Figure A3 shows SB and B1 and B2. Both B1 and especially B2 give smaller values of stress than SB. Again f_w is not known but should be adjusted experimentally. Figure A4 shows SB and D which in general have the same order

of magnitude. In order to compare the stresses more fairly it was decided to normalise the values so that the time-averaged stress at the Central North Sea location in every case was equal to the SB value. This location has the largest values of wind-stress. The normalised stresses are plotted in Figures A5 to A7.

Examining the stress time series some general observations may be made:

(i) In Figure A5 both K1 and K2 enhance the peak stresses. K1 has a tendency to produce very low or zero stress after reaching a peak. This may reflect the stage of wave development in that the peak frequency tends to become lower as the duration of the wind increases so after the peak of the wind the waves will be travelling faster than the wind.

(ii) In Figure A6 models B1 and B2 seem to reproduce the results of SB very closely. The inclusion of the wave phase speed effect in B2 enhances the peak stress values slightly. The reason for the excellent agreement is that these models are heavily biassed towards the high frequency waves which have slow phase speeds and rapidly reach equilibrium with the wind. Thus the only effect of importance to the roughness length is that the wave height increases with wind-speed which is modelled adequately by SB.

(iii) In Figure A7 model D shows enhancement of peak stresses as in K1 and K2. There is also a tendency for the stresses to be larger for rising winds than for falling winds, presumably a similar effect to that in K1 where the long waves around the spectral peak start to travel faster than the wind and their contribution to the drag drops off.

Table A3 shows a summary of the normalised time-averaged stresses at the 6 points expressed as a percentage of the SB values, which show the differences between different regions and wave climates, for the 6 models. The normalisation factor which has been applied to each model to obtain figures A5-A7 from figures A2-A4 is also given. The most marked regional variation is at the coastal North Sea position. All the wave-related stress models give very low stress at that position. The reason is that the winds at that point are offshore for the first half of the time period so that no waves were generated in the wave model and hence these methods predict zero stress. Probably a small residual stress value representing skin friction should be included. This is discussed later in section A5. When the winds come round to being onshore the waves and stresses start to build up. As mentioned before the B1 and B2 stresses are fairly close to SB with little regional variation. The K1 stresses seem generally rather low, presumably because of their tendency to drop to zero when the wave phase speed exceeds the wind speed. The most interesting results

are from K2 and D. Both show a reduction of stress in the southern North Sea and the Celtic Sea relative to other sea areas, the maximum stresses being obtained in the Central North Sea. This is related to the fetch-limited conditions applying in the southern North Sea and Celtic Sea. When the waves reach full development their phase speeds are maximised and the stresses are rather reduced compared to a developing sea. Thus either of the methods K2 and D could be expected to give a different regional distribution of stress with enhanced maximum stresses compared to SB.

A5 Model simulation with wave-dependent wind-stress

On the basis of the results from A4 method K2 was selected for a full trial in the extended shelf model (CXX). The last ten days of the first WHIST period were selected as they contained a significant wind event incorporating a shift in wind direction. The period studied was thus from 0z 31 January 1983 - 0z 10 February 1983.

First, the arrays of wind-stress calculated by method K2, equation (A4.2), were calculated for the whole of the wave model fine-mesh, every six hours. This is a rather time-consuming process, since the wave spectra have to be integrated at every grid-point but a large proportion of the time was consumed by reading the tape. The process could be considerably streamlined. The wind-stresses were then interpolated onto the CXX grid. The wind-stresses were concatenated with those previously calculated using method SB for the first WHIST period, in order to fill in gaps where the wave model did not supply any information at a sea-model grid point. Finally the wind-stresses and pressure data were written in the form required for input to the sea-model. The met. data was only supplied every 6 hours instead of every 3 hours as in the original runs using the SB formulation.

The CXX model was run for the 10-day period, Run 4, using elevations and currents at 0z 31 January from a previous run as the initial conditions. Time series of residual elevations and currents were derived and compared with observations, and with results for the same period using the original wind-stress. Only slight differences in surge prediction appear. The wave-modified wind stress tends to consistently underpredict negative surge peaks at coastal stations e.g. Sheerness. There are similarly slight differences in the currents but it is very difficult to assess the overall effect of the wave modified stress from graphical comparison.

In order to try to quantify the effect some simple statistics were computed. In particular, the RMS error, standard deviation of the error (based on differences between computed and observed surges) and correlation coefficient were computed for solutions using the SB and wave-modified stresses. Linear regression analyses were also carried out. The results suggested that the wave-modified stresses produced some improvement at tide gauges in deep water, but gave less satisfactory results in shallower water. This may be partly due to the deficiency relating to negative surges produced by offshore winds or to an inappropriate normalisation factor.

A modification could be made to the wave-dependent wind-stress calculation to correct the predictions for offshore winds (Donelan, personal communication), hence presumably improving the prediction of negative surges. The problem is due to the wave model having a threshold for wave prediction whereas in reality there will always be some waves. Also the spatial discretization of the wave and sea models are rather different so that the model coastlines do not exactly coincide. It is suggested that empirical formulae (DONELAN, HAMILTON & HUI, 1985) could be used to predict a wave height for this fetch-limited case. Assuming the waves are travelling in the same direction as the wind, the ratio U_{10}/c_p is given by

$$U_{10}/c_p = 11.6\ \tilde{x}^{0.23}\ , \qquad \text{(A5.1)}$$

where $\tilde{x}$ is the non-dimensional fetch. $\tilde{x} = xg/U^2_{10}$ where x is the actual fetch in the upwind direction: x will be determined by the grid-size for a coastal grid-point. Then the integral of the wave spectrum $\bar{\zeta}^2$ is given by

$$\frac{\bar{\zeta}^2 g^2}{U^4_{10}} = 0.00274\ \left(\frac{U_{10}}{C_p}\right)^{-3.3}\ .$$

A parametric distribution of the spectral energy could then be applied e.g. that given by DONELAN, HAMILTON & HUI (1985) or the JONSWAP spectrum (CARTER, 1982), before the chosen method for calculating the drag coefficient was used.

In order to examine the differences between the two types of wind-stress some arrays of wind-stress and current vectors were plotted. Figures A8 and A9 show wind-stresses for two times, 12z 1 February 1983 and 18z 5 February 1983. In each case (a) shows the wave-modified wind-stress and (b) the differences between the wave-modified wind-stress and the original wind-stress. The latter shows the effect on the wind-stress to be quite large in some areas. In the

first example, 12z on 1 Feb. 83, the wind-stresses associated with the depression in the North Sea were enhanced except near the coast and also wind-stresses west of Ireland were much stronger, but in the southern North Sea, the Irish Sea and off NW Scotland the wind-stresses were reduced. At 18z on 5 Feb. 83 the winds are strongest off the west and north west of Britain. The wind-stresses are enhanced by the wave-modified drag formula in this area. In the North Sea the wind-stresses are generally reduced. So it may be seen that there are large spatial variations in stress produced by this new formulation of the drag coefficient.

The different stresses produce significantly different surge currents in some areas and at some times, as can be seen from Figure A10.

A6 Summary of conclusions

(i) The investigation of the effects of waves on the wind-stress showed that it is feasible to compute a wave-modified drag coefficient which differs significantly locally in time and space from the original formulaiton.

(ii) In general the inclusion of wave effects enhances the peak wind-stresses.

(iii) Fetch-limited sea areas produce lower wave-modified drag coefficients than open ocean locations.

(iv) The effect of wave-modified wind-stress on coastal surges is small except in offshore winds where the model must be adjusted to increase the drag to more realistic values.

(v) The wave-modified wind-stress has more effect on offshore currents than on coastal sea levels.

(vi) There is still an uncertainty in the magnitude of the wind-stress which has been arbitrarily normalised by equating the average magnitude of the wind-stress at one point in the northern North Sea by the two methods. If the wind-stress in the southern North Sea were taken as the standard this would increase the relative magnitude of the wave-modified wind-stress elsewhere.

(vii) There are some limitations in wave data arising because the Met. Office wave model constrains the waves to follow the wind very closely. More interesting effects may appear with data from a more sophisticated wave model which allowed a longer relaxation time for wave adjustment to sudden wind changes e.g. after the passage of atmospheric fronts.

(viii) Statistical analysis of surges computed using the wave-modified and original wind stress formulations showed some improvement at certain locations due to the influence of waves.

REFERENCES

ARANUVACHAPUN, S. 1977 Wave refraction in the southern North Sea.
Ocean Engineering, 4, 91-99.

BANKS, J.E. 1974 A mathematical model of a river-shallow sea system used to investigate tide, surge and their interaction in the Thames-Southern North Sea region.
Philosophical Transactions of the Royal Society of London, A, 275, 567-609.

BARBER, N.F. 1949 The behaviour of waves on tidal streams.
Proceedings of the Royal Society of London A, 198, 81-93.

BATTJES, J.A. 1974 Computation of set-up, longshore currents, run-up and overtopping due to wind-generated waves.
Delft University of Technology, Dept. of Civil Engineering, Communications on Hydraulics Report no. 74-2, 244pp.

BRETHERTON, F.P. & GARRETT, C.J.R. 1969 Wavetrains in inhomogeneous moving media.
Proceedings of the Royal Society of London, A, 302, 529-554.

BYRNE, H.M. 1983 The variation of the drag coefficient in the marine surface boundary layer due to temporal and spatial variations of the surface wind and sea state.
U.S. National Oceanic and Atmospheric Administration, Technical Memorandum ERL PMEL-49, 116pp.

CARTER, D.J.T. 1982 Estimation of wave spectra from wave height and period.
Institute of Oceanographic Sciences, Report, No. 135, 20pp.

CAVALERI, L. & RIZZOLI, P.M. 1981 Wind wave prediction in shallow water: theory and applications.
Journal of Geophysical Research, 86, 10961-10973.

CHAO, Y.Y. 1987 Forecasting wave conditions affected by currents and topography.
U.S. National Oceanic and Atmospheric Administration, Ocean Products Center, Technical Note, OPC Contribution No. 10, 11pp. (Unpublished Manuscript).

CHARNOCK, H. 1955 Wind stress on a water surface.
Quarterly Journal of the Royal Meteorological Society, 81, 639-640.

CHRISTOFFERSEN, J.B. & JONSSON, I.G. 1985 Bed friction and dissipation in a combined current and wave motion.
Ocean Engineering, 12, 387-423.

DAVIES, A.M. 1988 On extracting current profiles from vertically integrated numerical models.
Coastal Engineering (in press).

DAVIES, A.M. & FLATHER, R.A. 1987 Computing extreme meteorologically induced currents, with application to the north-west European continental shelf.
Continental Shelf Research, 7, 643-638.

DONELAN, M.A. 1979 On the fraction of wind momentum retained by waves.
pp.141-159 in, Marine Forecasting, (ed. J.C.J. Nihoul). Proceedings of the 10th International Liege Colloquium on Ocean Hydrodynamics, 1978.
Amsterdam: Elsevier. 493pp.

DONELAN, M.A. 1980 Similarity theory applied to the forecasting of wave heights, periods and directions.
Proceedings of the Canadian Coastal Conference 1980, 47-61.

DONELAN, M.A. 1982 The dependence of the aerodynamic drag coefficient on wave parameters.
pp. 381-387 in, First International Conference on Meteorology and Air/Sea Interaction of the Coastal Zone, May 10-14, 1982, The Hague, Netherlands. Preprints.
Massachusetts: American Meteorological Society. 404pp.

DONELAN, M.A., HAMILTON, J. & HUI, W.H. 1985 Directional spectra of wind-generated waves.
Philosophical Transactions of the Royal Society of London, A, 315, 509-562.

FLATHER, R.A. 1984 A numerical investigation of the storm surge of 31 January and 1 February 1953 in the North Sea.
Quarterly Journal of the Royal Meteorological Society, 110, 591-612.

FLATHER, R.A. 1987 Estimates of extreme conditions of tide and surge using a numerical model of the north-west European continental shelf.
Estuarine, Coastal and Shelf Science, 24, 69-93.

FLATHER, R.A. & WOLF, J. 1986 Storm surge current and wave effect investigation - Phase 1.
Institute of Oceanographic Sciences, Internal Document, No 254 (3 vols) (unpublished manuscript).

GADD, A.J. 1985 The 15-level weather prediction model.
Meteorological Magazine, 114, 222-226.

GAO, Q.D. 1986 Extension of the 3rd generation ocean wave model with refraction.
Koninklijk Nederlands Meteorologisch Instituut, Wetenschappelijke Rapporten, WR-86-5, 9pp. & figs.

GARRATT, J.R. 1977 Review of drag coefficients over oceans and continents.
Monthly Weather Review, 105, 915-929.

GEERNAERI, G.L., KATSAROS, K.B. & RICHTER, K. 1986 Variation of the drag coefficient and its dependence on sea state.
Journal of Geophysical Research, 91, 7667-7679.

GOLDING, B. 1983 A wave prediction system for real-time sea state forecasting.
Quarterly Journal of the Royal Meteorological Society, 109, 393-416.

GRANT, W.D. & MADSEN, O.S. 1979 Combined wave and current interaction with a rough bottom.
Journal of Geophysical Research, 84, 1797-1808.

HASSELMANN, K. 1974 On the spectral dissipation of ocean waves due to white-capping.
Boundary-Layer Meteorology, 6, 107-125.

HASSELMANN, K., BARNETT, T.P., BOUWS, E., CARLSON, H., CARTWRIGHT, D.E., ENKE, K., EWING, J.A., GIENAPP, H., HASSELMANN, D.E., KRUSEMAN, P., MEERBURG, A., MULLER, P., OLBERS, D.J., RICHTER, K., SELL, W. & WALDEN, H. 1973 Measurements of wind-wave growth and swell-decay during the Joint North Sea Wave Project (JONSWAP).
Deutsche Hydrographische Zeitschrift Erganzungsheft, A, No. 12, 95pp.

HASSELMANN, S. & HASSELMANN, K. 1985 Computations and parameterizations of the nonlinear energy transfer in a gravity-wave spectrum. Part 1: A new method for efficient computations of the exact nonlinear transfer integral.
Journal of Physical Oceanography, 15, 1369-1377.

HEAPS, N.S. 1983 Storm surges, 1967-1982.
Geophysical Journal of the Royal Astronomical Society, 74, 331-376.

HSU, S.A. 1974 A dynamic roughness equation and its application to wind stress determination at the air-sea interface.
Journal of Physical Oceanography, 4, 116-120.

JAMES, I.D. 1983 The effects of wind waves on sea level at the coast.
Institute of Oceanographic Sciences, Report, No. 155, 66pp.

KING, H.L., DAVIES, A.G. & SOULSBY, R.L. 1985 A numerical model of the turbulent boundary layer beneath surface waves and tides.
Institute of Oceanographic Sciences, Report, No. 196, 90pp.

KINSMAN, B. 1965 Wind waves : their generation and propagation on the ocean surface.
Englewood Cliffs, N.J.: Prentice-Hall. 676pp

KITAIGORODSKII, S.A. 1973 The physics of air-sea interaction.
Jerusalem: Israel program for scientific translations, 237pp.

KITAIGORODSKII, S.A. & VOLKOV, Y.A. 1965 On the roughness parameter of the sea surface and the calculation of momentum flux in the near-water layer of the atmosphere.
Izvestiya Atmospheric and Oceanic Physics, 1, 973-988.

KOMEN, G.J. 1986 Activities of the WAM (Wave Modelling) Group.
pp.121-127 in, Advances in underwater technology and offshore engineering, Volume 6: Oceanology.
London: Graham & Trotman for the Society for Underwater Technology. 486pp.

KOMEN, G.J. & RIEPMA, H.W. 1981 Residual vorticity induced by the action of tidal currents in combination with bottom topography in the Southern Bight of the North Sea.
Geophysical and Astrophysical Fluid Dynamics, 18, 93-110.

LeBLOND, P.H. & MYSAK, L.A. 1978 Waves in the ocean.
Amsterdam: Elsevier. 602pp.

LONGUET-HIGGINS, M.S. & STEWART, R.W. 1964 Radiation stresses in water waves; a physical discussion with applications.
Deep-Sea Research, 11A, 529-562.

MELVILLE, W.K. 1977 Wind stress and roughness length over breaking waves.
Journal of Physical Oceanography, 7, 702-710.

MINISTRY OF AGRICULTURE, FISHERIES & FOOD. 1985 Report of the Research Consultative Committee on Flood Protection.
London: Ministry of Agriculture, Fisheries & Food. 88pp.

MUNK, W. 1955 Wind stress on water: an hypothesis.
Quarterly Journal of the Royal Meteorological Society, 81, 320-332.

MURTY, T.S. 1984 Storm surges - meteorological ocean tides.
Canadian Bulletin of Fisheries and Aquatic Sciences, 212, 897pp.

PEREGRINE, D.H. & JONSSON, I.G. 1983 Interaction of waves and currents. U.S. Army, Corps of Engineers, Coastal Engineering Research Center, Fort Belvoir, Va., Miscellaneous Report No. 83-6, 88pp.

PHILLIPS, O.M. 1977 The dynamics of the upper ocean. Cambridge University Press. 336pp.

PROCTOR, R. & FLATHER, R.A. 1983 Routine storm surge forecasting using numerical models: procedures and computer programs for use on the CDC CYBER 205E at the British Meteorological Office. Institute of Oceanographic Sciences, Report, No. 167, 171pp.

SMITH, S.D. & BANKE, E.G. 1975 Variation of the sea surface drag coefficient with wind speed. Quarterly Journal of the Royal Meteorological Society, 101, 665-673.

SNYDER, R.L., DOBSON, F.W., ELLIOT, J.A. & LONG, R.B. 1981 Array measurements of atmospheric pressure fluctuations above surface gravity waves. Journal of Fluid Mechanics, 102, 1-59.

SROKOSZ, M.A. 1985 Wave-current interactions: a review of some problems. Institute of Oceanographic Sciences, Report, No. 212, 34pp.

SWAMP GROUP. 1985 Ocean wave modelling. Principal results of a wave model intercomparison study conducted by the Sea Wave Modelling Project (SWAMP) and first presented at a symposium on Wave Dynamics and Radio Probing of the Ocean Surface, May 13-20 1981, Miami, Florida. New York: Plenum. 256pp.

TAYLOR, P.A. & GENT, P.R. 1978 A numerical investigation of variations in the drag coefficient for air flow above water waves. Quarterly Journal of the Royal Meteorological Society, 104, 979-988.

TOWNEND, I.M. & SAVELL, I.A. 1985 The application of ray methods to wave refraction studies. pp. 137-164 in, Offshore and coastal modelling, (ed. P.P.G. Dyke, A.O. Moscardini & E.H. Robson). (Proceedings of the seventh POLYMODEL Conference held Sunderland Polytechnic, May 1984.) New York: Springer-Verlag. 399pp. (Lecture Notes on Coastal and Estuarine Studies, 12.)

VINCENT, C.E. 1979 The interaction of wind-generated sea waves with tidal currents. Journal of Physical Oceanography, 9, 748-755.

WOLF, J. & FLATHER, R.A. 1986 Storm surge current and wave effect investigation - Phase 2.
Institute of Oceanographic Sciences, Internal Document, No. 267 (unpublished manuscript).

WU, J. 1982 Wind stress coefficients over sea surface from breeze to hurricane.
Journal of Geophysical Research, 87, 9704-9706.

YOO, D. & O'CONNOR, B.A. 1987 Bed friction model of wave-current interacted flow.
ASCZ Delaware Conference 1987 on Coastal Hydrodynamics (in press).

LIST OF SYMBOLS

A	constant in surface drag coefficient expression
A_D	empirical constant in Donelan's surface drag coefficient model
A_H	horizontal eddy viscosity coefficient ($m^2 s^{-1}$)
A_K	coefficient in surface drag formulation = $0.12\sqrt{2\pi A}$
A_S	empirical constant in expression for near-shore set-up
a	wave amplitude (m)
a_c	Charnock's constant
B	constant in surface drag coefficient expression
b	constant in bottom drag coefficient model = 0.0747
C_S, C_B	surface/bottom drag coefficients
C_{BC}, C_{BW}	friction coefficients in bottom drag coefficient model
C_{LW}, C_{SW}	long wave/short wave surface drag coefficients
$\underset{\sim}{c}, \underset{\sim}{c}_g$	wave phase velocity, wave group velocity (ms^{-1})
c, c_g	wave phase speed, wave group speed (ms^{-1})
D	total depth of water (m) = $h + \zeta$
$E=E(f,\theta)$	(wave energy density spectrum)/$\frac{1}{2}\rho g$ (M^2 radians^{-1}Hz^{-1})
$\bar{E}_W, \bar{E}_{PM}$	total wave energy in wind sea spectrum/Pierson-Moskowitz spectrum (m^2 radians^{-1}Hz^{-1})
f	wave frequency (Hz)
f_c	Coriolis parameter (= $2\Omega\sin\phi$)
f_w	parameter in Byrne's surface drag coefficient model
g	gravitational acceleration = 9.81 (ms^{-2})
H	significant wave height (m)
h	undisturbed water depth (m)
J	parameter in bottom drag coefficient model
K	von Karman's constant = 0.4
$\underset{\sim}{k}$	wavenumber (radians m^{-1}), $k = \lvert\underset{\sim}{k}\rvert$
l_A	apparent roughness parameter in bottom drag coefficient model (m)
l_N	Nikuradse length scale (m)
$\langle\underset{\sim}{M}\rangle$	average momentum of the waves per unit area of the sea surface ($kgm^{-1}s^{-1}$)
m	parameter in bottom drag coefficient model
$N(\underset{\sim}{k})$	wave-action density wavenumber spectrum (m^4s radians^{-4})
n	constant in bottom drag coefficient model = 0.367
p_a	atmospheric pressure (Nm^{-2})

LIST OF SYMBOLS (continued)

$\langle Q \rangle$	spatial wave energy density = wave energy per unit area of sea surface ($J\ m^{-2}$)
$R_{xx}, R_{xy}, R_{yz}, R_{yy}$	radiation stresses ($J\ m^{-2}$)
Re_s	sea-state Reynolds number
r	constant in bottom drag coefficient model = 0.450
S	net source function in wave model ($m^2 radians^{-1}$)
S_{ds}	dissipation of wave energy by wave breaking and bottom friction (m^2 $radians^{-1}$)
S_{in}	energy input to the waves from the wind (m^2 $radians^{-1}$)
S_{nl}	re-distribution of energy within the wave spectrum by non-linear interactions (m^2 $radians^{-1}$)
t	time (s)
$\underset{\sim}{U}, \underset{\sim}{U}(z), \underset{\sim}{U}_z$	wind velocity at a height z above the sea surface (ms^{-1})
$U, U(z), U_z$	wind speed at a height z above the sea surface (ms^{-1})
$\underset{\sim}{u}$	depth-averaged current velocity vector (ms^{-1}) = (u,v)
$\langle \underset{\sim}{u} \rangle$	mean sea-bed wave velocity (ms^{-1})
u_M	equivalent depth-averaged mean flow induced by waves (ms^{-1})
$\underset{\sim}{u}_{WBM}$	wave-particle current just outside the wave boundary layer (ms^{-1})
u_*	friction velocity (ms^{-1})
w	vertical current velocity component (ms^{-1})
X	linear term in M.O. model wind input source term (m^2 $radians^{-1}$)
$\underset{\sim}{x}$	position vector (m) = (x,y)
$\tilde{x}$	dimensionless fetch
Y	non-linear term in M.O. model wind input source term (s^{-1})
z	vertical dimension, positive upwards, origin sea surface (m)
$z_o, z_o', z_{LW}, z_{SW}$	roughness length (m)
α	integral wave steepness parameter
α_{PM}	theoretical value of integral wave steepness parameter for Pierson-Moskowitz spectrum
β	constant in wind input source function
$\underset{\sim}{\Gamma}$	extra terms in momentum equation due to wave action (kgm^{-1} s^{-2})
γ	coefficient in definition of wind sea peak frequency
Δ_W	thickness of wave boundary layer (m)
δ	mean current velocity direction (radians)
δA	element in wavenumber space ($radians^2$ m^{-1})

LIST OF SYMBOLS (continued)

ε	peak width in definition of wind sea peak frequency
ζ	sea surface elevation (m)
$\bar{\zeta}$	change in mean sea level (set-up) (m)
θ	wave direction (radians)
θ_p	direction of peak of bottom wave spectrum (radians)
λ	wavelength (m)
ξ	constant in bottom drag coefficient model = 0.5013
ρ, ρ_a	density of sea water, density and air (kg m^{-3})
σ	parameter in bottom drag coefficient model
$\underset{\sim}{\tau}_S, \underset{\sim}{\tau}_B$	surface/bottom stress (N m^{-2})
$\underset{\sim}{\tau}_{BC}, \underset{\sim}{\tau}_{BW}$	mean flow/wave bottom stresses (N m^{-2})
ϕ	latitude (°N)
ϕ_1	constant in wave dissipation source term = 0.005
ψ	wind direction (radians)
$\underset{\sim}{\Omega}$	planetary angular velocity (radians s^{-1})
ω	angular frequency of waves (radians s^{-1}) = 'apparent' frequency
$\bar{\omega}$	mean frequency of waves
ν	kinematic viscosity of air (m^2 s^{-1})
μ	vertical eddy viscosity (kg m^{-1} s^{-1})

SUBSCRIPTS (unless otherwise defined)

o	denotes a quantity in the co-ordinate system moving with the current, u
P	denotes a quantity corresponding to the peak frequency of the wave spectrum

LIST OF TABLES

5.1 WHIST storms

5.2 Comparison points for wave model data

5.3 Wave set-up

5.4 Order of magnitude of terms in equation of motion

5.5 Changes in wavenumber (m^{-1}) for a range of frequencies as a result of changes in water depth

5.6 Changes in wave group velocity (ms^{-1}) for a range of frequencies as a result of changes in water depth

5.7 Changes in water direction (degrees) for a range of frequencies as a result of changes in water depth

5.8 Wave energy budget

A.1 Coefficients A and B in equation A2.3

A.2 Locations chosen for comparisons of wind-stress

A.3 Comparison of time-averaged wind stress obtained by 6 models at 6 locations.

TABLE 5.1 WHIST Storms

Storm no.	Start time	End time	No. of 3h values
1	3z 03/01/83	0z 05/01/83	16
2	3z 06/01/83	0z 08/01/83	16
3	3z 09/01/83	0z 11/01/83	16
4	3z 18/01/83	0z 20/01/83	16
5	3z 01/02/83	0z 03/02/83	16

TABLE 5.2 Comparison Points

Point no.	Location	Station	Water depth (m)	Selected points
1	52.0°N 3.6°E	Euro	20	*
2	52.6°N 4.1°E	Ijmuiden	20	
3	53.2°N 3.2°E	K13	31	*
4	54.7°N 7.2°E	FPN	34	*
5	56.5°N 3.2°E	Ekofisk	74	*
6	59.3°N 4.8°E	Utsira	201	
7	61.0°N 1.5°E	Brent	140	
8	61.2°N 1.2°E	North Cormorant	150	
9	61.3°N 1.9°E	Statfjord	175	*
10	65.0°N 7.5°E	Haltenbanken	265	
11	66.3°N 9.5°E	Traenebanken	240	

TABLE 5.3 Wave Set-up (m)

For Wave-period = 10 second

Water depth (m)	Wave height (m) 1	2	3	4	5	6
1	-0.06	0	0	0	0	0
2	-0.03	-0.12	0	0	0	0
3	-0.02	-0.08	-0.17	0	0	0
4	-0.01	-0.06	-0.13	-0.22	0	0
5	-0.01	-0.04	-0.10	-0.17	-0.27	0
6	-0.01	-0.03	-0.08	-0.14	-0.22	-0.32
7	-0.01	-0.02	-0.07	-0.12	-0.18	-0.26
8	-0.01	-0.02	-0.06	-0.10	-0.16	-0.22
9	-0.01	-0.02	-0.05	-0.09	-0.13	-0.19
10	0	-0.02	-0.04	-0.07	-0.12	-0.17
12	0	-0.01	-0.03	-0.06	-0.09	-0.13
14	0	-0.01	-0.03	-0.05	-0.07	-0.11
16	0	-0.01	-0.02	-0.04	-0.06	-0.09
18	0	-0.01	-0.02	-0.03	-0.05	-0.07
20	0	-0.01	-0.01	-0.03	-0.04	-0.06

For wave-period = 5 seconds

Water depth (m)	Wave height (m) 1	2	3	4	5	6
1	-0.06	0	0	0	0	0
2	-0.02	-0.10	0	0	0	0
3	-0.01	-0.06	-0.13	0	0	0
4	-0.01	-0.04	-0.09	-0.15	0	0
5	-0.01	-0.03	-0.06	-0.11	-0.17	0
6	0	-0.02	-0.04	-0.08	-0.12	-0.17
7	0	-0.01	-0.03	-0.06	-0.09	-0.12
8	0	-0.01	-0.02	-0.04	-0.06	-0.09
9	0	-0.01	-0.02	-0.03	-0.05	-0.07
10	0	-0.01	-0.01	-0.02	-0.03	-0.05
12	0	0	-0.01	-0.01	-0.02	-0.03
14	0	0	0	-0.01	-0.01	-0.01
16	0	0	0	0	-0.01	-0.01
18	0	0	0	0	0	0
20	0	0	0	0	0	0

TABLE 5.4 Order of magnitude of terms in the equation of motion

	(a) Depth = 50m Grid size = 30km	(b) Depth = 10m Grid size = 30km	(c) Depth = 10m Grid size = 5km
$\frac{\partial \underset{\sim}{u}}{\partial t}$	$O(10^{-4})$	$O(10^{-4})$	$O(10^{-4})$
$\underset{\sim}{u}.\nabla\underset{\sim}{u}$	$O(10^{-5})$	$O(10^{-5})$	$O(10^{-4})$
$2\underset{\sim}{\Omega}x\underset{\sim}{u}$	$O(10^{-4})$	$O(10^{-4})$	$O(10^{-4})$
$g\nabla\zeta$	$O(10^{-4})$	$O(10^{-4})$	$O(10^{-4})$
$\frac{1}{\rho}\nabla p_a$	$O(10^{-6})$	$O(10^{-6})$	$O(10^{-6})$
$\frac{\underset{\sim}{\tau}_S}{\rho D}$	$O(10^{-5})$	$O(10^{-4})$	$O(10^{-4})$
$\frac{\underset{\sim}{\tau}_S}{\rho D}$	$O(10^{-5})$	$O(10^{-4})$	$O(10^{-4})$
$A_H\nabla^2\underset{\sim}{u}$	$O(10^{-7})$	$O(10^{-8})$	$O(10^{-7})$
$\frac{\nabla\{(\underset{\sim}{c} - 2\underset{\sim}{c}_g).\langle\underset{\sim}{M}\rangle\}}{2\rho D}$	$O(10^{-7})$	$O(10^{-6})$	$O(10^{-5})$
$\frac{\underset{\sim}{u}\nabla.\langle\underset{\sim}{M}\rangle}{\rho D}$	$O(10^{-7})$	$O(10^{-6})$	$O(10^{-5})$
$\frac{\langle\underset{\sim}{M}\rangle x\nabla x\underset{\sim}{u}}{\rho D}$	$O(10^{-7})$	$O(10^{-6})$	$O(10^{-5})$

Frequency (Hz) / Depth (m)	0.0673	0.0740	0.0814	0.0895	0.0985	0.1083	0.1192	0.1311	0.1442	0.1586	0.1745
18	0.0336	0.0374	0.0419	0.0469	0.0528	0.0597	0.0680	0.0780	0.0904	0.105	0.125
19	0.0328	0.0366	0.0409	0.0459	0.0517	0.0587	0.0670	0.0770	0.0895	0.105	0.124
20	0.0321	0.0358	0.0401	0.0450	0.0508	0.0577	0.0660	0.0761	0.0887	0.104	0.124
21	0.0314	0.0351	0.0393	0.0442	0.0499	0.0568	0.0651	0.0753	0.0880	0.130	0.124
22	0.0308	0.0344	0.0386	0.0434	0.0492	0.0560	0.0644	0.0746	0.0874	0.103	0.123

TABLE 5.5 Changes in wavenumber (m^{-1}) for a range of frequencies as a result of changes in water depth

Frequency (Hz) / Depth (m)	0.0673	0.0740	0.0814	0.0895	0.0985	0.1083	0.1192	0.1311	0.1442	0.1586	0.1745
18	11.25	10.86	10.40	9.88	9.27	8.60	7.85	7.07	6.27	5.52	4.82
19	11.46	11.04	10.54	9.98	9.34	8.62	7.84	7.03	6.21	5.46	4.77
20	11.46	11.19	10.67	10.07	9.39	8.64	7.82	6.99	6.15	5.40	4.72
21	11.82	11.34	10.78	10.15	9.43	8.64	7.80	6.94	6.10	5.35	4.68
22	11.99	11.48	10.88	10.22	9.46	8.64	7.77	6.89	6.04	5.30	4.65

TABLE 5.6 Changes in wave group velocity (ms^{-1}) for a range of frequencies as a result of changes in water depth

Frequency (Hz) / Depth (m)	0.0673	0.0740	0.0814	0.0895	0.0985	0.1083	0.1192	0.1311	0.1442	0.1586	0.1745
18	2.59	2.51	2.41	2.28	2.13	1.94	1.71	1.43	1.11	0.78	0.47
19	1.27	1.23	1.18	1.11	1.04	0.94	0.82	0.68	0.52	0.36	0.21
20	-	-	-	-	-	-	-	-	-	-	-
21	1.22	1.18	1.13	1.06	0.98	0.88	0.76	0.61	0.46	0.30	0.17
22	2.41	2.32	2.21	2.07	1.91	1.70	1.45	1.17	0.86	0.56	0.30

TABLE 5.7 Changes in wave direction (degrees) for a range of frequencies as a result of changes in water depth

TABLE 5.8 Wave energy budget

Point No.	1	3	5	9
$\frac{\partial \langle Q \rangle}{\partial t}$	2.12	1.42	1.93	1.94
$\underset{\sim}{u}.\underset{\sim}{\nabla}\langle Q \rangle$	0.31	0.14	0.04	0.03
$\frac{1}{2}\rho g \int\int \underset{\sim}{c}_g.\underset{\sim}{\nabla}E$	2.66	2.66	2.33	2.12
Current refraction + radiation stress	0.34	0.19	0.09	0.13
Depth refraction	0.69	0.003	0.21	0.32
Input source term	3.23	3.82	2.58	1.47
Bottom friction	1.48	0.55	0.16	0.03
Dissipation source term	1.00	1.00	1.00	1.00

LIST OF FIGURES

Figure 2.1 Grid of sea model CSX showing pressure points (X) of M.O. 15 level atmospheric model.

Figure 2.2 Finite difference grid of the extended continental shelf sea model, CXX.

Figure 5.1 CXX grid with the M.O. fine mesh wave model (X) showing locations of WAM wave model data (o).

Figure 5.2
(a) Elevation time series from CXX, days 1-40 1983
(b) East component of current CXX, " " 1983
(c) North component of current CXX, " " 1983
(d) Custer diagram of wind velocity for WHIST storm
(e) WAM directional wave spectra at 6Z 1 February 1983 and 12Z 1 February 1983 at point no. 5
(f) M.O. and WAM directional wave spectra at 12Z 1 February 1983 at point no. 4
(g) Significant wave height time series for WHIST storms
——— M.O. X WAM

Figure 5.3
(a) Surface drag coefficient, M.O. waves
——— Smith & Banke x Kitaigorodskii
(b) Surface drag coefficient, WAM waves
——— Smith & Banke x Kitaigorodskii

Figure 5.4 Bottom drag coefficient

Figure 5.5
(a) Surface stress (N/m^2)
(b) Bottom stress
(c) Surface stress - Bottom stress

Figure 5.6 (a) Time series of terms in wave energy equation.

Figure 5.6 (b) Time series of terms in wave energy equation.

Figure A1 CXX grid with the fine mesh wave model plus locations used for comparisons of wind-stress.

Figure A2 Comparison of wind-stress at six locations from methods SB, B1 and B2.

Figure A3 Comparison of wind-stress at six locations from methods SB, B1 and B2.

Figure A4 Comparison of wind-stress at six locations for methods SB and D.

Figure A5 As A2 but with wave-modified wind-stress normalised.

Figure A6 As A3 but with wave-modified wind-stress normalised.

Figure A7 As A4 but with wave-modified wind-stress normalised.

Figure A8 (a) Spatial array of wind-stress vectors computed with wave-modified drag coefficient.
12Z 1 February 1983.

Figure A8 (b) Spatial arrays of differences between the wave-modified wind-stress and the original wind-stress.
12Z 1 February 1983.

Figure A9 (a) Spatial array of wind-stress vectors computed with wave-modified drage coefficient.
18Z 5 February 1983.

Figure A9 (b) Spatial arrays of differences between the wave-modified wind stress and the original wind-stress.
18Z 5 February 1983.

Figure A10 (a) Spatial arrays of residual currents computed with original wind-stress, 12Z 1 February 1983.
(b) Spatial arrays of differences in residual currents between wave-modified wind-stress case and original wind-stress case, 12Z 1 February 1983.

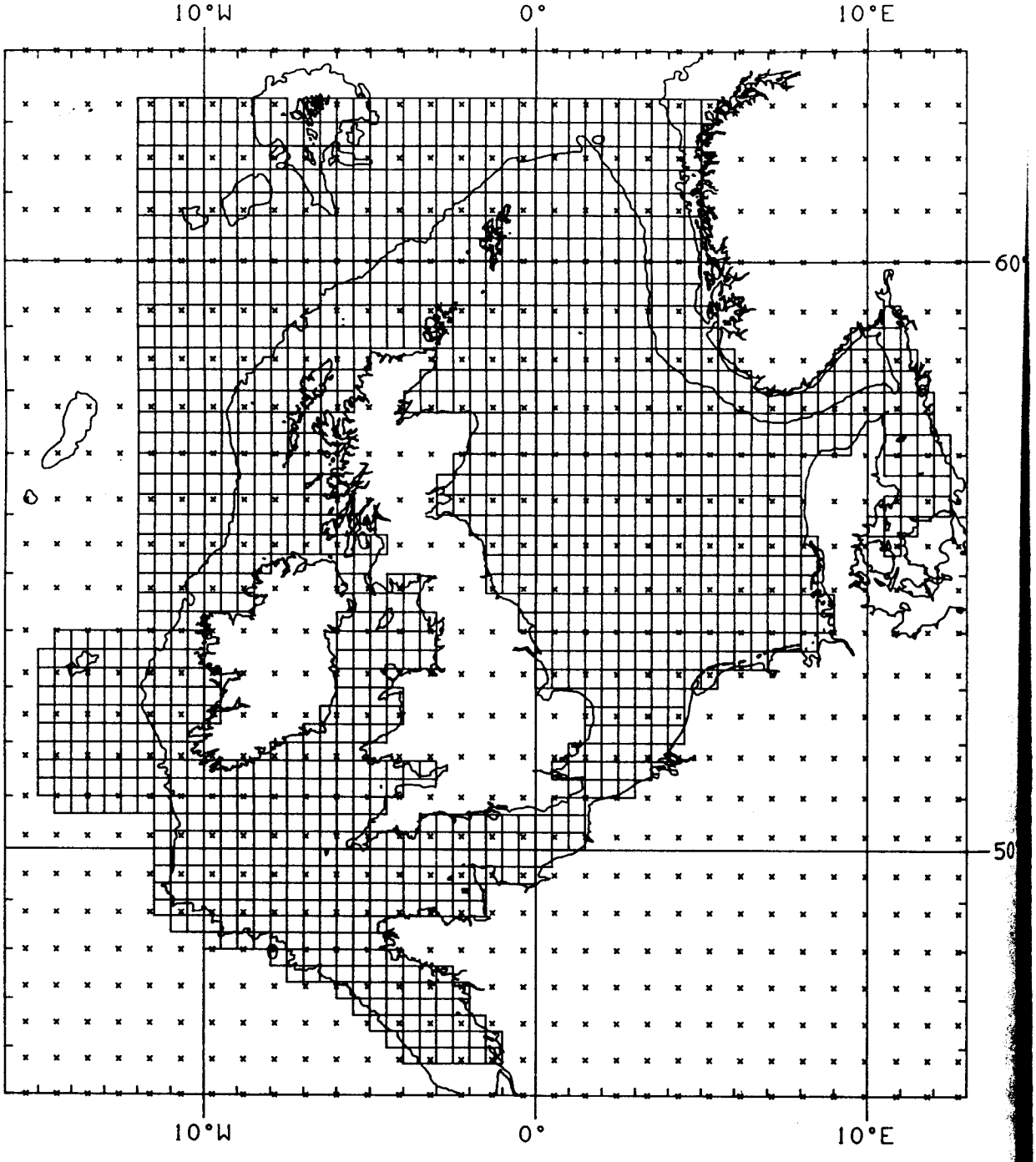

Figure 2.1 Grid of sea model CSX showing pressure points (X) of M.O. 15 level atmospheric model.

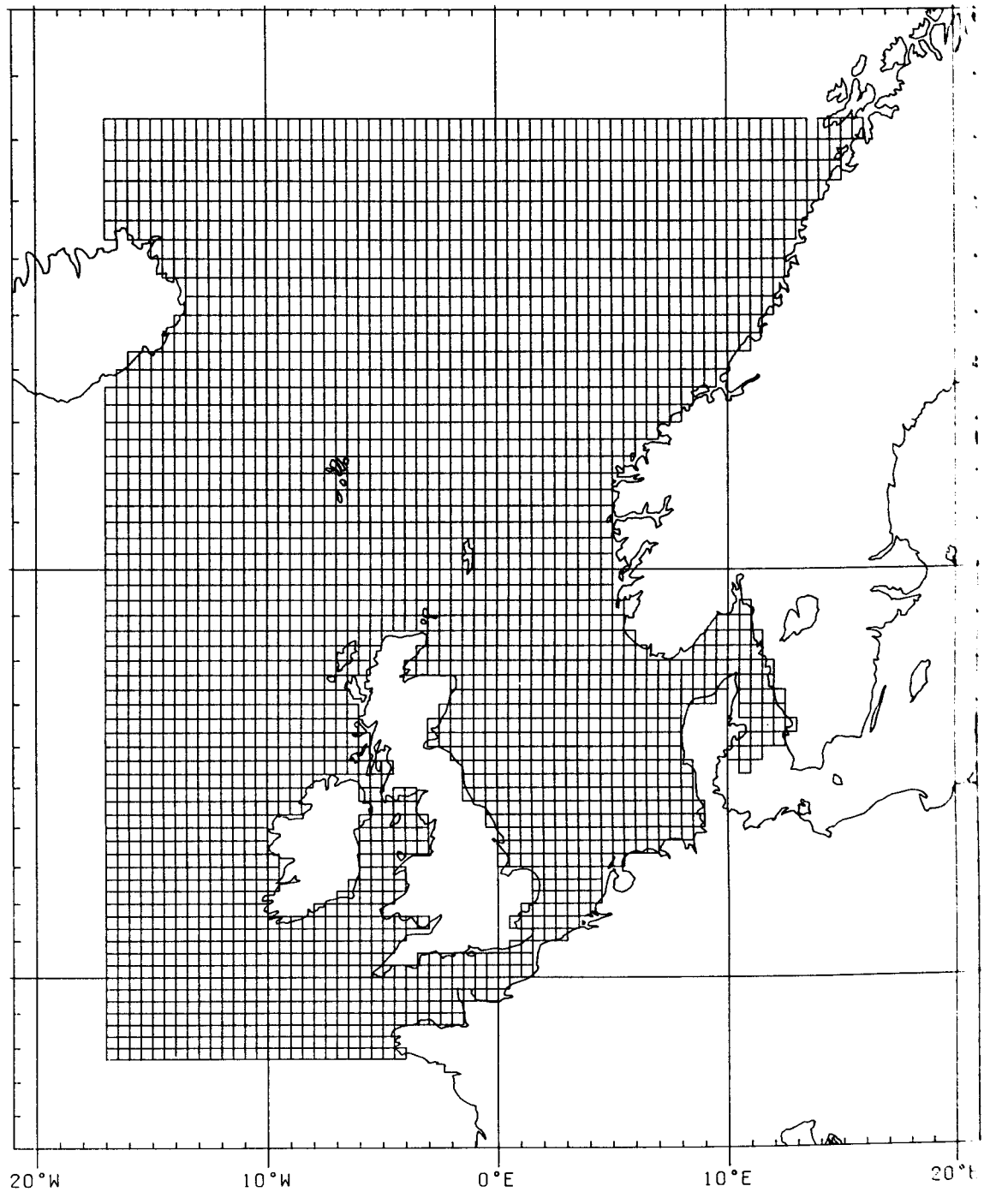

Figure 2.2 Finite difference grid of the extended continental shelf sea model, CXX.

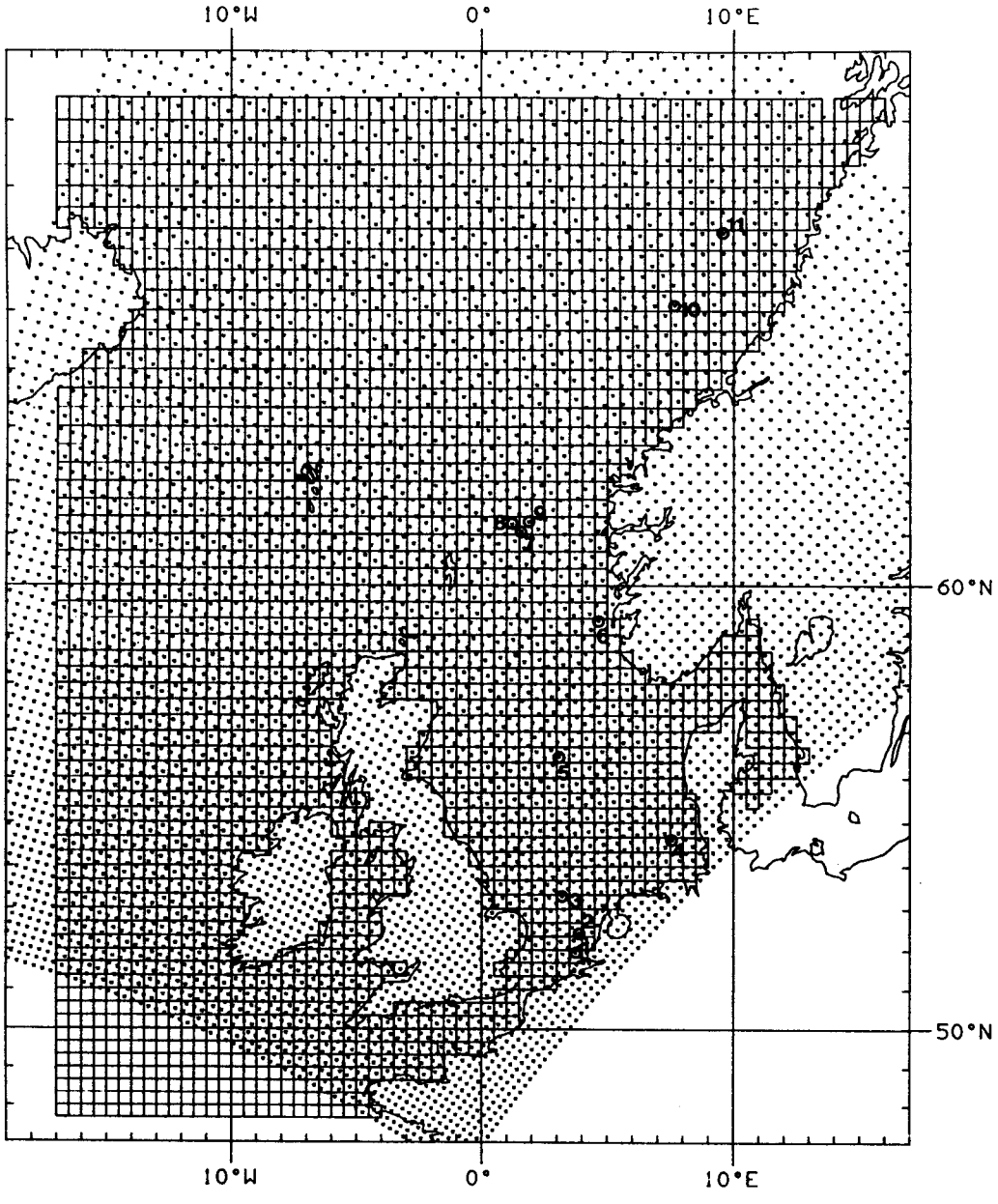

Figure 5.1 CXX grid with the M.O. fine mesh wave model (X) showing locations of WAM wave model data (o).

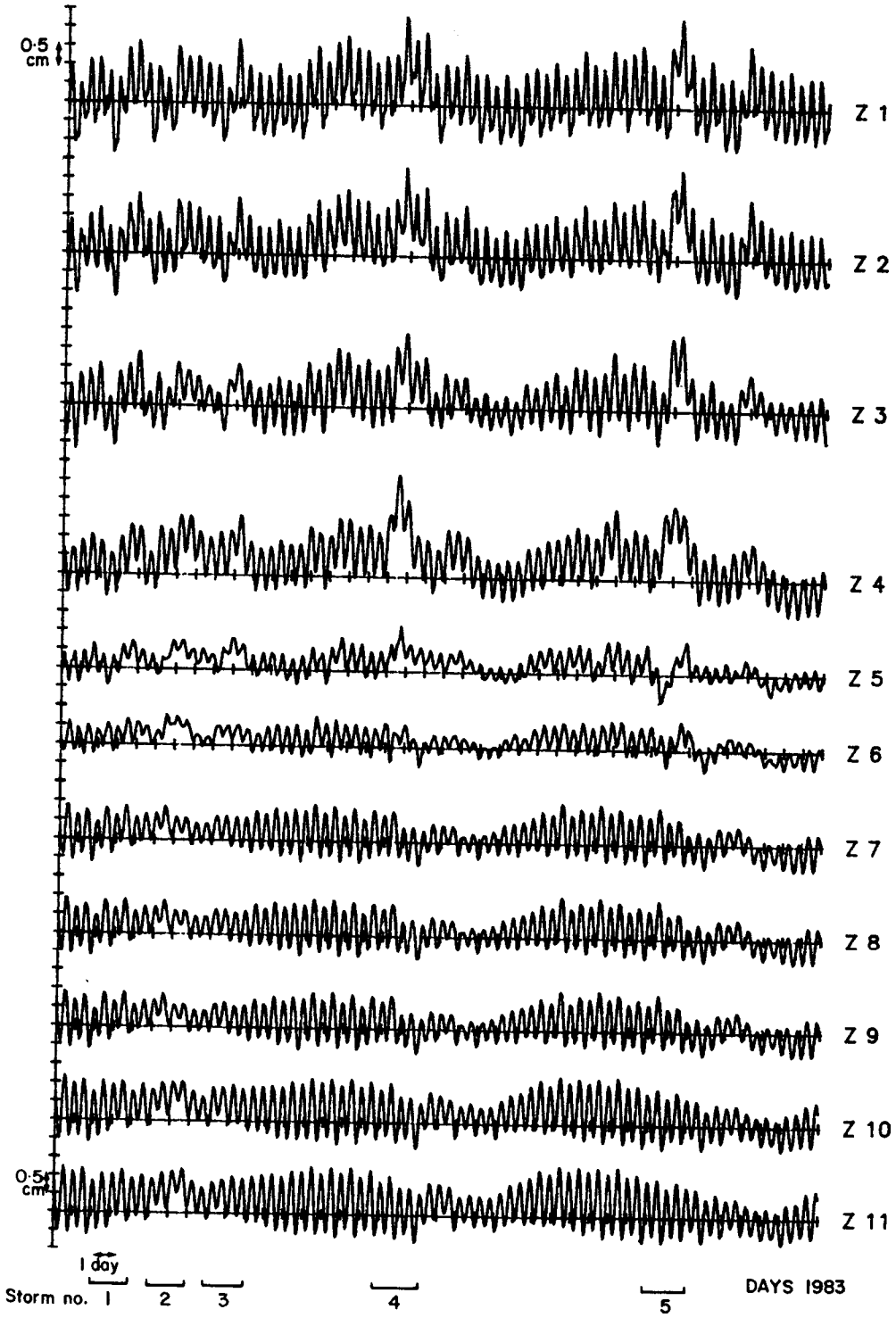

Figure 5.2 (a) Elevation time series from CXX, days 1-40 1983

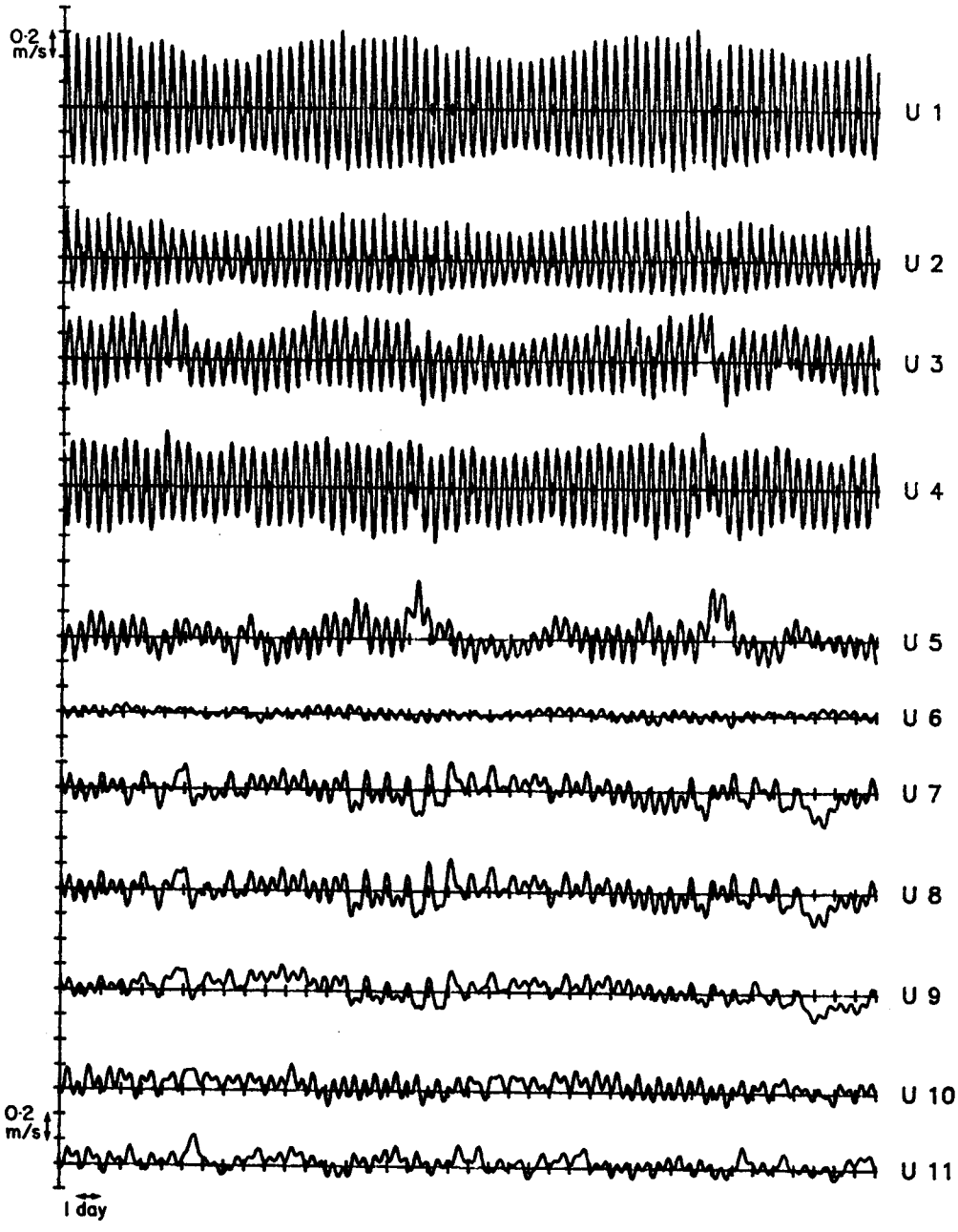

Figure 5.2 (b) East component of current CXX, days 1-40 1983

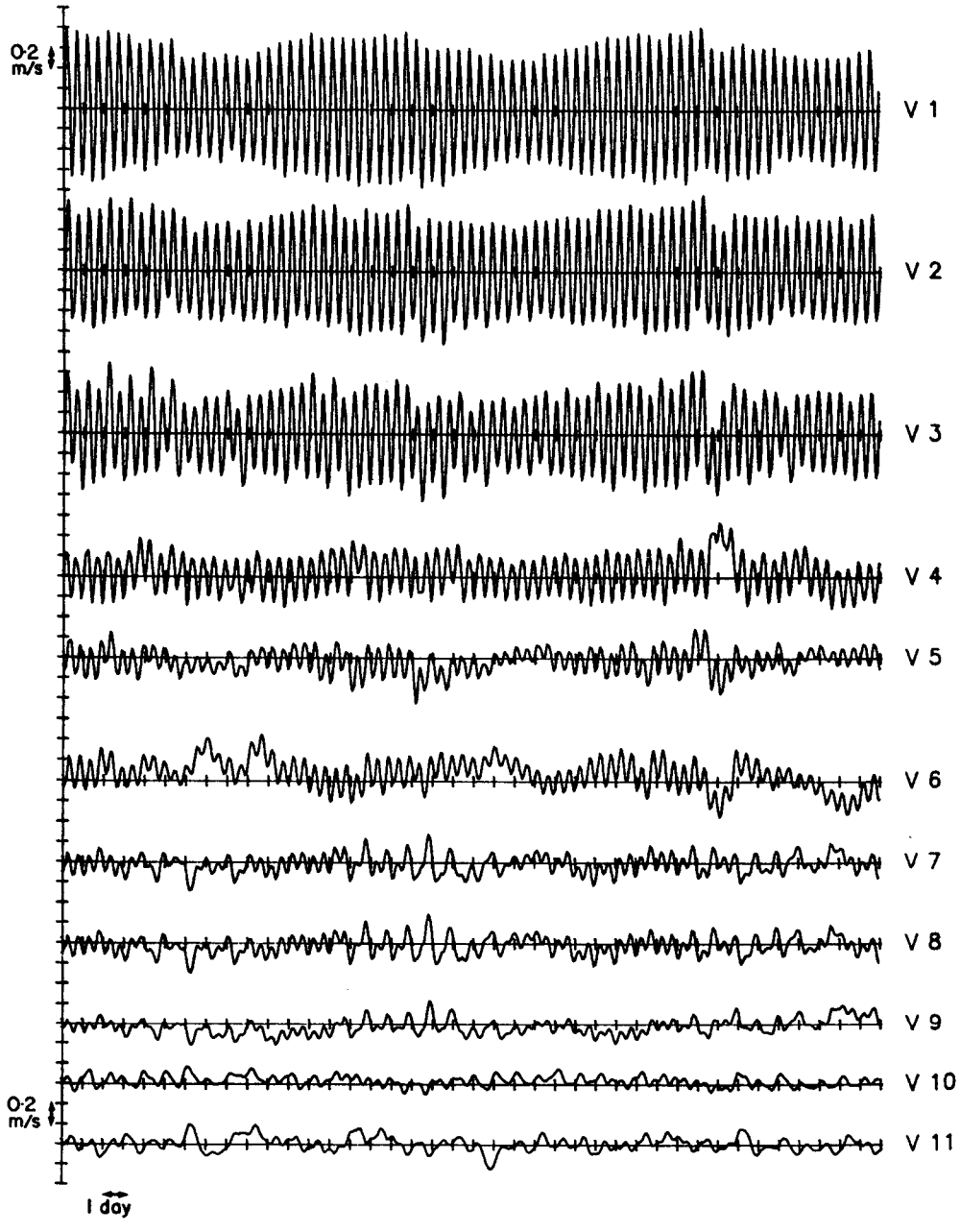

Figure 5.2 (c) North component of current CXX, days 1-40 1983

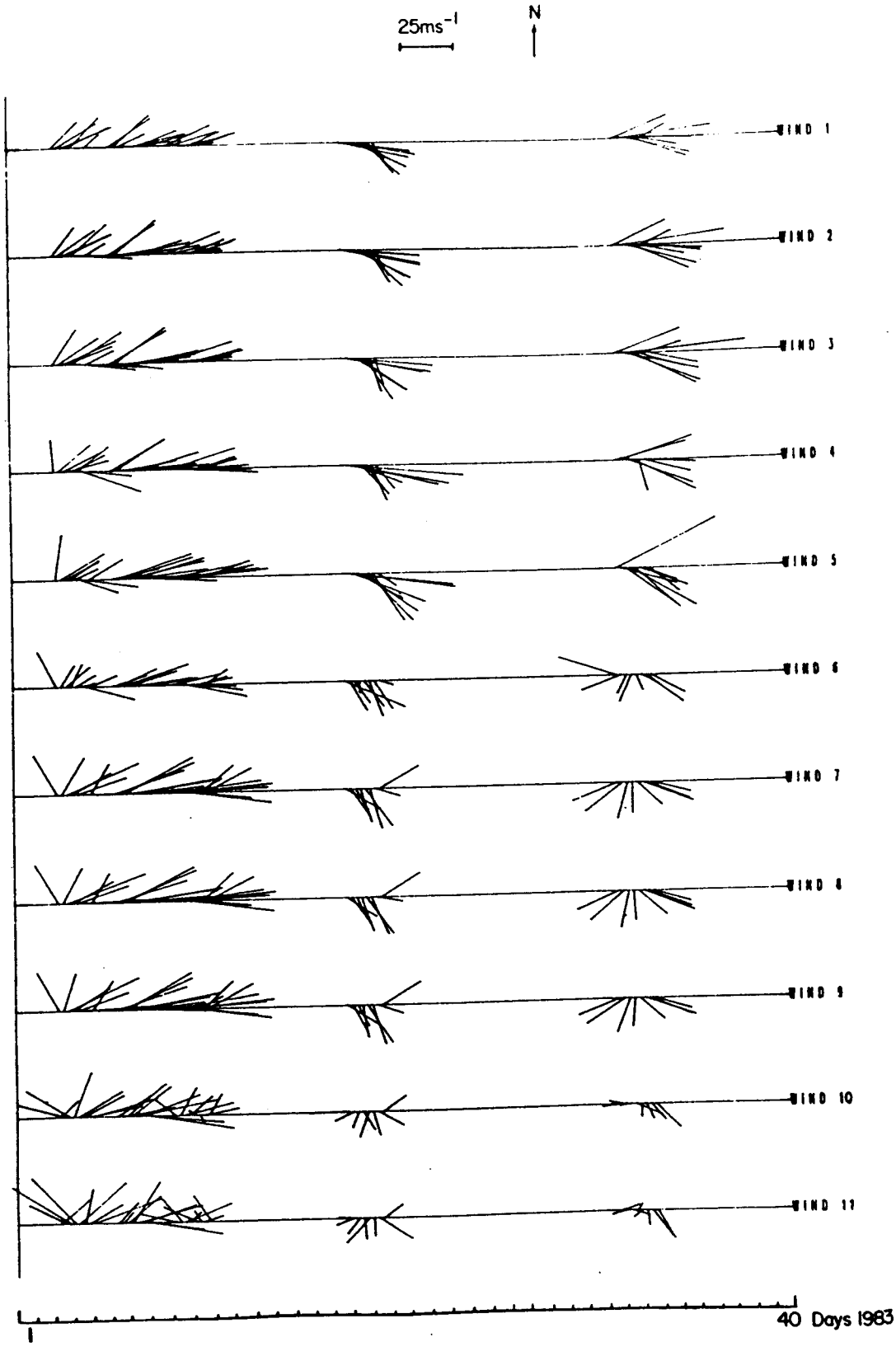

Figure 5.2 (d) Custer diagram of wind velocity for WHIST storms

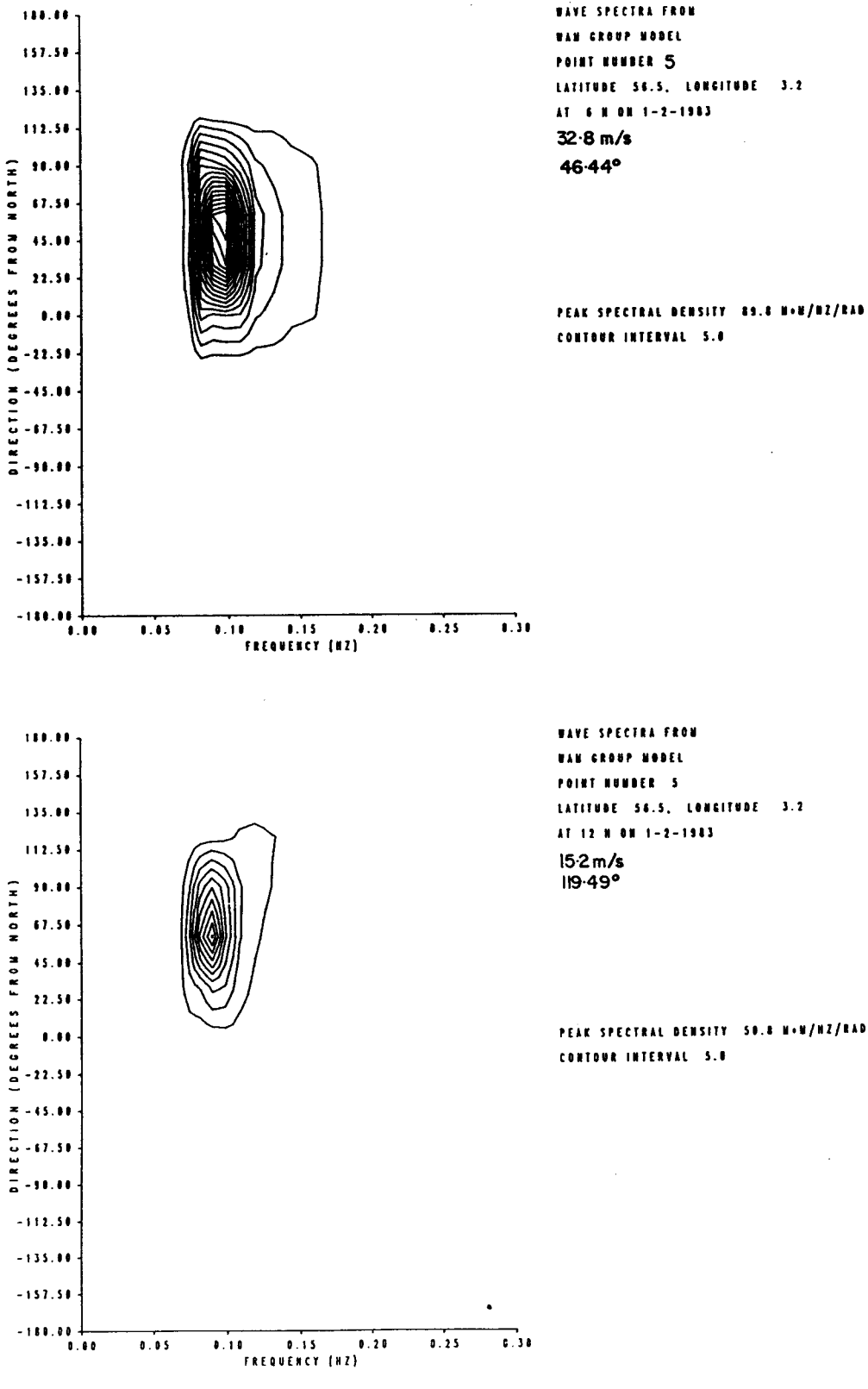

Figure 5.2 (e) WAM directional wave spectra at 6Z 1 February 1983 and 12Z 1 February 1983 at point no. 5

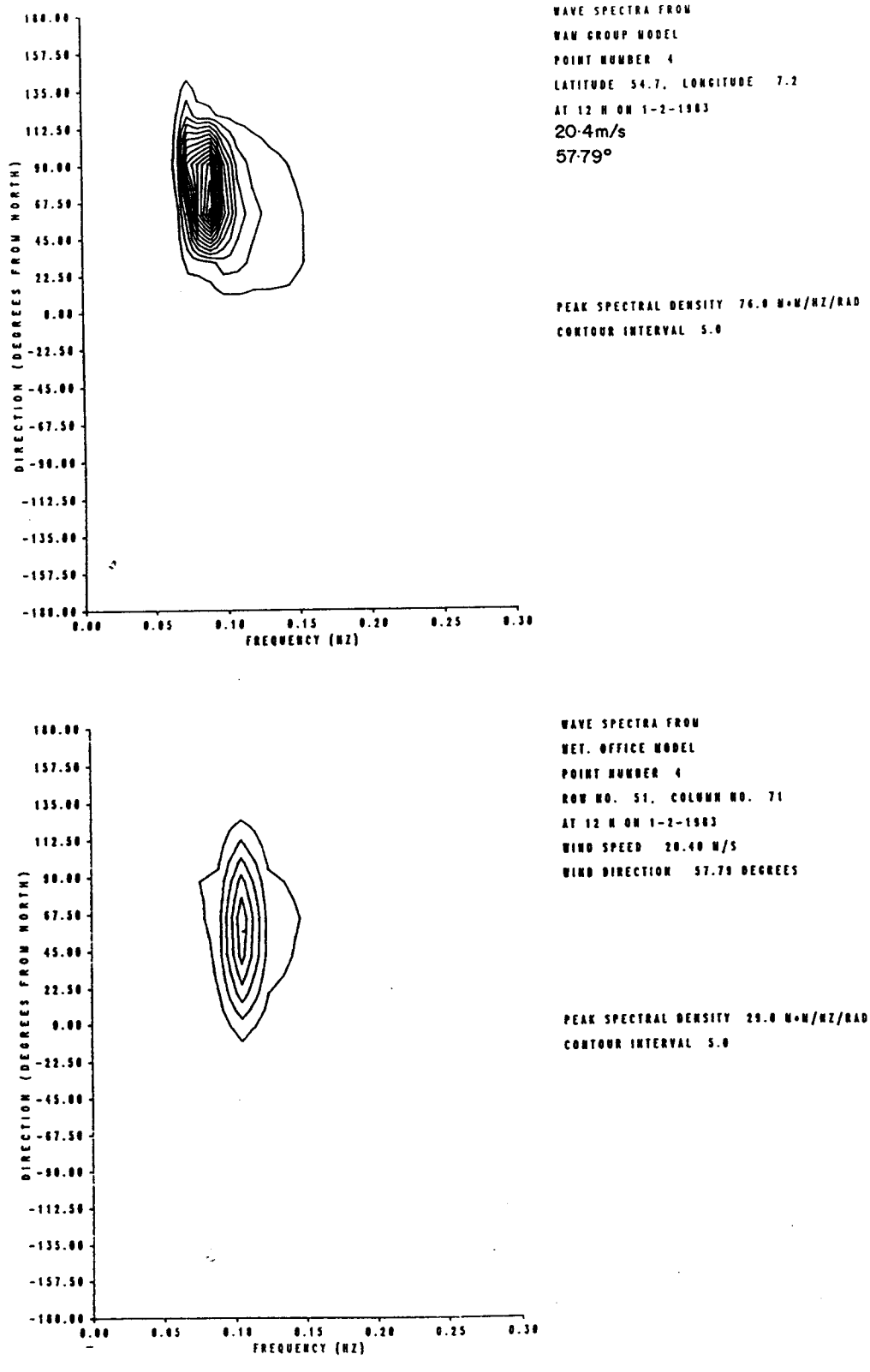

Figure 5.2 (f) M.O. and WAM directional wave spectra at 12Z 1 February 1983 at point no. 4

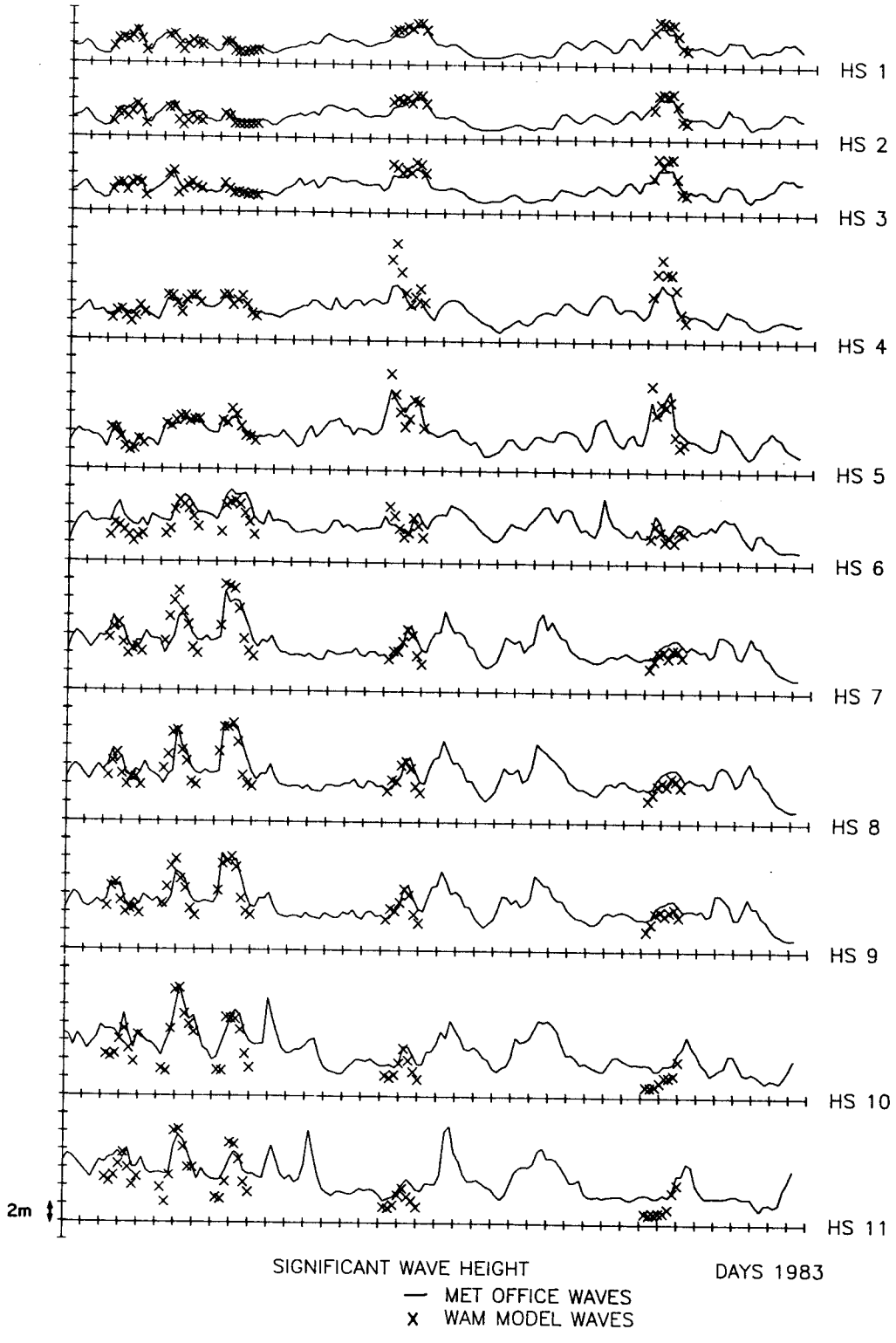

Figure 5.2 (g) Significant wave height time series for WHIST storms
——— M.O. X WAM

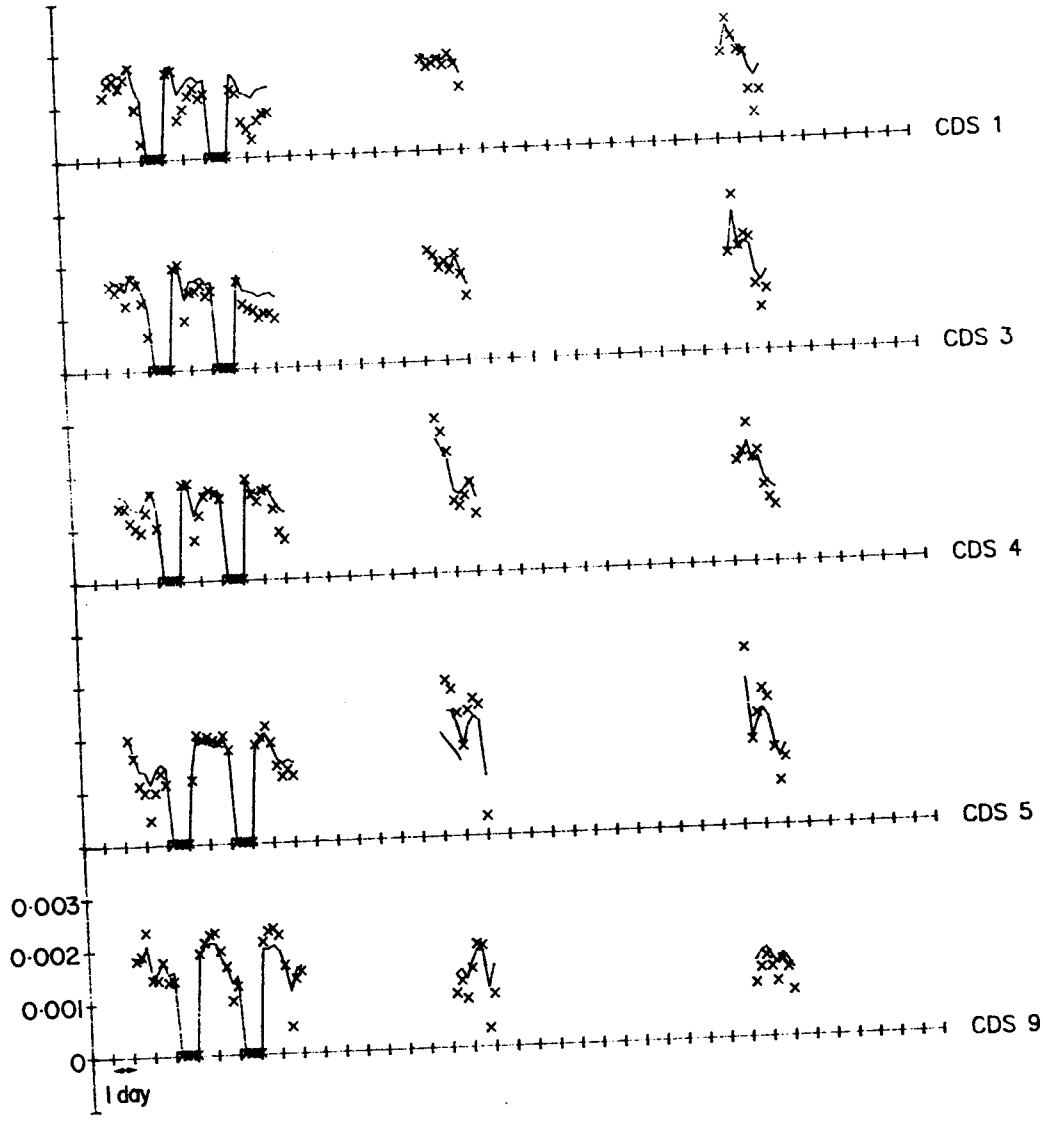

Figure 5.3 (a) Surface drag coefficient, M.O. waves
——— Smith & Banke x Kitaigorodskii

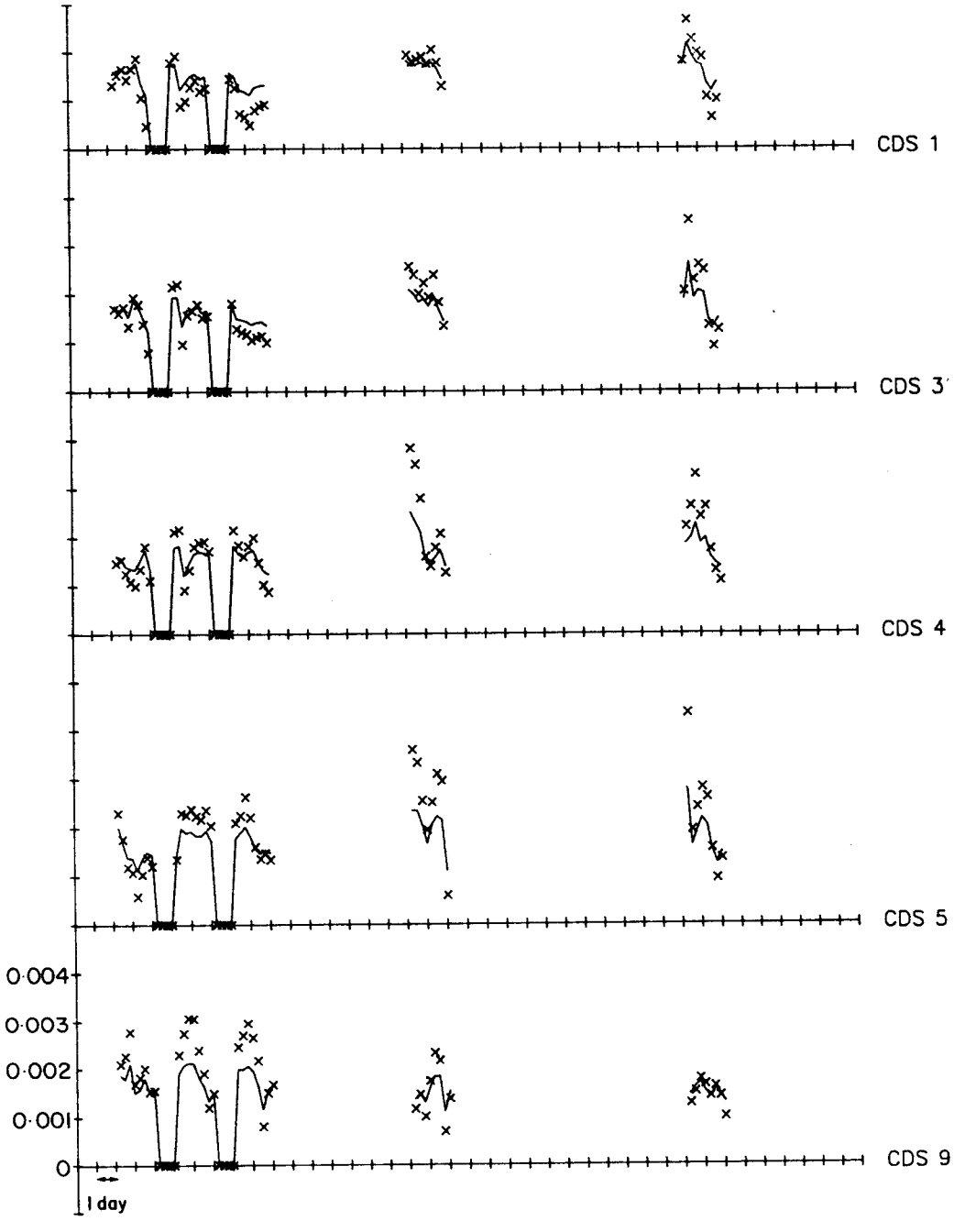

Figure 5.3 (b) Surface drag coefficient, WAM waves
——— Smith & Banke x Kitaigorodskii

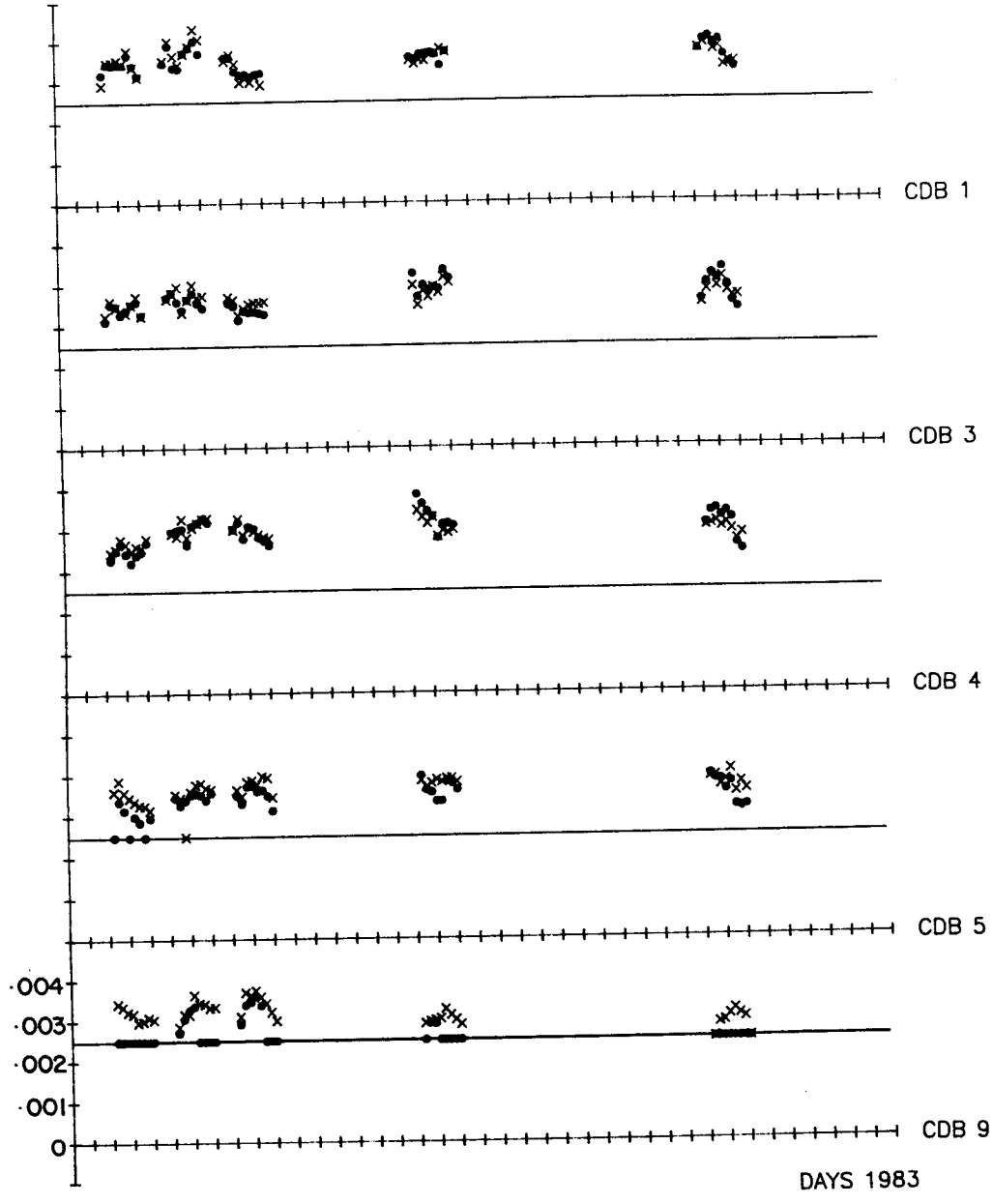

Figure 5.4 Bottom drag coefficient

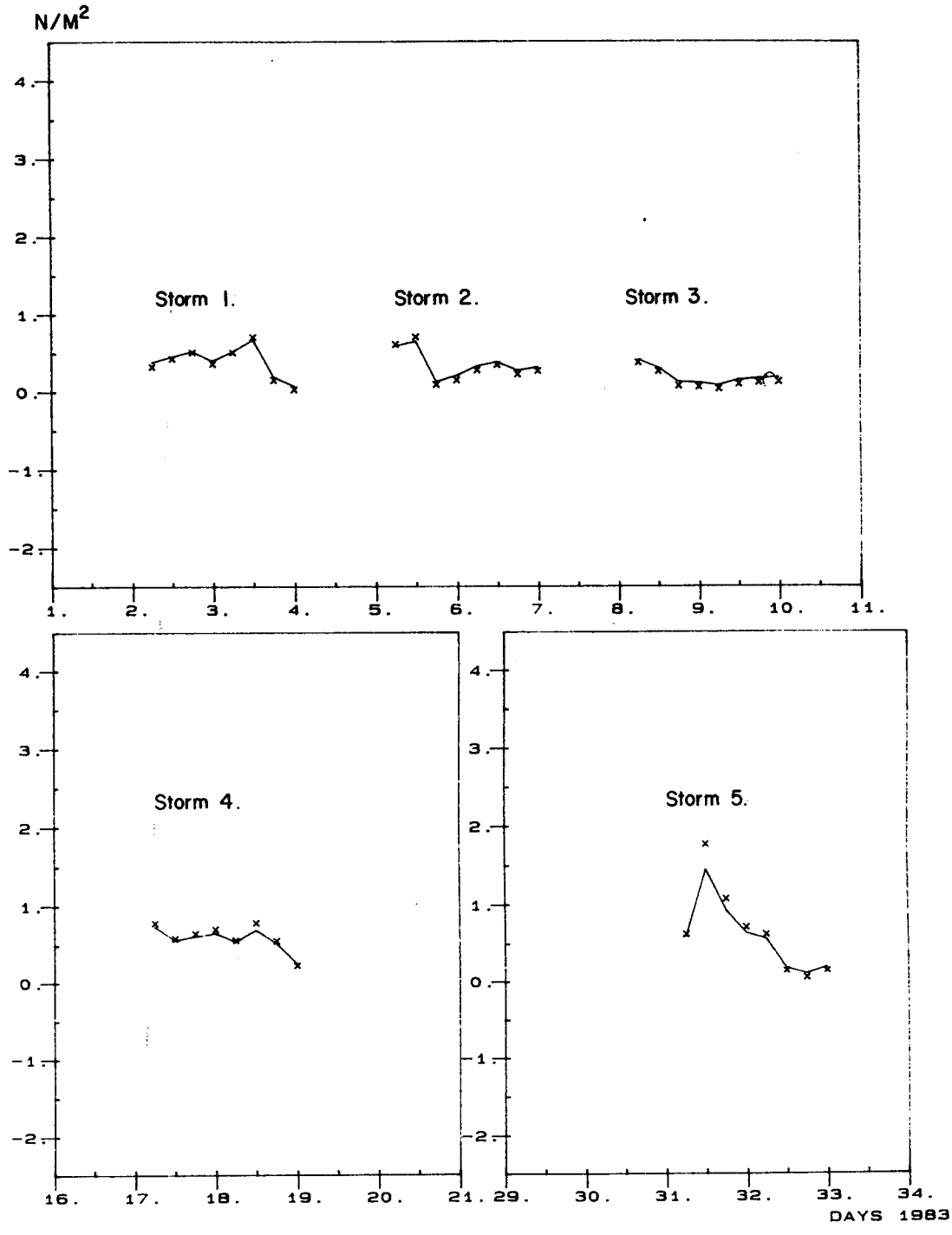
N/M2
Storm 1.
Storm 2.
Storm 3.
Storm 4.
Storm 5.
DAYS 1983
SURFACE STRESS, POINT NO 1

Figure 5.5 (a)

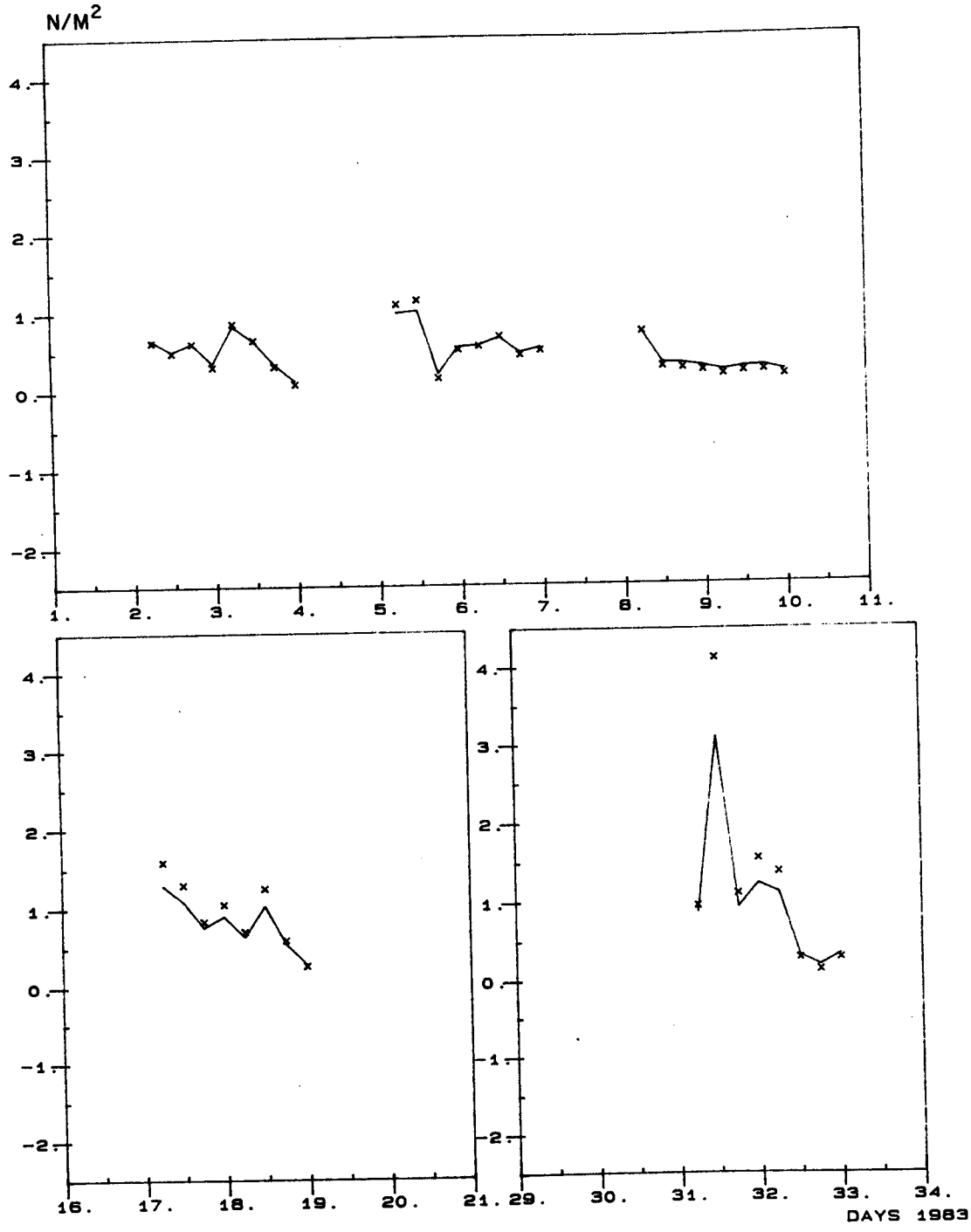
N/M2
4.
3.
2.
1.
0.
-1.
-2.
1. 2. 3. 4. 5. 6. 7. 8. 9. 10. 11.
16. 17. 18. 19. 20. 21. 29. 30. 31. 32. 33. 34.
DAYS 1983
SURFACE STRESS, POINT NO 3

Figure 5.5 (a)

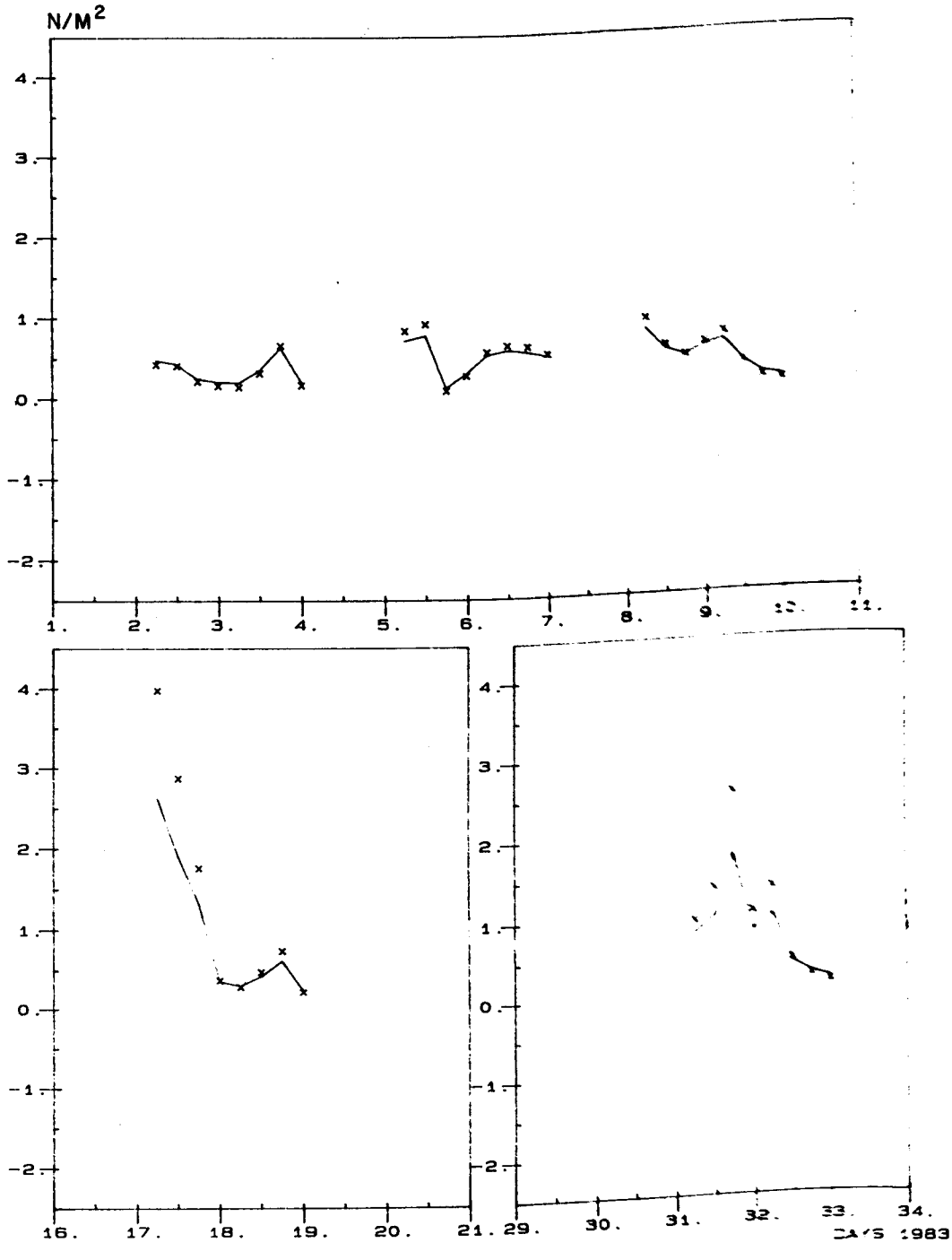
N/M2
4.
3.
2.
1.
0.
-1.
-2.
1. 2. 3. 4. 5. 6. 7. 8. 9. 11.
16. 17. 18. 19. 20. 21. 29. 30. 31. 32. 33. 34.
DAYS 1983
SURFACE STRESS, POINT NO 4

Figure 5.5 (a)

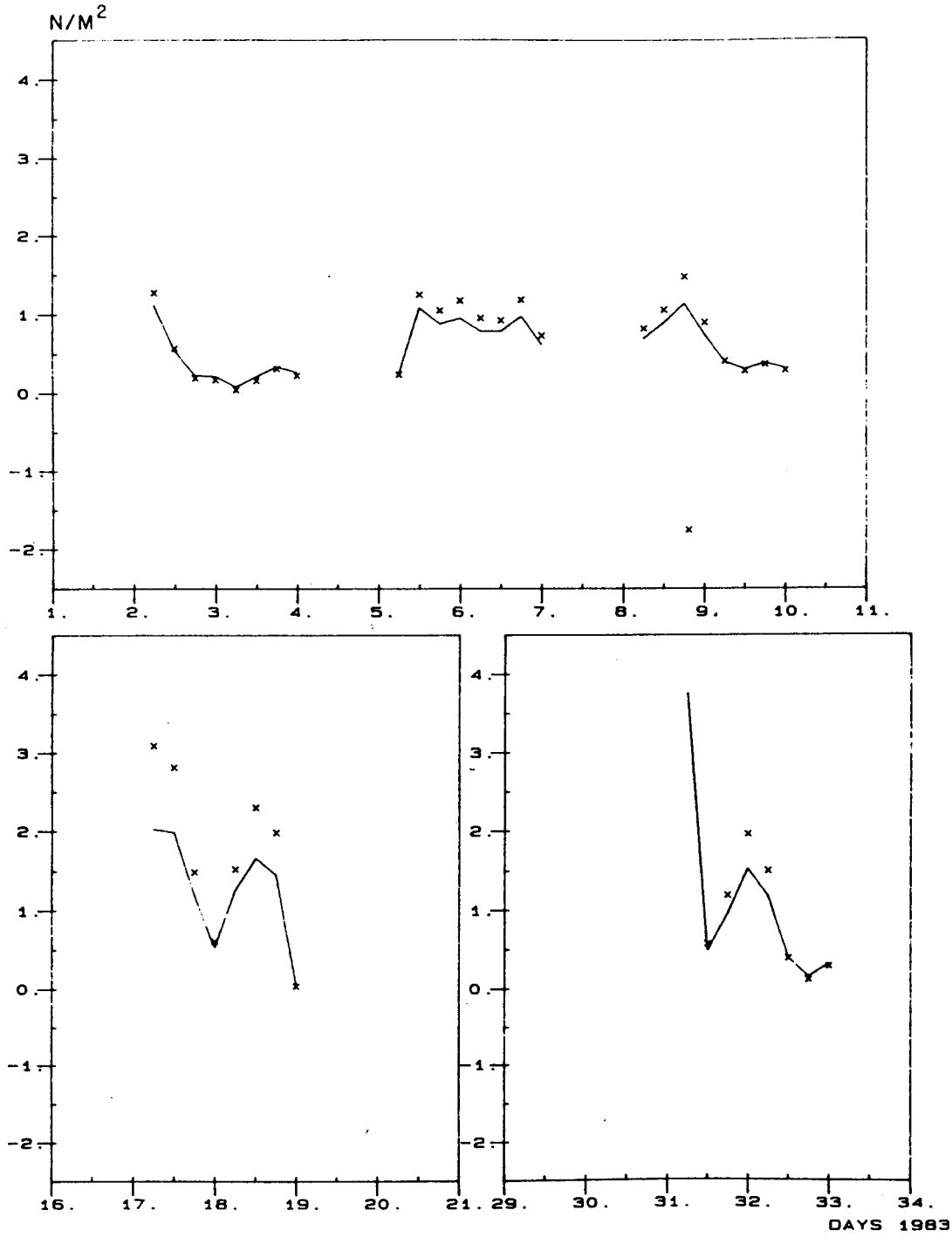
N/M2
4.
3.
2.
1.
0.
-1.
-2.
1. 2. 3. 4. 5. 6. 7. 8. 9. 10. 11.
16. 17. 18. 19. 20. 21.
29. 30. 31. 32. 33. 34.
DAYS 1983
SURFACE STRESS, POINT NO 5

Figure 5.5 (a)

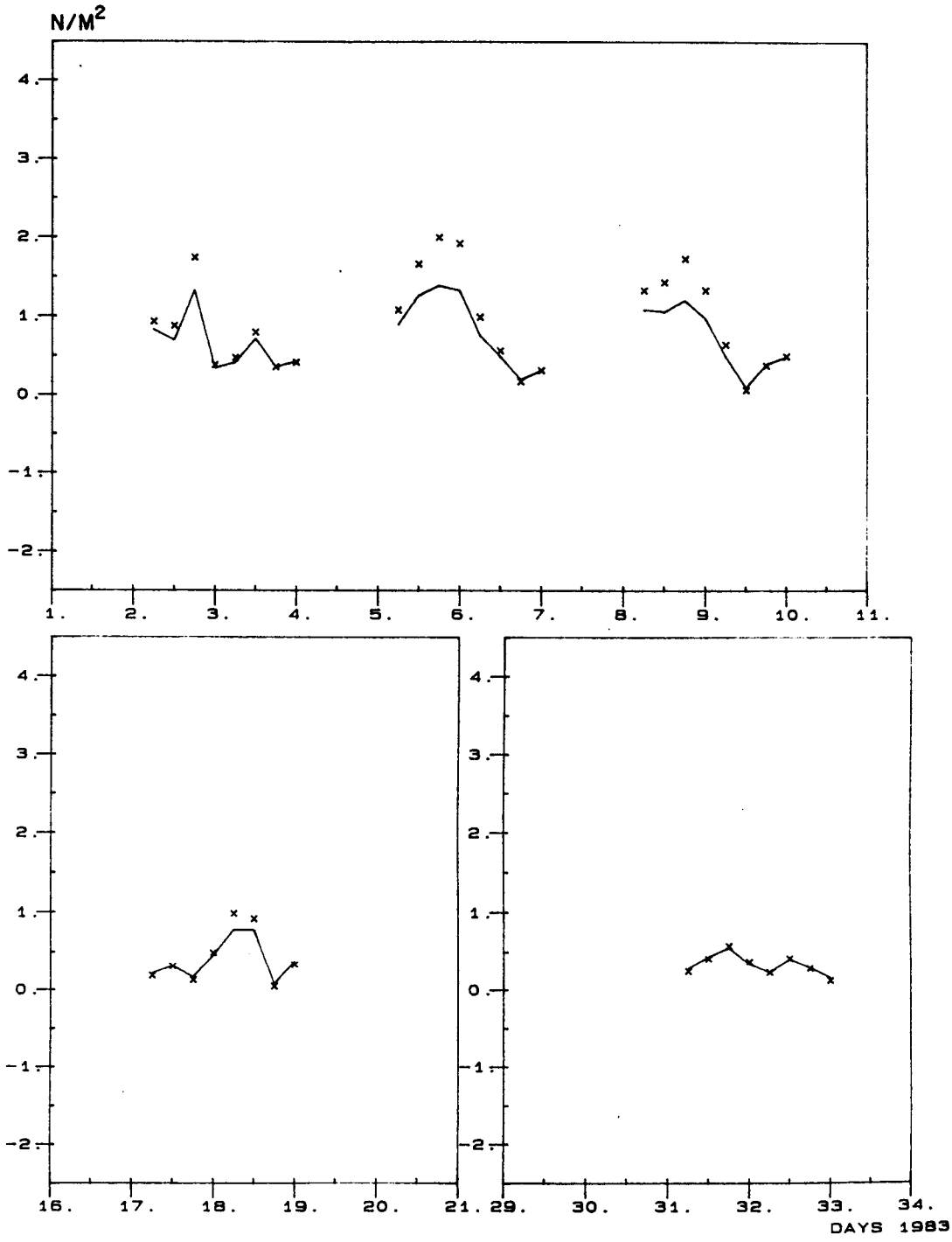
N/M2
4.
3.
2.
1.
0.
-1.
-2.
1. 2. 3. 4. 5. 6. 7. 8. 9. 10. 11.
16. 17. 18. 19. 20. 21.
29. 30. 31. 32. 33. 34.
DAYS 1983
SURFACE STRESS, POINT NO 9

Figure 5.5 (a)

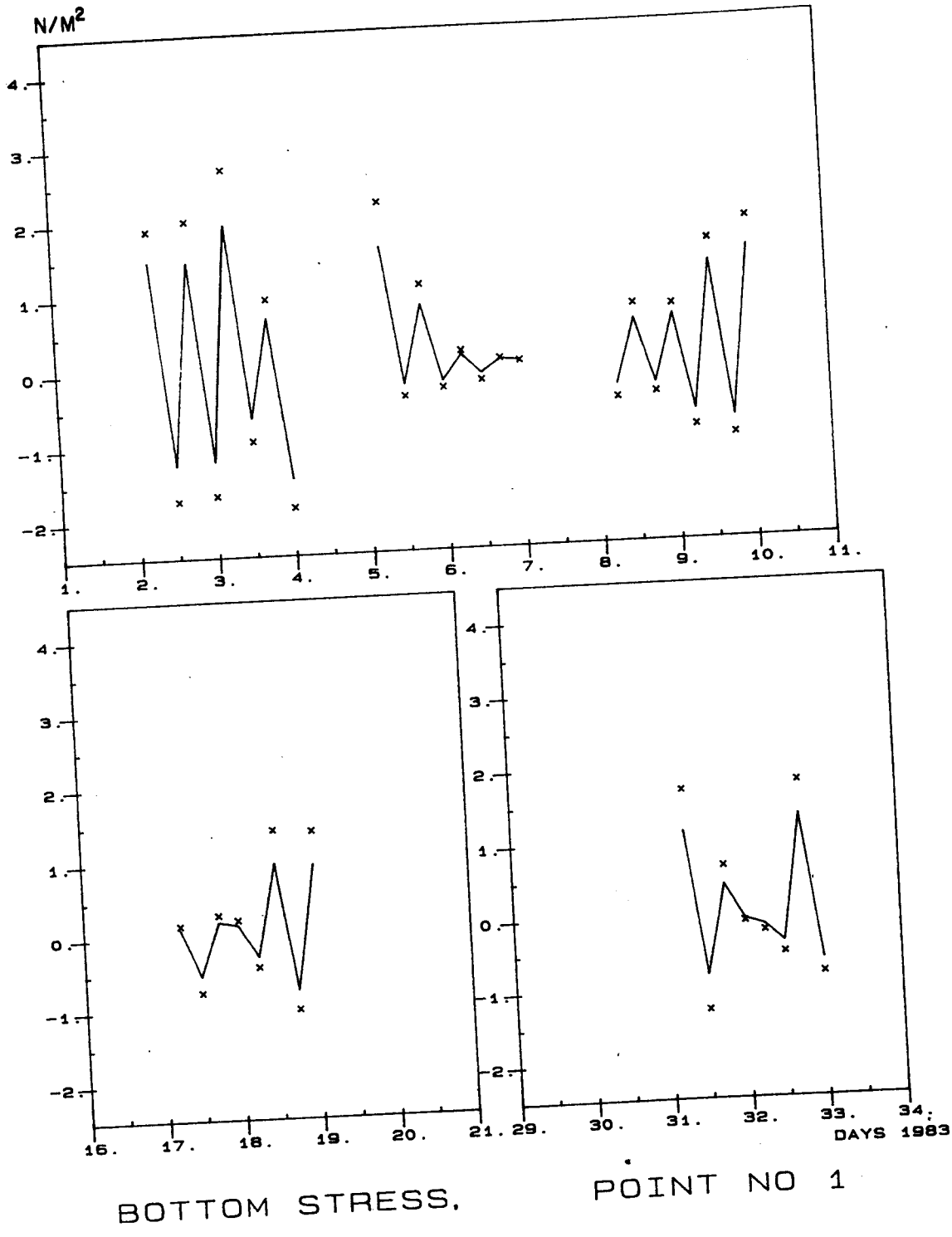
N/M2
4.
3.
2.
1.
0.
-1.
-2.
1. 2. 3. 4. 5. 6. 7. 8. 9. 10. 11.
16. 17. 18. 19. 20. 21.
29. 30. 31. 32. 33. 34.
DAYS 1983
BOTTOM STRESS, POINT NO 1

Figure 5.5 (b)

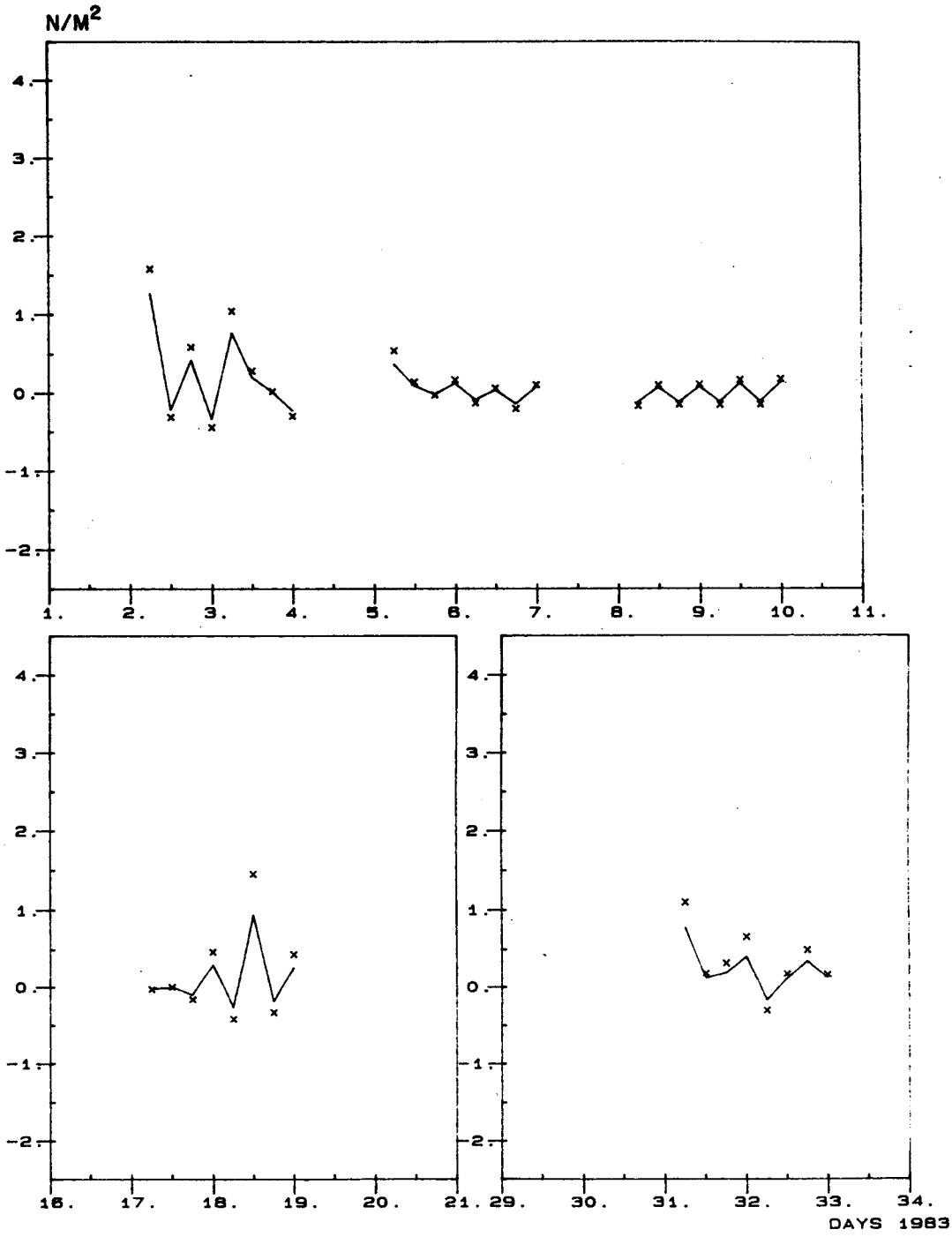
N/M2
4.
3.
2.
1.
0.
-1.
-2.
1. 2. 3. 4. 5. 6. 7. 8. 9. 10. 11.
16. 17. 18. 19. 20. 21. 29. 30. 31. 32. 33. 34.
DAYS 1983
BOTTOM STRESS, POINT NO 3

Figure 5.5 (b)

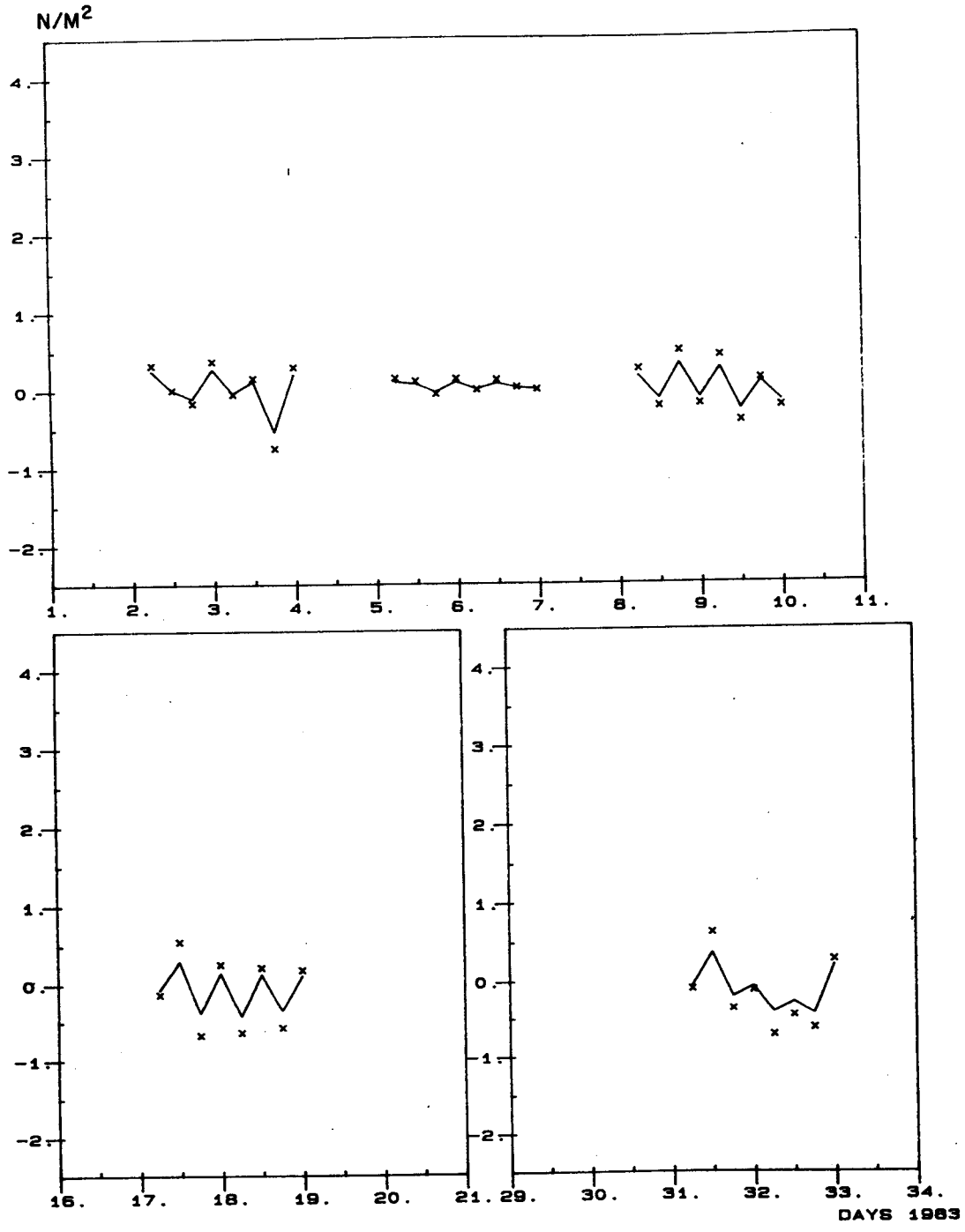
N/M2
4.
3.
2.
1.
0.
-1.
-2.
1. 2. 3. 4. 5. 6. 7. 8. 9. 10. 11.
16. 17. 18. 19. 20. 21. 29. 30. 31. 32. 33. 34.
DAYS 1983
BOTTOM STRESS, POINT NO 4

Figure 5.5 (b)

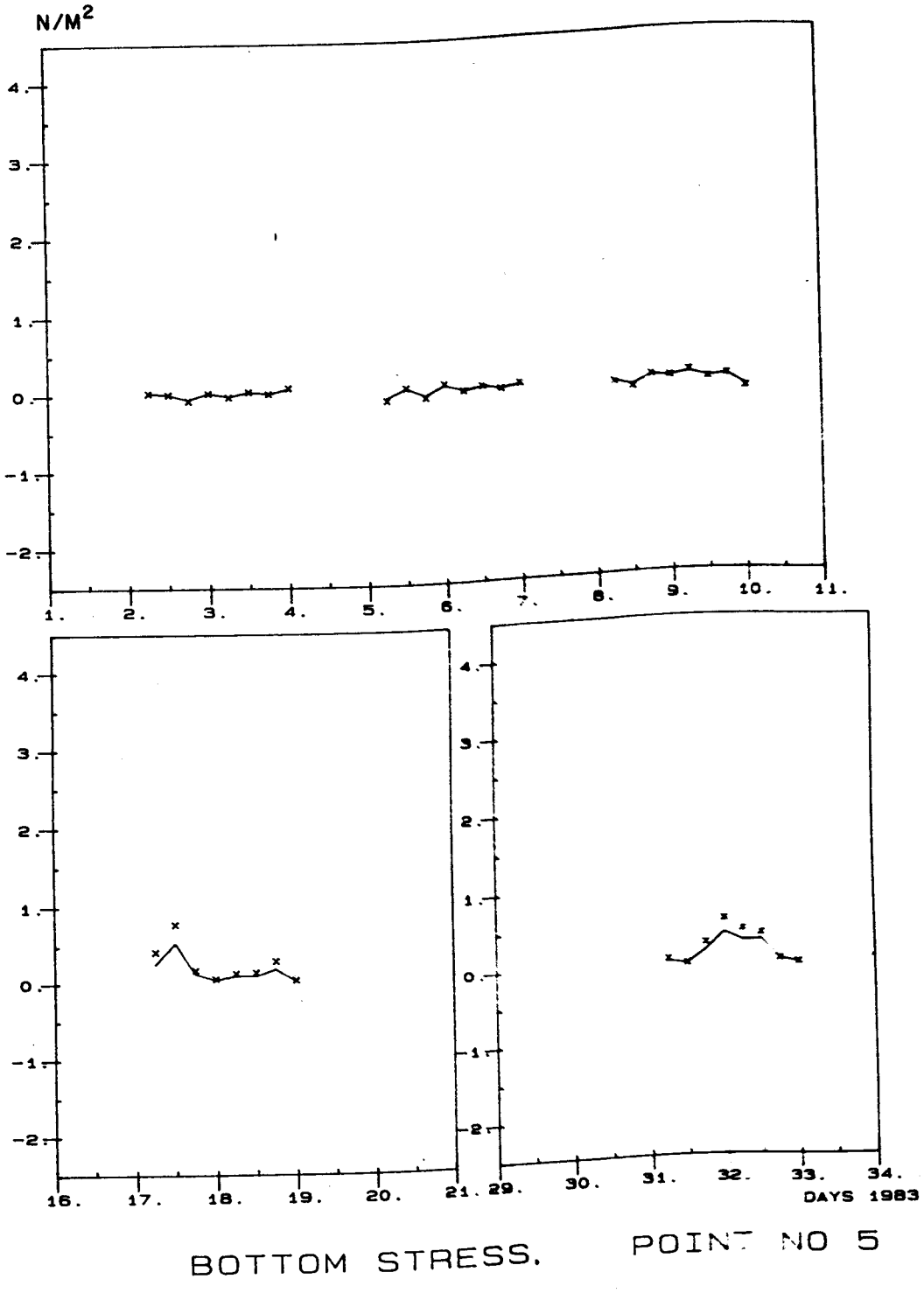
N/M2
4.
3.
2.
1.
0.
-1.
-2.
1. 2. 3. 4. 5. 6. 7. 8. 9. 10. 11.
16. 17. 18. 19. 20. 21. 29. 30. 31. 32. 33. 34.
DAYS 1983
BOTTOM STRESS. POINT NO 5

Figure 5.5 (b)

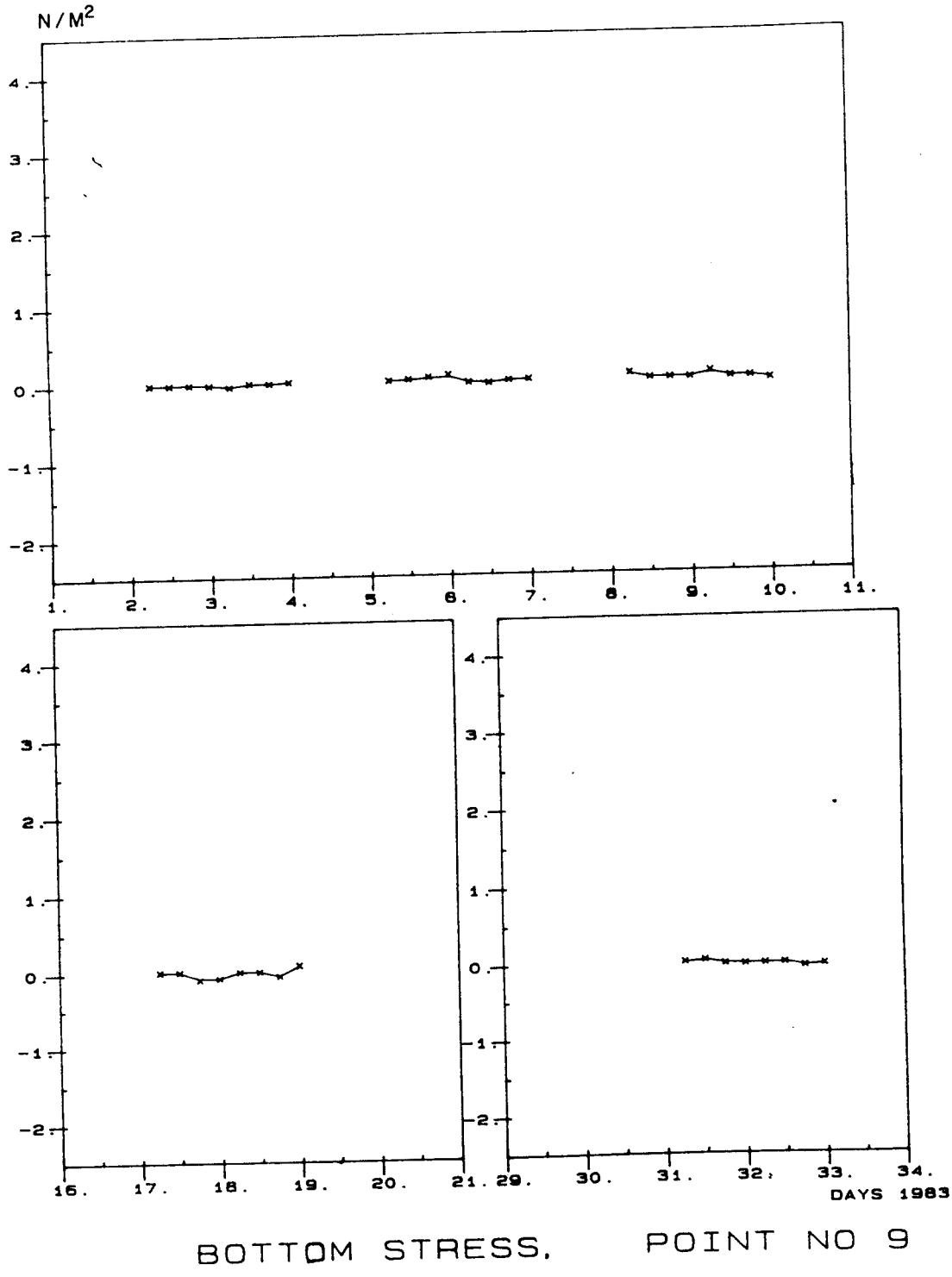
N/M2
4.
3.
2.
1.
0.
-1.
-2.
1. 2. 3. 4. 5. 6. 7. 8. 9. 10. 11.
16. 17. 18. 19. 20. 21. 29. 30. 31. 32. 33. 34.
DAYS 1983
BOTTOM STRESS, POINT NO 9

Figure 5.5 (b)

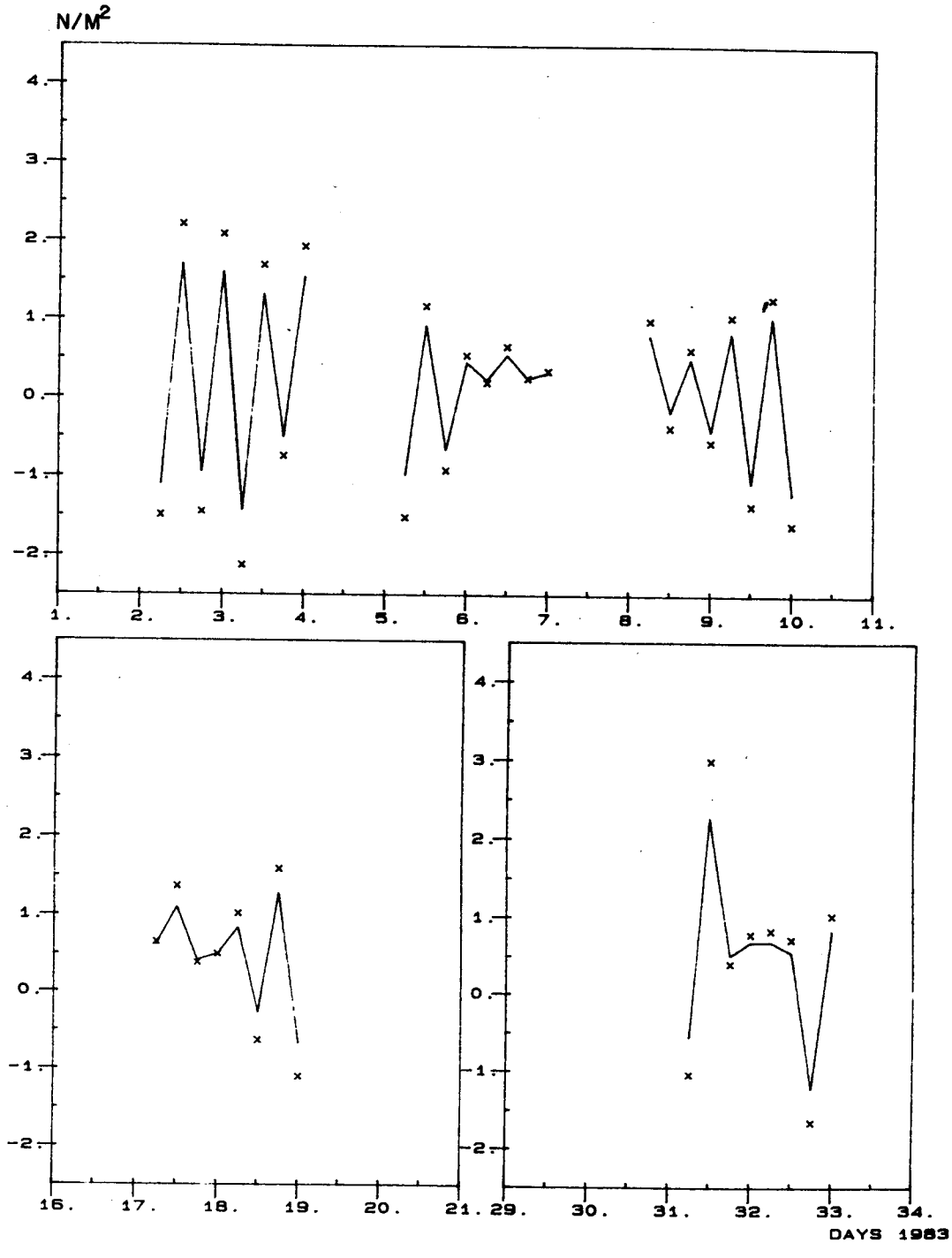
N/M2
4.
3.
2.
1.
0.
-1.
-2.
1. 2. 3. 4. 5. 6. 7. 8. 9. 10. 11.
16. 17. 18. 19. 20. 21.
29. 30. 31. 32. 33. 34.
DAYS 1983
SURFACE-BOTTOM STRESS,POINT NO 1

Figure 5.5 (c)

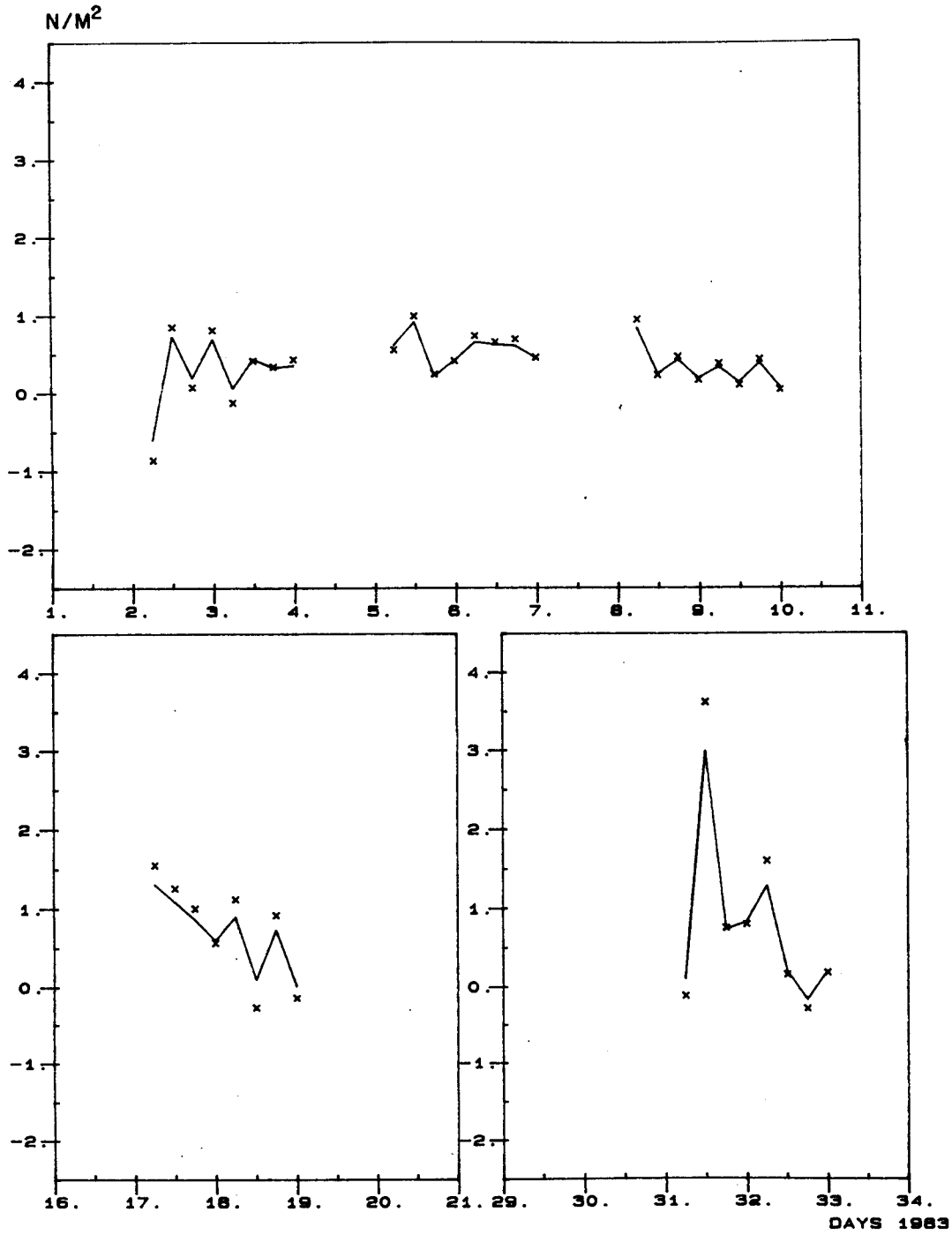
N/M2
4.
3.
2.
1.
0.
-1.
-2.
1. 2. 3. 4. 5. 6. 7. 8. 9. 10. 11.
16. 17. 18. 19. 20. 21. 29. 30. 31. 32. 33. 34.
DAYS 1983
SURFACE-BOTTOM STRESS, POINT NO 3

Figure 5.5 (c)

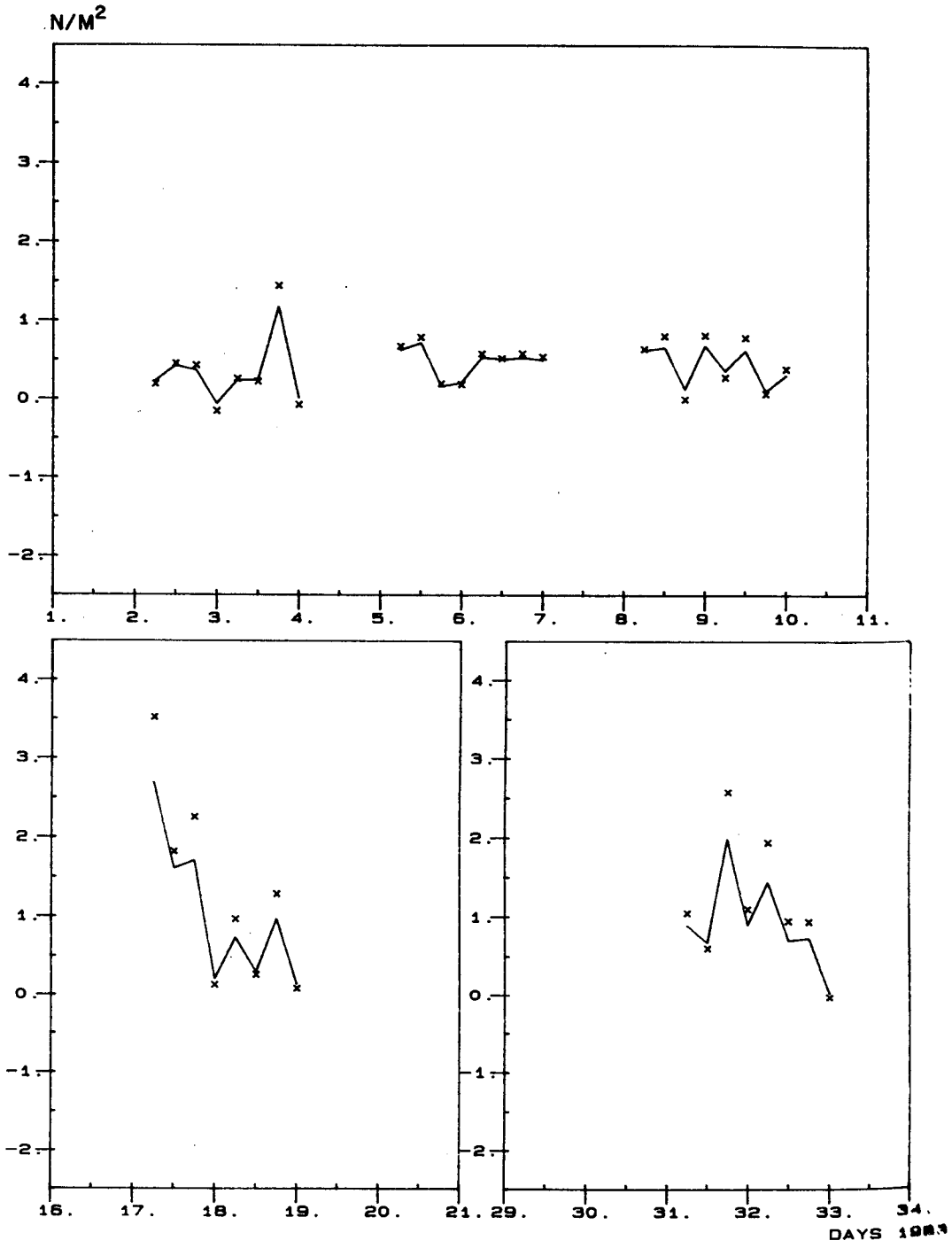
N/M2
4.
3.
2.
1.
0.
-1.
-2.
1. 2. 3. 4. 5. 6. 7. 8. 9. 10. 11.
16. 17. 18. 19. 20. 21.
29. 30. 31. 32. 33. 34.
DAYS 1983
SURFACE-BOTTOM STRESS, POINT NO 4

Figure 5.5 (c)

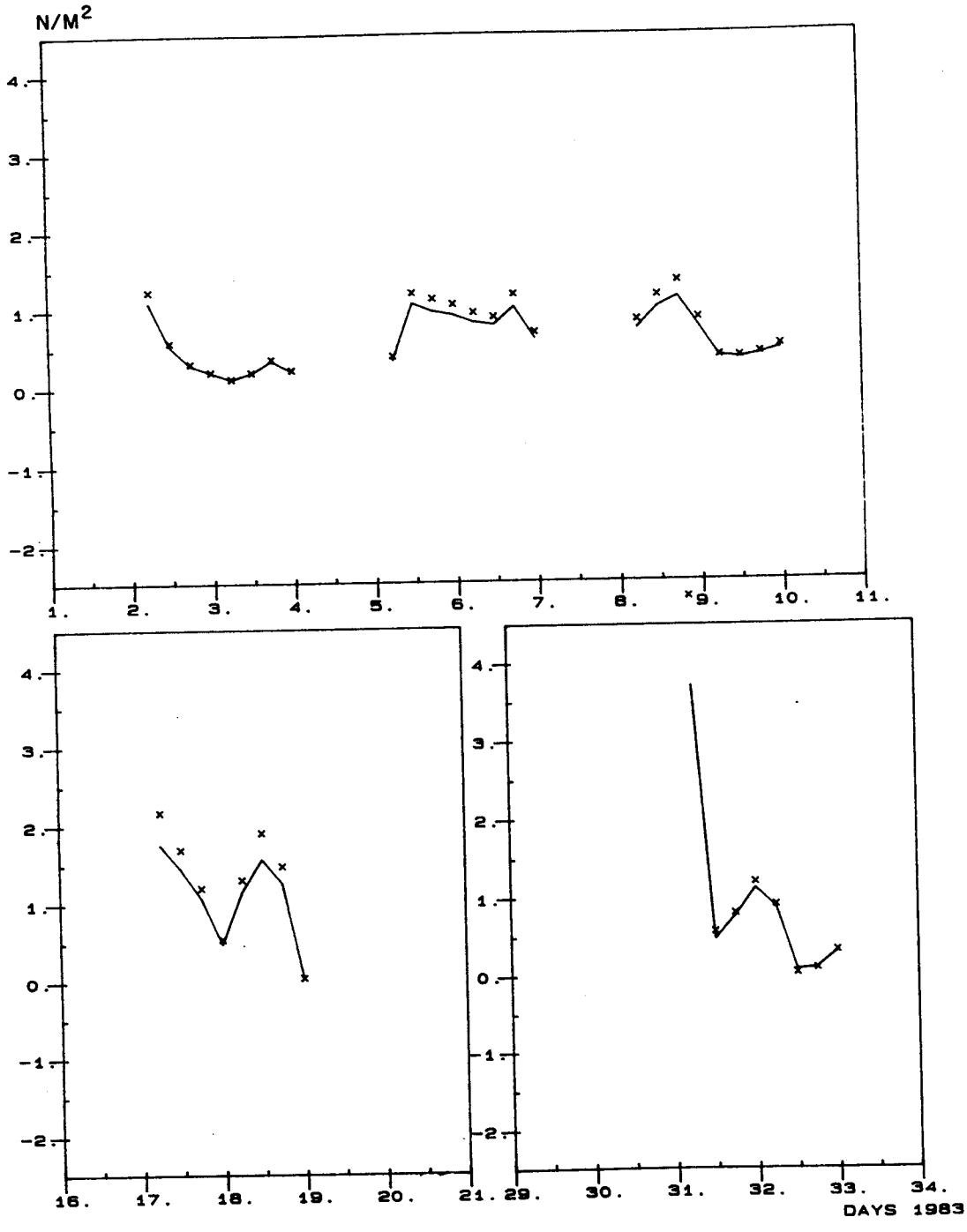
N/M2
4.
3.
2.
1.
0.
-1.
-2.
1. 2. 3. 4. 5. 6. 7. 8. 9. 10. 11.
16. 17. 18. 19. 20. 21. 29. 30. 31. 32. 33. 34.
DAYS 1983
SURFACE-BOTTOM STRESS, POINT NO 5

Figure 5.5 (c)

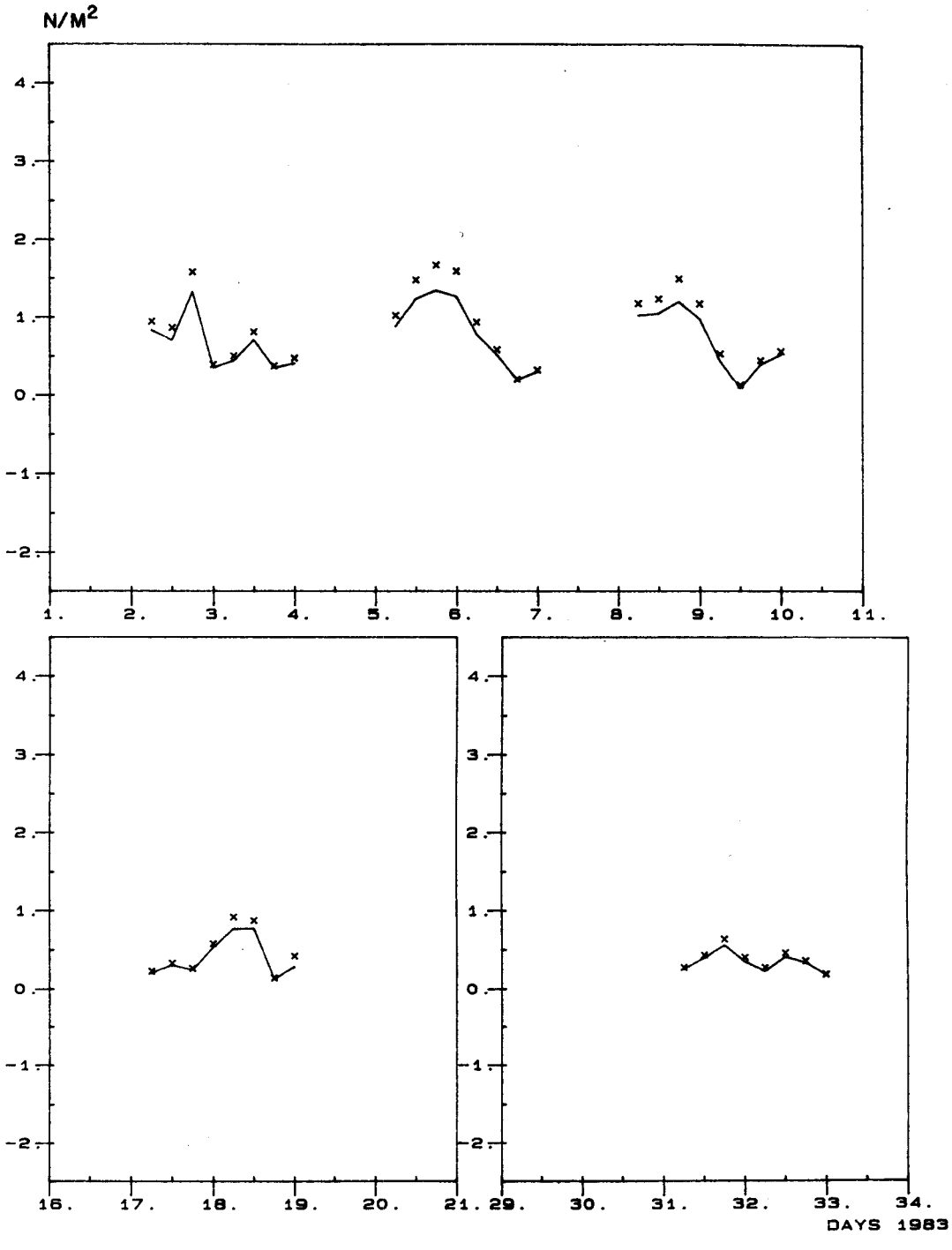
N/M2
4.
3.
2.
1.
0.
-1.
-2.
1. 2. 3. 4. 5. 6. 7. 8. 9. 10. 11.
16. 17. 18. 19. 20. 21.
29. 30. 31. 32. 33. 34.
DAYS 1983
SURFACE-BOTTOM STRESS, POINT NO 9

Figure 5.5 (c)

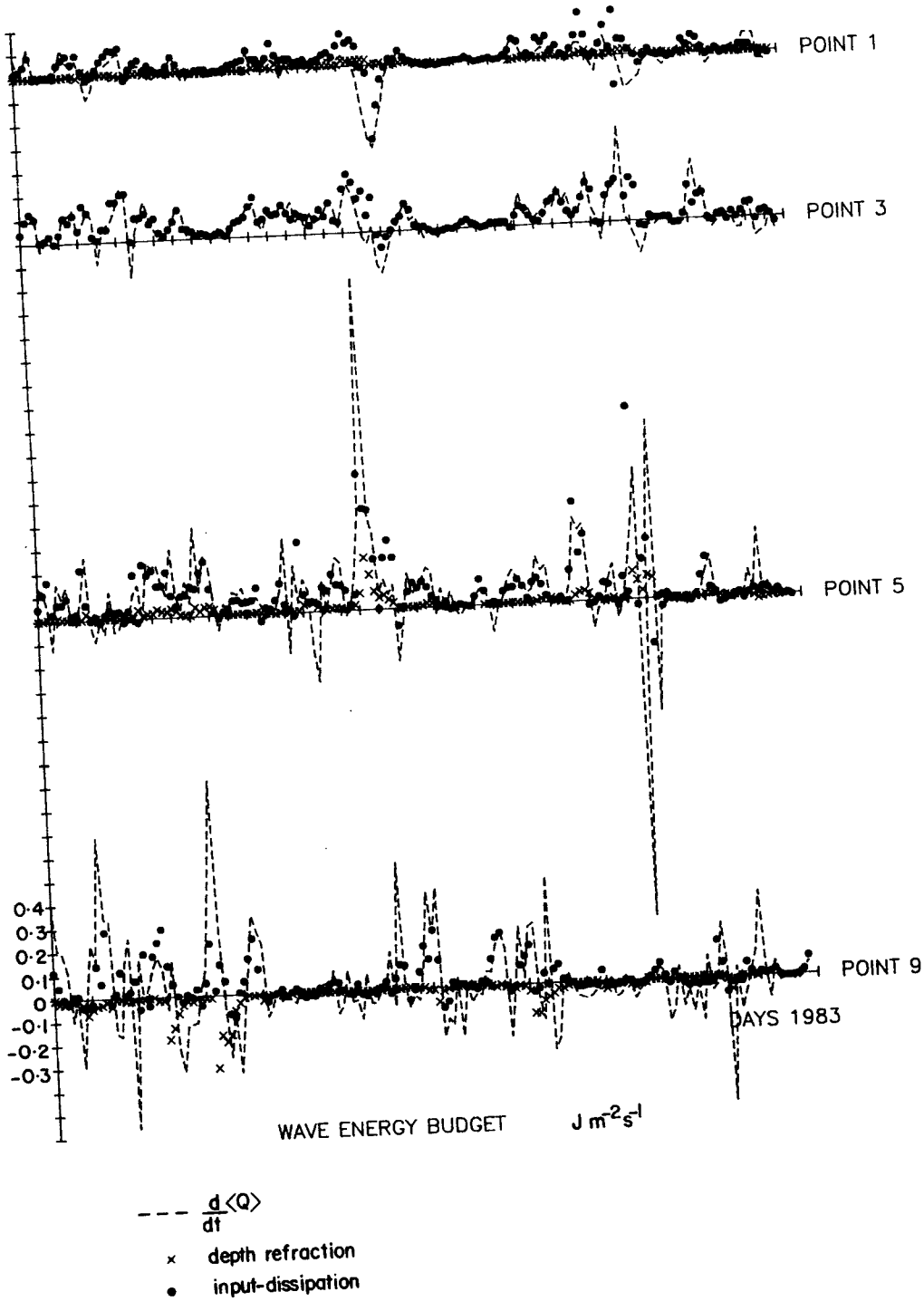

Figure 5.6 (a) Time series of terms in wave energy equation.

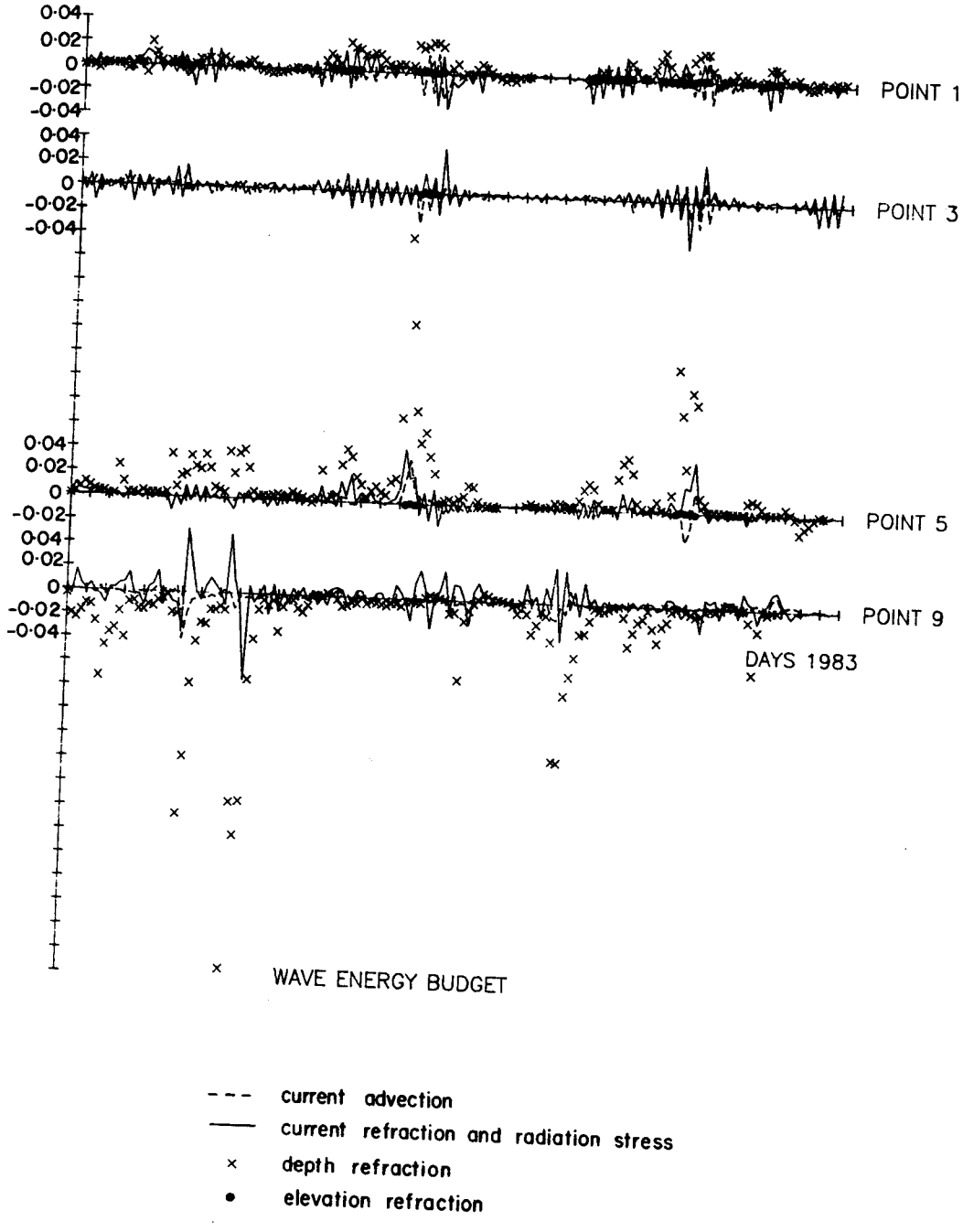

Figure 5.6 (b) Time series of terms in wave energy equation.

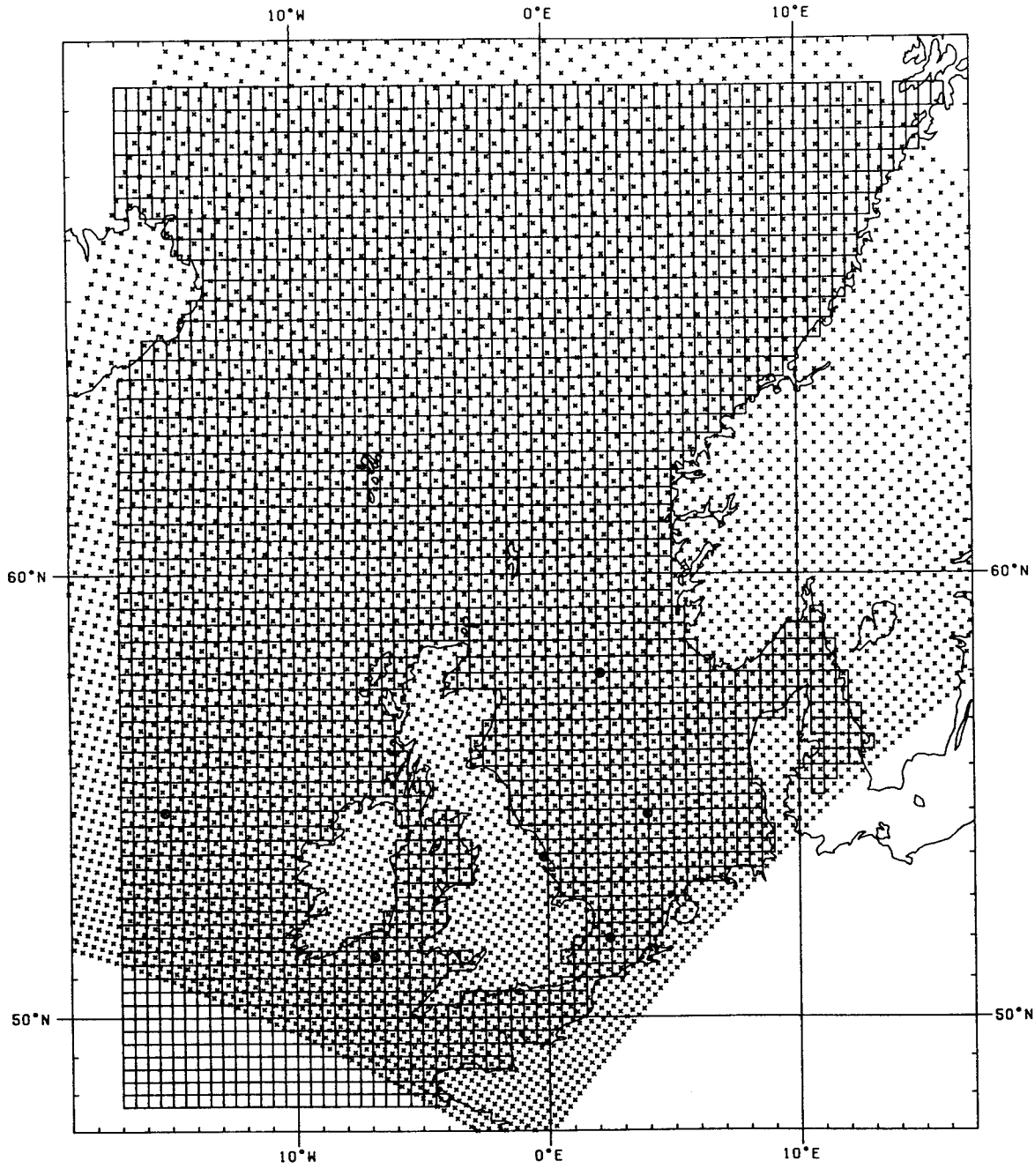

Figure A1 CXX grid with the fine mesh wave model plus locations used for comparisons of wind-stress.

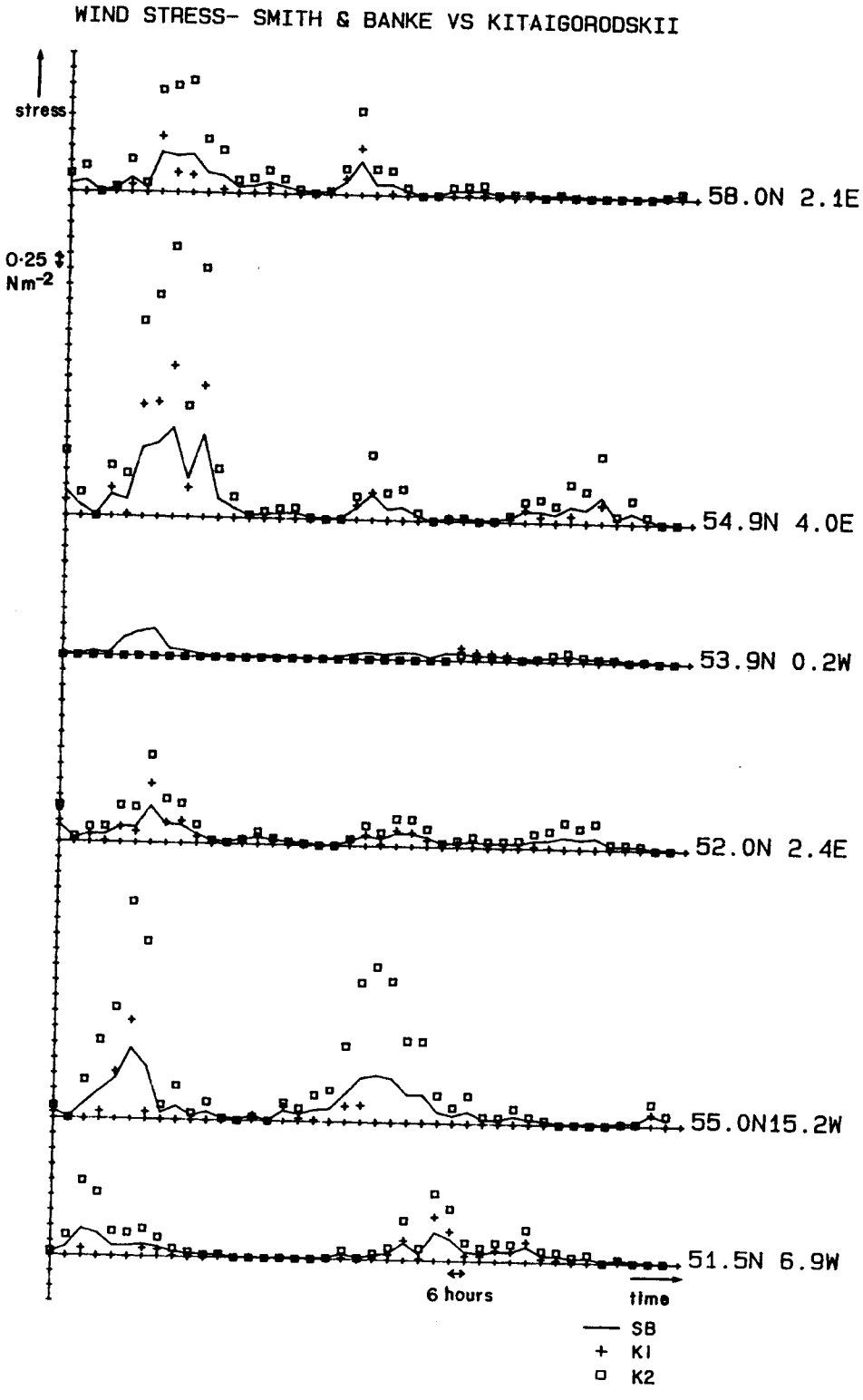

Figure A2 Comparison of wind-stress at six locations from methods SB, B1 and B2.

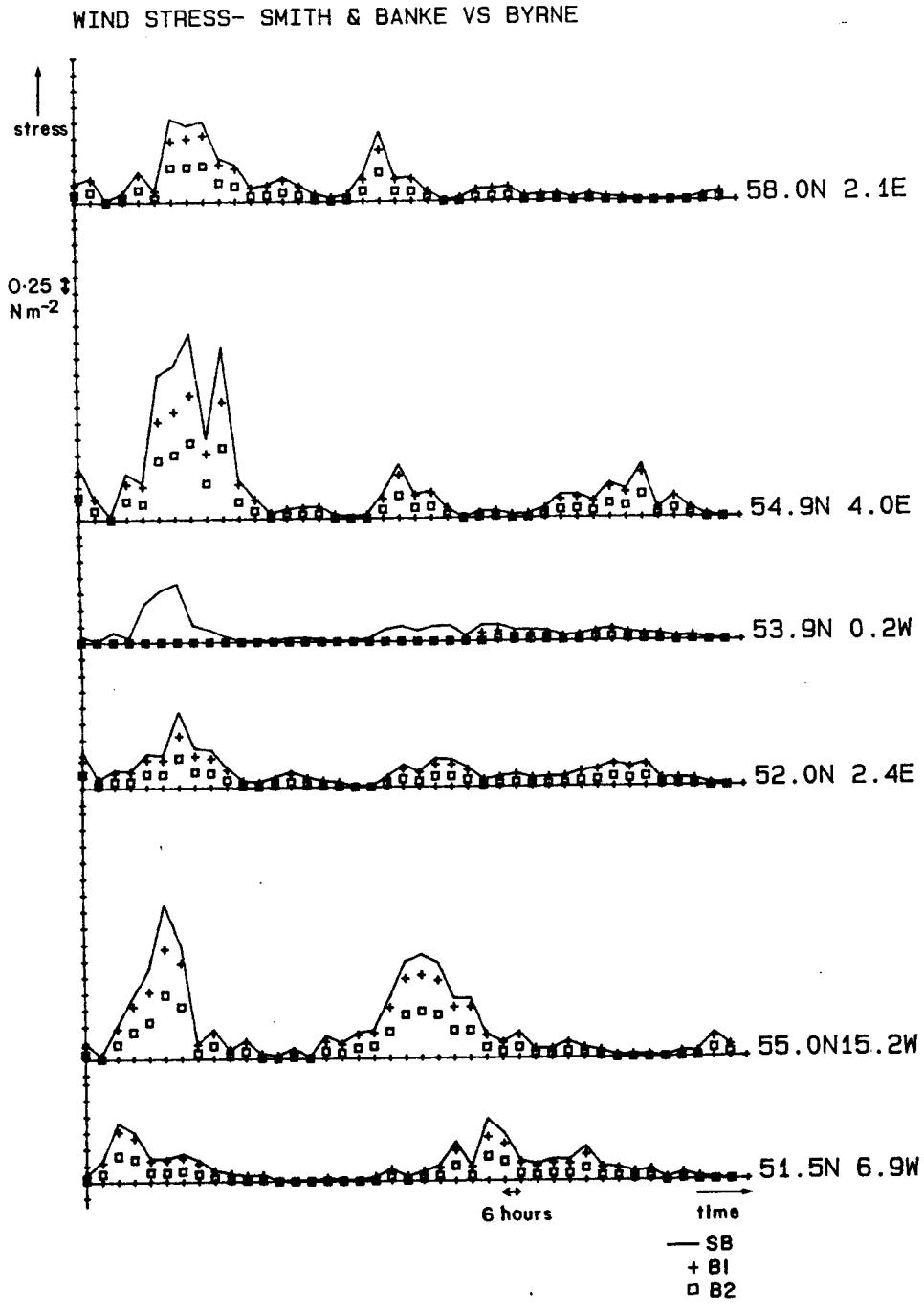

Figure A3 Comparison of wind-stress at six locations from methods SB, B1 and B2.

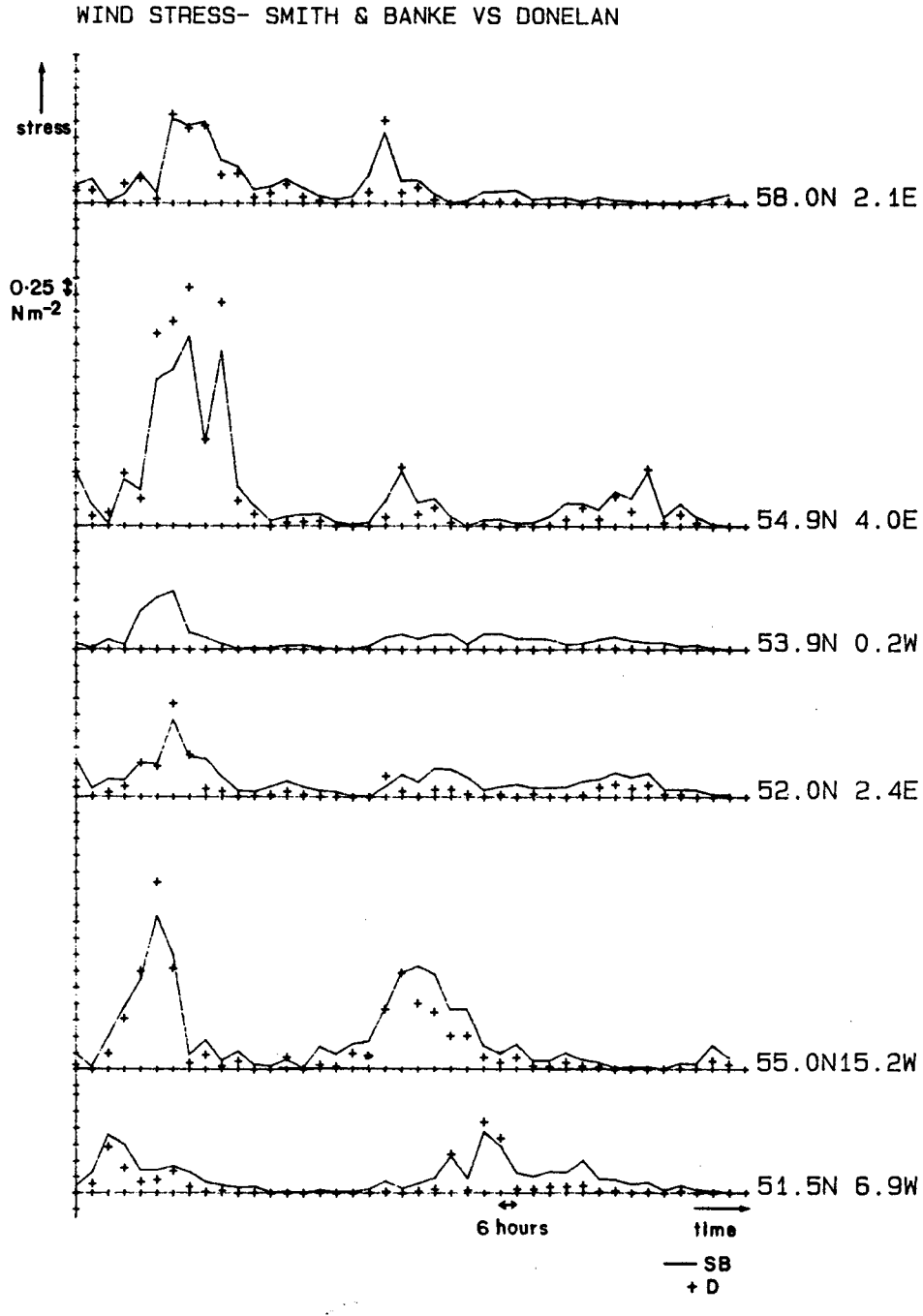

Figure A4 Comparison of wind-stress at six locations for methods SB and D.

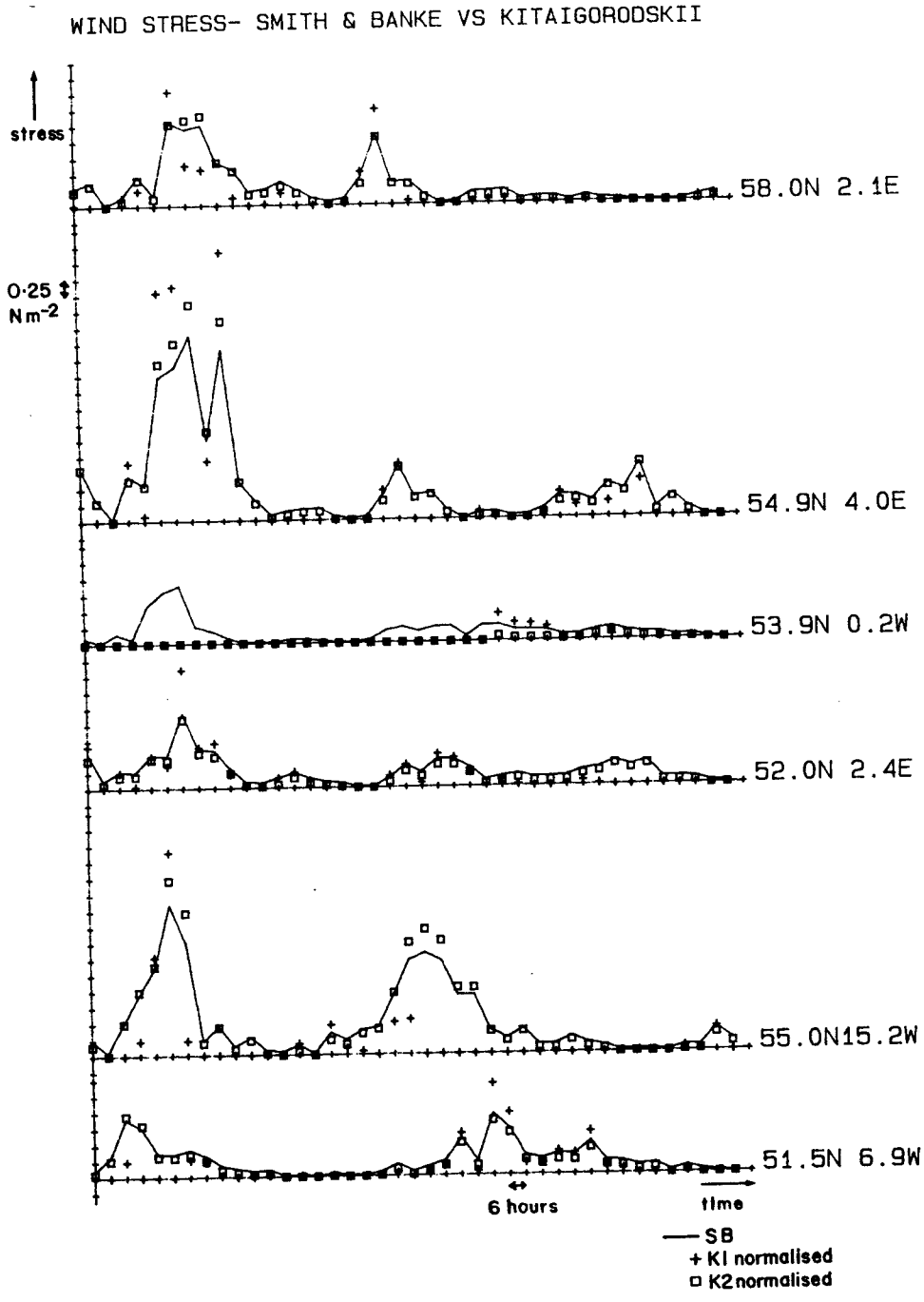

Figure A5 As A2 but with wave-modified wind-stress normalised.

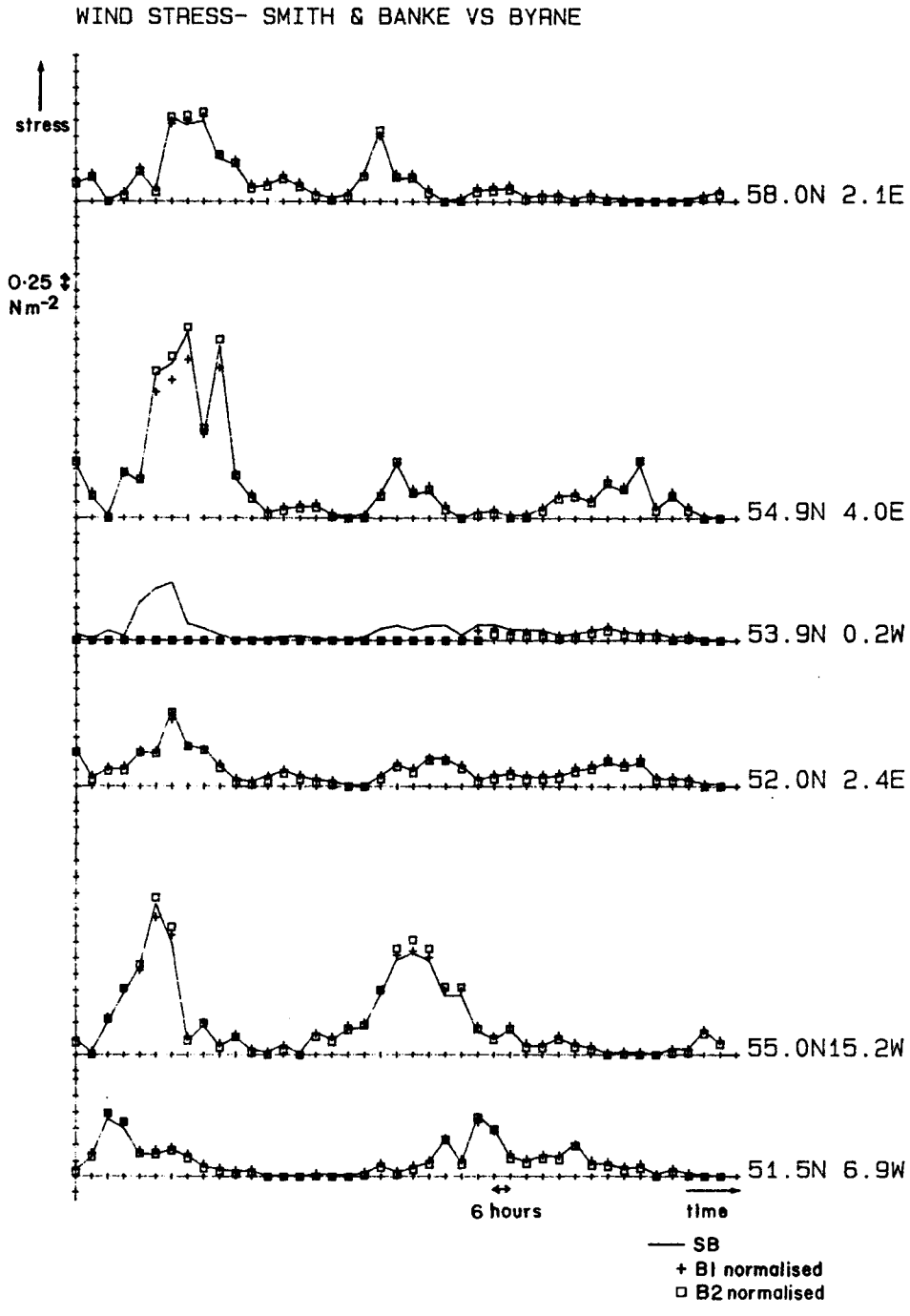

Figure A6 As A3 but with wave-modified wind-stress normalised.

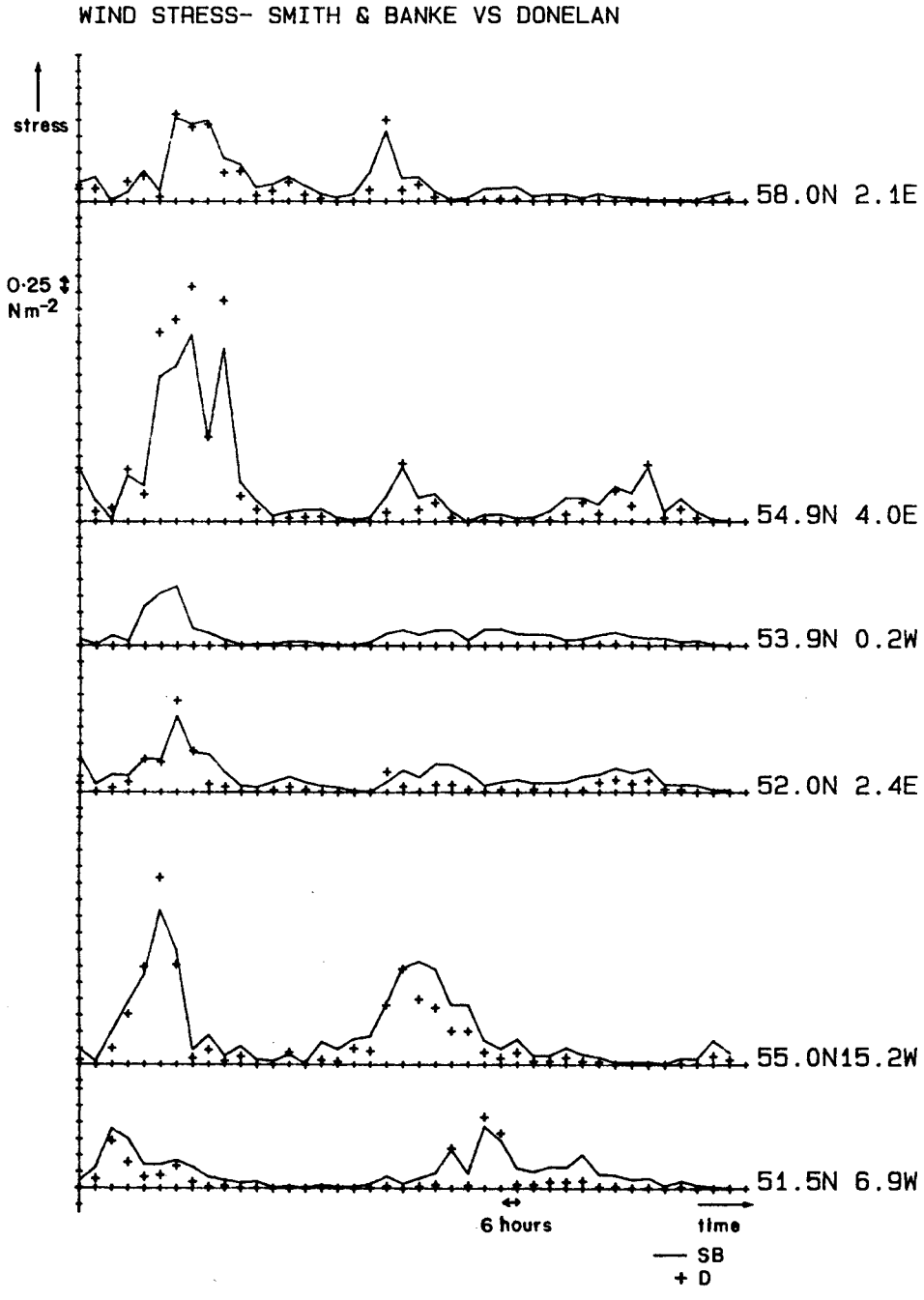

Figure A7 As A4 but with wave-modified wind-stress normalised.

(b) Spatial arrays of differences between the wave-modified wind-stress and the original wind-stress. 12Z 1 February 1983.

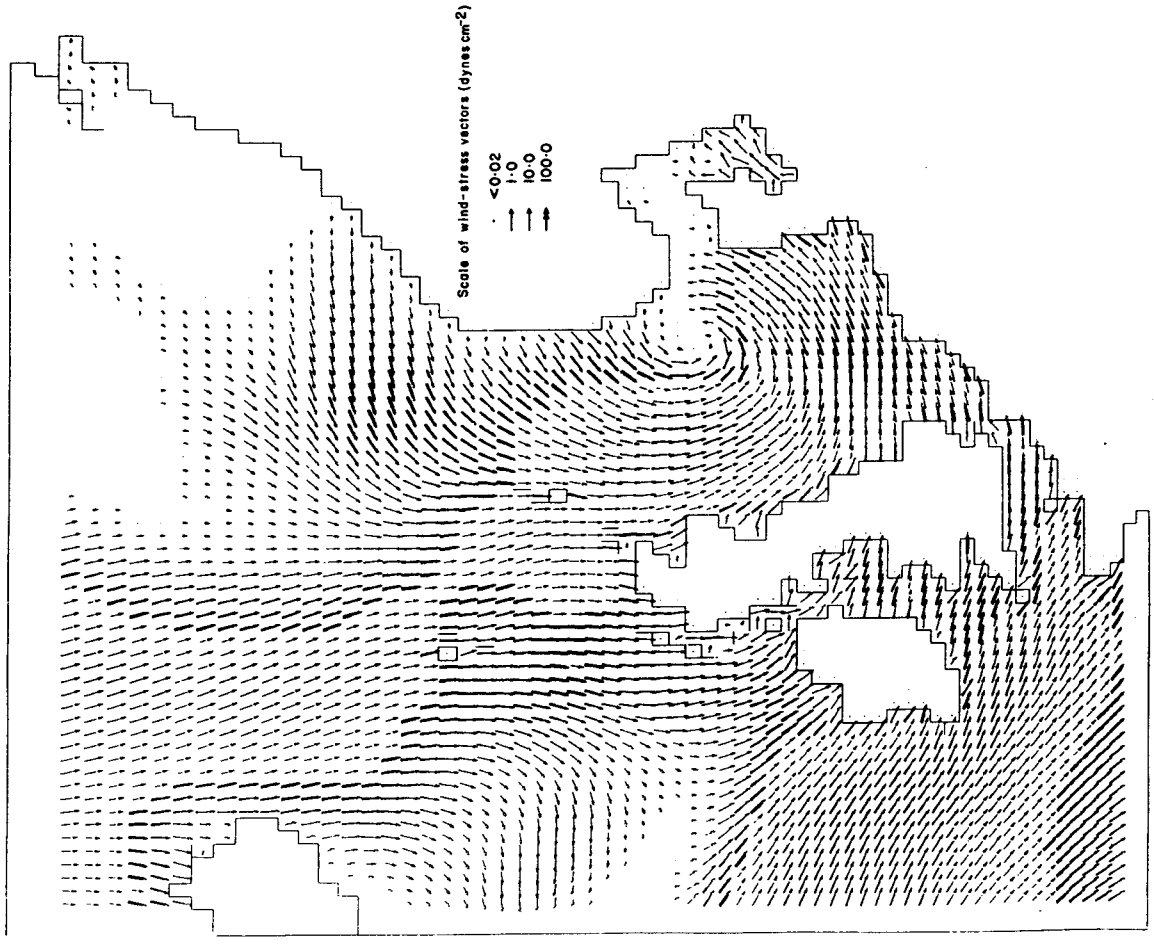

(a) Spatial array of wind-stress vectors computed with wave-modified drag coefficient. 12Z 1 February 1983.

Figure A8

(b) Spatial arrays of differences between the wave-modified wind stress and the original wind-stress. 18Z 5 February 1983.

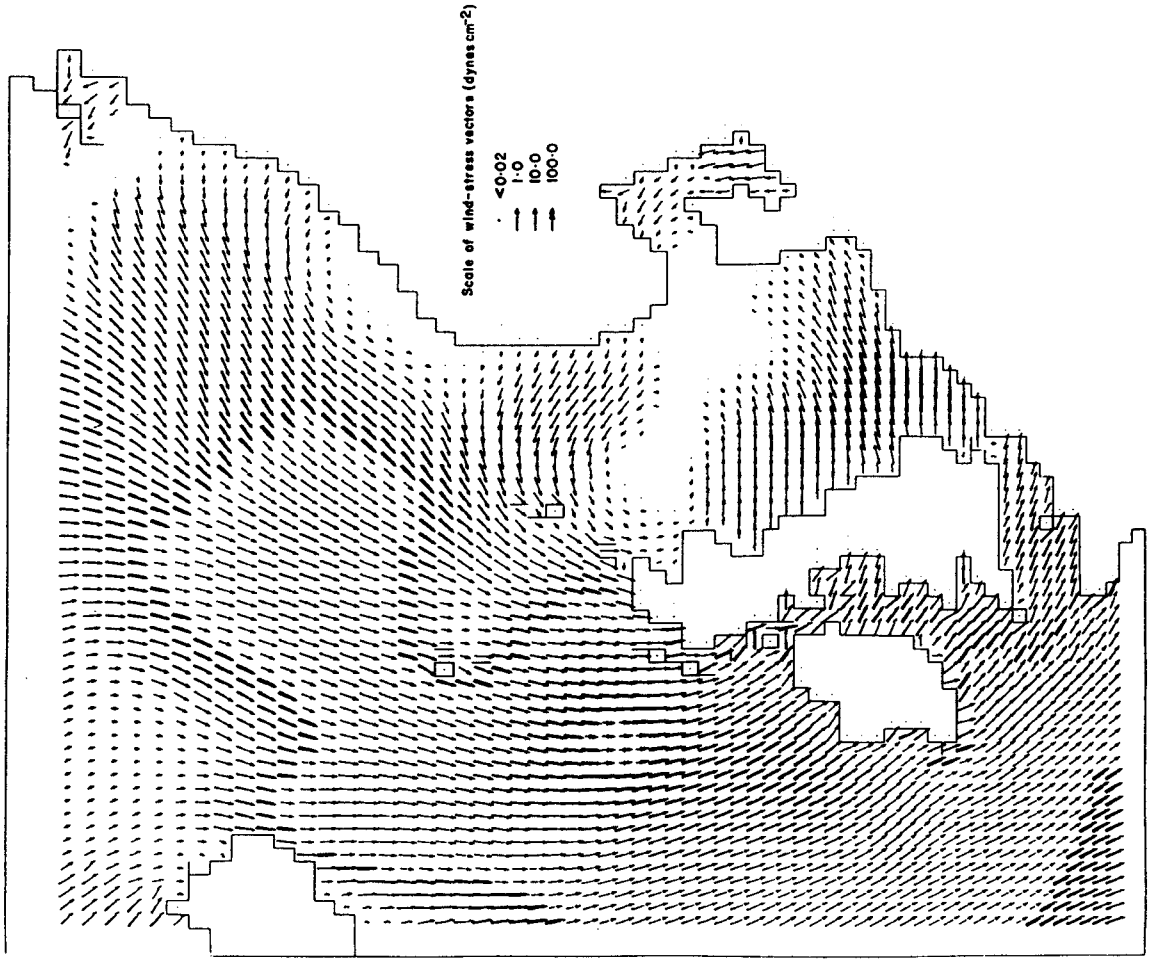

(a) Spatial array of wind-stress vectors computed with wave-modified drage coefficient. 18Z 5 February 1983.

Figure A9

(a) Spatial arrays of residual currents computed with original wind-stress, 12Z 1 February 1983.

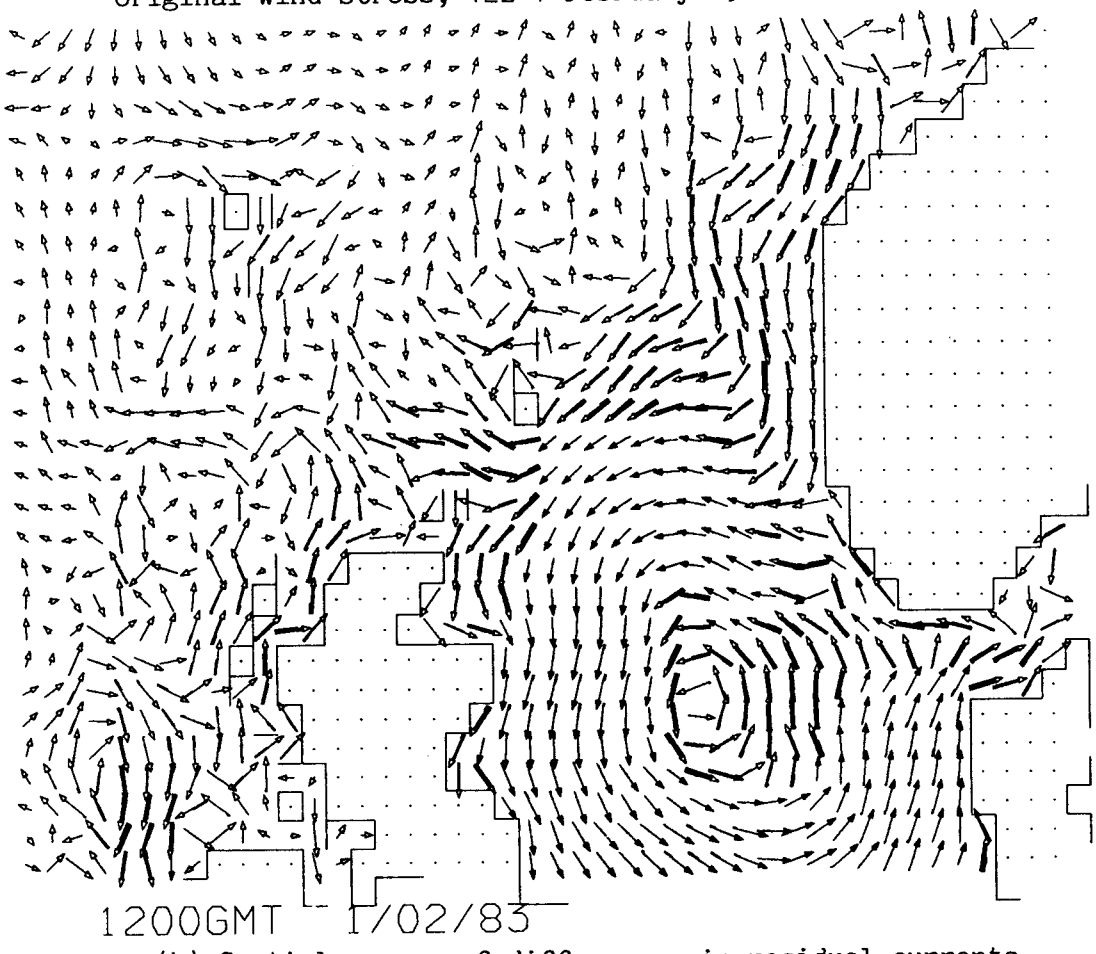

(b) Spatial arrays of differences in residual currents between wave-modified wind-stress case and original wind-stress case, 12Z 1 February 1983.

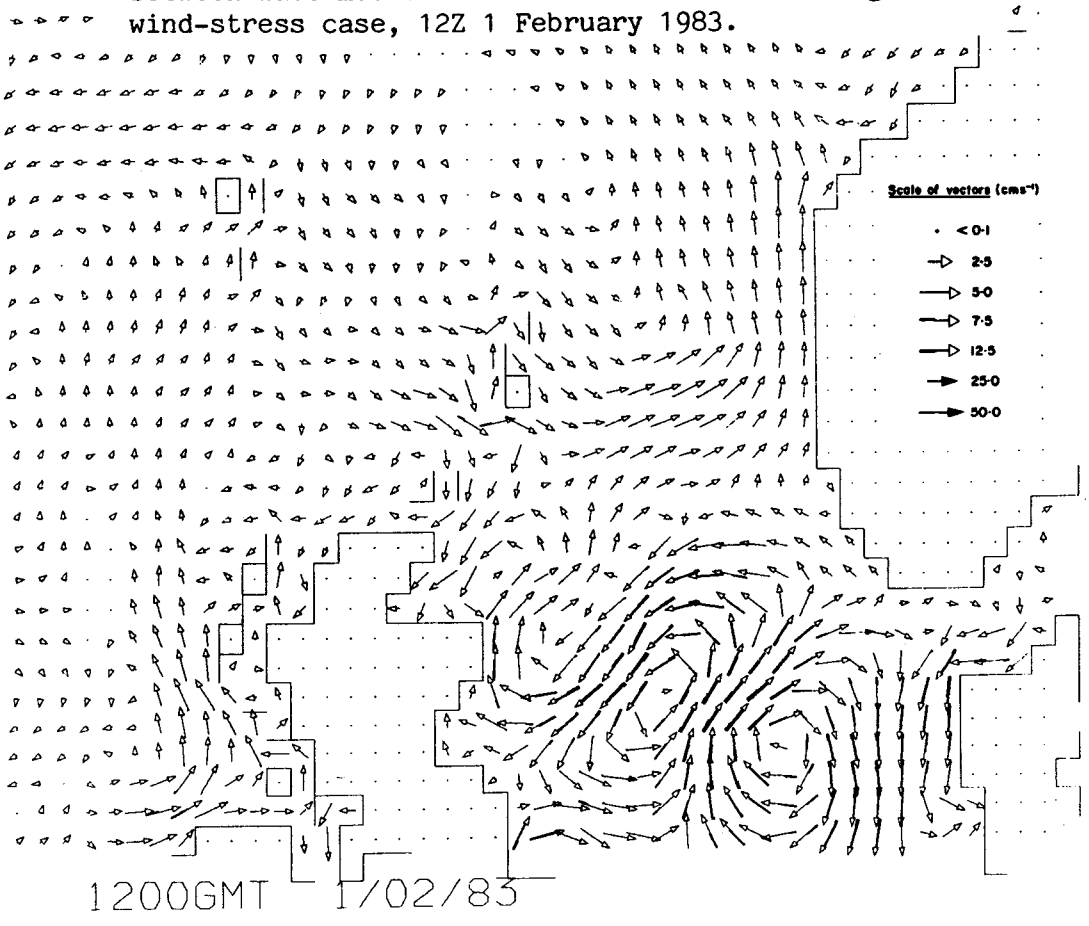

Figure A10

(a) Spatial arrays of residual currents computed with wind stress and the original wind-stress. 18Z 5 February 1983.

(b) Spatial arrays of differences between the wave-modified drage coefficient. 18Z 5 February 1983.